https://doi.org/10.15388/vu.thesis.840
https://orcid.org/0000-0001-8206-0776

VILNIUS UNIVERSITY
CENTER FOR PHYSICAL SCIENCES AND TECHNOLOGY

Julija Sarvutienė

The Application of Electrochemical and QCM Sensors in Studying Interactions Involving High Molecular Weight Compounds

DOCTORAL DISSERTATION

Natural Sciences,
Chemistry (N 003)

VILNIUS 2025

This dissertation was prepared between 2019 and 2025 State Research Institute Center for Physical Sciences and Technology). The Research Council of Lithuania supported the research with scholarships granted for academic accomplishments in 2023.

Academic Supervisor – Assoc. Prof. Dr. Urtė PRENTICE (Center for Physical Sciences and Technology, Natural Sciences, Chemistry – N 003).
Scientific Consultant – Dr. Deivis PLAUŠINAITIS (Vilnius University, Natural Sciences, Chemistry – N 003).

Chairperson – Dr. Renata BUTKUTĖ (Center for Physical Sciences and Technology of the State Research Institute, Technological Sciences, Materials Engineering – T 008),
Members:
Prof. Dr. Henrikas CESIULIS (Vilnius University, Natural Sciences, Chemistry – N 003),
Dr. Natalija GERMAN (Department of Immunology, State Research Institute Centre for Innovative Medicine, Natural Sciences, Chemistry – N 003),
Dr. Renata KARPICZ (Center for Physical Sciences and Technology (FTMC), Natural Sciences, Physics – N 002),
Prof. Dr. Yasemin OZTEKIN (Selcuk University, Türkiye, Natural Sciences, Chemistry – N 003).

This doctoral dissertation will be defended in a public meeting of the Dissertation Defence Panel at 14:00 on 24 October 2025 at Meeting Room D401 of the State Research Institute Center for Physical Sciences and Technology.
Address: Saulėtekio 3, Vilnius, Lithuania, tel. +37052648884; e-mail: office@ftmc.lt

The text of this dissertation can be accessed at Vilnius University Library, Universiteto 3, Vilnius, Lithuania, as well as on the website of Vilnius University: *www.vu.lt/lt/naujienos/ivykiu-kalendorius*

https://doi.org/10.15388/vu.thesis.840
https://orcid.org/0000-0001-8206-0776

VILNIAUS UNIVERSITETAS
VMTI FIZINIŲ IR TECHNOLOGIJOS MOKSLŲ CENTRAS

Julija Sarvutienė

Elektrocheminių ir QCM jutiklių taikymas didelės molekulinės masės junginių sąveikos tyrimuose

DAKTARO DISERTACIJA

Gamtos mokslai,
Chemija (N 003)

VILNIUS 2025

Disertacija rengta 2019–2025 metais Valstybiniame mokslinių tyrimų institute Fizinių ir technologijos mokslų centre. Mokslinius tyrimus rėmė Lietuvos mokslo taryba 2023 metais.

Mokslinė vadovė – doc. dr. Urtė Prentice (Fizinių ir technologijos mokslų centras, gamtos mokslai, chemija – N 003).
Mokslinis konsultantas – dr. Deivis Plaušinaitis (Vilniaus universitetas, gamtos mokslai, chemija – N 003)

Gynimo taryba:
Pirmininkė – dr. Renata Butkutė (Valstybinis mokslinių tyrimų institutas Fizinių ir technologijos mokslų centras, technologijos mokslai, medžiagų inžinerija – T 008).
Nariai:
prof. dr. Henrikas Cesiulis (Vilniaus universitetas, gamtos mokslai, chemija – N 003),
dr. Natalija German (IMC, Valstybinis mokslinių tyrimų institutas Inovatyvios medicinos centras, gamtos mokslai, chemija – N 003),
dr. Renata Karpicz (Fizinių ir technologijos mokslų centras, gamtos mokslai, fizika – N 002),
prof. dr. Yasemin Oztekin (Selcuk universitetas (Turkija), gamtos mokslai, chemija – N 003).

Disertacija ginama viešame Gynimo tarybos posėdyje 2025 m. spalio 24 d., 14 val. Valstybinio mokslinių tyrimų instituto Fizinių ir technologijos mokslų centro D401 konferencijų salėje. **Adresas:** Saulėtekio al. 3, Vilnius, Lietuva tel. +37052648884; el. paštas: office@ftmc.lt

Disertaciją galima peržiūrėti Vilniaus universiteto bibliotekose ir VU interneto svetainėje adresu: https://www.vu.lt/naujienos/ivykiu-kalendorius

ACKNOWLEDGMENTS

I want to extend my heartfelt gratitude to everyone who contributed to the preparation of this dissertation and supported me throughout this process with their encouragement and motivation.

I am especially thankful to Prof. Habil. Dr. Arūnas Ramanavičius for inviting me to join the department. His trust, constructive feedback, patience, and continued optimism have been invaluable as I worked on my doctoral thesis.

I am deeply grateful to my supervisor, Assoc. Prof. Dr. Urtė Prentice, who has always been my first point of contact during times of uncertainty. Her positivity, supportive attitude, guidance, and patience have greatly helped me throughout the writing of this dissertation.

I would also like to express my sincere appreciation to Dr. Deivis Plaušinaitis for his professionalism, insightful consultations, support, and collaboration in analyzing kinetic data. Working together in a supportive and inspiring research environment has been truly fulfilling. His expertise, dedication, and willingness to share ideas were essential to this work.

Finally, I would like to thank my family for their unwavering support and encouragement and for reminding me of what truly matters. This journey has been challenging, but their belief in me has made it possible.

TABLE OF CONTENTS

INTRODUCTION 8

1. LITERATURE REVIEW 10
1.1. Biological macromolecules 10
1.1.1. DNA-modifying enzymes 11
1.1.2. Protein biomarkers 16
1.1.2.1. BAFF protein 16
1.1.2.2. VEGF protein 17
1.2. Self-assembled monolayers (SAM) Strategies for Biosensor Applications . 18
1.2.1. SAM on Gold Nanoparticles 19
1.2.2. SAM for DNA-modifying enzymes 20
1.2.3. The limitation of SAM-based analytical systems 25
1.2.4. Quartz Crystal Microbalance (QCM) 26
1.2.5. Fourier Transform Infrared Spectroscopy (FTIR) 28
2. EXPERIMENTAL SECTION 31
2.1. Materials and equipment 31
2.2. T7 DNA polymerase studies 31
2.2.1. Free T7 DNA polymerase studies 31
2.2.1.1. DNA fragments extraction from agarose gel protocol 32
2.2.1.2. Free T7 DNA polymerase 3'→5' exonuclease activity study 32
2.2.2. T7 DNA polymerase-based sensor study 33
2.2.2.1. Cleaning protocol for the gold QSense® 33
2.2.2.2. SAM formation study 34
2.2.2.3. T7 DNA polymerase masking study 35
2.2.2.4. SAM activation and T7 DNA polymerase immobilization study .. 35
2.2.2.5. T7 DNA polymerase-based sensor 3'→5' exonuclease activity study 37
2.2.2.6. T7 DNA polymerase-based sensor re-usage study 37
2.2.2.7. T7 DNA polymerase-based sensor hydrolysis study 37
2.3. BAFF protein study 38
2.3.1. Free BAFF protein study 38
2.3.2. BAFF protein-based sensor study 38
2.3.2.1. SAM activation and BAFF immobilization study 38
2.3.2.2. SAM deactivation study 39
2.3.2.3. BAFF protein-based sensor evolution study 39
2.4. VEGF protein study 40
3. RESULTS AND DISCUSSION 41
3.1. T7 DNA polymerase study results 41
3.1.1. Free T7 DNA polymerase study results 41
3.1.2. T7 DNA polymerase-based sensor study results 54
3.1.2.1. QSense® sensor after cleaning characterization 54
3.1.2.2. SAM surface characterization 55

3.1.2.3. Characterization of enzyme-based sensor QCM data 58
3.1.2.4. Characterization of enzyme-based sensor kinetic models..... 60
3.1.2.5. Characterization of enzyme-based sensor re-usage 65
3.1.2.6. Characterization of enzyme-based sensor hydrolysis 69
3.2. BAFF protein study results 76
3.2.1. Free BAFF study results..... 76
3.2.2. Characterization of BAFF-based sensor QCM data 76
3.2.3. Characterization of BAFF-based sensor kinetic models 78
3.3. VEGF protein study results..... 81
CONCLUSION..... 84
SANTRAUKA..... 86
ĮVADAS..... 86
TYRIMO METODIKA 91
REZULTATŲ APTARIMAS..... 97
IŠVADOS..... 106
REFERENCES 107
LIST OF PUBLICATIONS..... 118
LIST OF CONFERENCE PRESENTATIONS..... 119
CURRICULUM VITAE 120

INTRODUCTION

Understanding the interplay between genetic mechanisms and immune system regulation is fundamental for advancing biosensor technologies aimed at precise molecular diagnostics. DNA-modifying enzymes, such as T7 DNA polymerase, play a crucial role in essential biological processes, including DNA replication, repair, and proofreading. Their substrate specificity and catalytic efficiency make them suitable candidates for integration into biosensing platforms, where enzymatic activity can be harnessed for sensitive and specific DNA detection. Equally important is the role of immune-related proteins, such as the *B-Cell Activating Factor* (BAFF), a cytokine crucial for B-cell maturation, survival, and immune function. BAFF has garnered significant attention not only for its physiological relevance but also for its involvement in autoimmune disorders, positioning it as a potential diagnostic marker.

This research focuses on the surface immobilization of T7 DNA polymerase and BAFF for use in label-free biosensors. By examining their functional retention and interaction capabilities on chemically modified sensor surfaces, this work aims to contribute to the development of diagnostic platforms that integrate both genetic and immunological detection elements. The dual focus of this study reflects the growing need for interdisciplinary solutions in biomedical diagnostics, combining enzymatic precision with immune specificity to improve sensitivity, reusability, and application in complex biological systems

Research Aim

This research aims to investigate the immobilization, reusability, and enzymatic efficiency of T7 DNA polymerase on functionalized biosensor surfaces and to explore its potential for molecular diagnostics. Additionally, the study extends to developing and characterizing a BAFF-based biosensor for DNA interaction detection, addressing both genetic and immunological aspects relevant to biosensor design.

Objectives

- To develop a T7 DNA polymerase-based biosensor using gold-coated electrodes and a variety of compositions of *Self-Assembled Monolayer* (SAM) mixtures and evaluate its immobilization efficiency and enzymatic activity.
- To assess the 3'→5' exonuclease activity of immobilized T7 DNA polymerase, focusing on its stability and reusability under various reaction conditions.
- To investigate the proteolysis of immobilized T7 DNA polymerase using Proteinase K and to evaluate proteolytic kinetics on gold-coated electrodes with different SAM compositions.
- To construct a BAFF-based biosensor using gold-coated electrodes with SAM mixture compositions and demonstrate its functionality through DNA interaction monitoring using QCM (*Quartz Crystal Microbalance*).
- To fit experimental QCM data to kinetic models (first-, second-, and n-order) for both BAFF and T7 DNA polymerase biosensor systems and determine the best model describing the adsorption behavior.

Scientific Novelty

- A novel immobilization strategy has been developed for masked T7 DNA polymerase on gold-coated QCM electrodes with SAM mixture compositions, maintaining active site accessibility and enzymatic function.

- This thesis has demonstrated immobilized T7 DNA polymerase reusability through multi-cycle exonuclease assays, revealing optimal reaction conditions that preserve enzyme activity.
- This thesis has implemented quantitative analysis of immobilized T7 DNA polymerase hydrolysis by Proteinase K, thereby providing a unique insight into surface-bound proteolysis using QCM-based kinetic modeling.
- First-time demonstration has been achieved of BAFF protein immobilization and functional DNA recognition on gold-coated QCM electrodes with self-assembled SAM monolayer mixture compositions, by using QCM, with real-time monitoring of interaction dynamics.
- Application of first, second, and n-order kinetic modeling has been performed to surface adsorption data, revealing complex interaction behaviors beyond classical adsorption models.

Statements to be Defended

1. Masked T7 DNA polymerase can be effectively immobilized on SAM-modified gold electrodes, forming a stable and functional biosensor with kinetically validated enzymatic activity.
2. Functional T7 DNA polymerase biosensors can maintain reusability.
3. Surface-bound enzyme stability can be evaluated through real-time, label-free QCM monitoring and kinetic analysis of proteolytic degradation.
4. BAFF immobilized on self-assembled monolayer functionalized gold electrodes enables the label-free detection of target DNA sequences, and its interaction kinetics can be reliably described by models supporting biosensor sensitivity and specificity.

1. LITERATURE REVIEW

This section examines existing studies, perspectives, and theories relevant to the research questions, specifically focusing on DNA-modifying enzymes and their applications in biosensor technology [1]. Additionally, the review addresses the significance of immune system-related proteins, such as the B-cell activating factor, in diagnostics. By analyzing the current body of knowledge, this review identifies key gaps and limitations in previous research that the present study aims to address. In doing so, it justifies the need for the proposed study and highlights its potential contributions to molecular biology, immunology, and biosensor development. The aim is to integrate and evaluate the relevant literature critically, establishing a foundation for the experimental work and theoretical advancements discussed throughout this dissertation.

Building on the foundational understanding of DNA-modifying enzymes, their integration into biosensor technologies has become a significant area of research. Application of these enzymes in biosensors dates back to the pioneering work by Clark and Lyons, who developed the first glucose biosensor in 1962 [2]. This milestone laid the groundwork for incorporating enzymatic reactions in diagnostic devices, thus marking the beginning of biosensor technologies that rely on the catalytic activity of enzymes. Since then, the field has expanded, with DNA-modifying enzymes becoming integral to developing biosensors for detecting genetic material and facilitating high-sensitivity detection in molecular diagnostics. Integration of these enzymes with nanomaterials has led to highly efficient biosensors characterized by enhanced specificity, sensitivity, and selectivity, lower detection limits, faster reaction kinetics, and reduced sample and reagent consumption [3]. Furthermore, coupling enzymatic reactions involving DNA-modifying enzymes with advanced physical detection methods has driven the development of innovative DNA sensor platforms. During the COVID-19 pandemic, these enzymes were pivotal in designing RNA and DNA sensors enabling precise nucleic acid detection [4]. Their catalytic ability to modify DNA substrates underscores their significance in biosensing applications. Additionally, DNA-modifying enzymes facilitate the integration of amplification techniques, such as isothermal amplification and *Polymerase Chain Reaction* (PCR), into biosensor architectures, significantly improving detection sensitivity [5,6]. Their versatility allows for the development of multiplexed platforms capable of detecting multiple targets simultaneously, thus making them highly suitable for diagnostic applications. The use of engineered or mutant enzymes tailored for specific reactions has further expanded the functional capabilities of DNA sensors. These advancements highlight the indispensable role of DNA-modifying enzymes in biosensor technology, paving the way for future innovations in personalized medicine, environmental monitoring, and point-of-care diagnostics.

1.1. Biological Macromolecules

Biological macromolecules are large, complex molecules that are crucial for the cellular structure, function, and regulation. The term ‘macromolecule’ typically refers to molecules with a high molecular weight, generally exceeding 1,000 Daltons (Da). In biological systems, these macromolecules usually vary from 10 kDa to several gigadaltons (GDa), with examples such as ribosomes at approximately 2.5 MDa, and human genomic DNA at about 3.2 GDa [7,8]. Biomacromolecules, which are composed of repeating monomeric units connected by covalent bonds to create extensive polymeric structures, are differentiated from smaller biomolecules like metabolites, hormones, and simple sugars by their significant size and complexity. The four primary classes of biological macromolecules – proteins, nucleic acids,

carbohydrates, and lipids – each serve unique roles in various cellular and physiological processes.

- Proteins are responsible for enzymatic catalysis (e.g., DNA-modifying enzymes like DNA polymerases), structural support (e.g., collagen), signal transduction (e.g., growth factors), transport (e.g., hemoglobin), and immune defense (e.g., antibodies).
- Nucleic acids store and transmit genetic information, regulate gene expression, and catalyze reactions (e.g., ribozymes).
- Carbohydrates (Polysaccharides) play roles in energy storage (e.g., glycogen, starch), structural support (e.g., cellulose, chitin), cellular communication (e.g., glycoproteins, glycolipids), and immune responses.
- Lipids are involved in membrane formation (e.g., phospholipids), energy storage (e.g., triglycerides), and signaling molecules (e.g., steroids, prostaglandins), facilitating signal transduction and molecular interactions.

Biological macromolecules are not only essential for maintaining the cellular structure and function but also represent highly suitable materials for biosensor development. Their considerable molecular weight, structural complexity, and capacity for selective interactions make them excellent candidates for constructing stable and functional recognition interfaces. Among them, DNA-modifying enzymes are of particular importance as their interactions with nucleic acids and ability to alter the DNA structure are fundamental for genetic stability and the regulation of gene expression. Beyond their biological role, these enzymes have also been successfully adapted as recognition and catalytic elements in biosensor platforms. Their unique properties enable biosensors to mimic natural biological systems and ensure high sensitivity, selectivity, and reproducibility in analyte detection. Thus, biological macromolecules – and DNA-modifying enzymes in particular – serve as indispensable building blocks for the development of advanced biosensing technologies.

1.1.1. DNA-modifying enzymes

Proteins serve as fundamental biological macromolecules responsible for catalyzing biochemical reactions, including those involved in DNA processing. Among them, DNA-modifying enzymes, such as DNA polymerases, play a crucial role in DNA replication, repair, and recombination. These enzymes are essential for maintaining genetic integrity by synthesizing new DNA strands with high specificity and fidelity. DNA polymerases are large, multi-domain proteins typically ranging from 60 kDa to over 200 kDa, which makes them biological macromolecules due to their high molecular weight and structural complexity [8]. They function by adding deoxyribonucleotides to a growing DNA strand, guided by a complementary template strand, and cleaving deoxyribonucleotides to proofread and correct errors in DNA strands. *Figure 1* broadly represents the interplay between polymerases, exonucleases, and other nucleic acid-processing enzymes involved in DNA synthesis, repair, and modification.

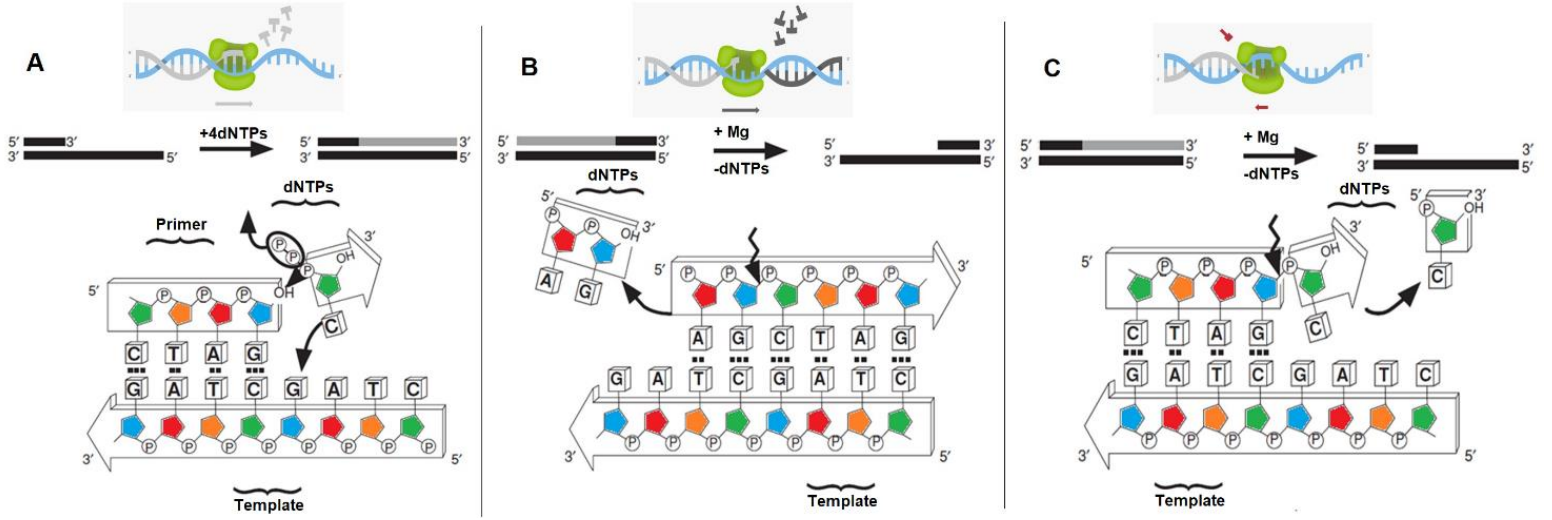


Figure 1. DNA-modifying enzyme activities: Polymerization, Proofreading, and Hydrolysis. This figure illustrates the key activities of DNA-modifying enzymes, including DNA polymerization (**A**), mismatch recognition (**B**), and hydrolytic cleavage (**C**). These functions are essential for DNA replication, repair, and processing. (A) DNA Polymerization activity: DNA polymerases catalyze the addition of nucleotides to a growing DNA strand in the 5'-to-3' direction using deoxynucleotide triphosphates (dNTPs). This activity is crucial for DNA replication and repair. (B) Mismatch recognition and enzyme transition: Certain DNA-modifying enzymes, including proofreading DNA polymerases and nucleases, recognize mismatches or damaged DNA. This leads to a transition where the enzyme may switch from polymerization to exonuclease activity or recruit repair mechanisms. (C) DNA hydrolysis and exonuclease activity: Many DNA-modifying enzymes, including exonucleases and some DNA polymerases with proofreading functions, degrade DNA by cleaving phosphodiester bonds. Exonucleases act in the 3'→5' or 5'→3' direction, depending on the enzyme type, removing nucleotides for error correction or processing DNA intermediates during repair

DNA-modifying enzymes are specialized biomolecules composed of linear chains of amino acids (see *Table 1*) linked by peptide bonds that fold into intricate primary, secondary, tertiary, and sometimes quaternary structures, enabling them to perform biochemical functions [9].

Table 1. Characterization of amino acids

Group	Amino Acid	Abbreviation	Side Chain Type
Nonpolar (Hydrophobic)	Glycine	Gly (G)	Most minor, non-chiral, flexible
	Alanine	Ala (A)	Methyl (-CH_3), simple and small
	Valine	Val (V)	Branched chain
	Leucine	Leu (L)	Branched chain
	Isoleucine	Ile (I)	Branched chain, a structural isomer of leucine
	Methionine	Met (M)	Contains sulfur (-CH_2-CH_2-S-CH_3), essential for start codon (AUG)
	Proline	Pro (P)	Cyclic, rigid, disrupts α-helices
Polar, Uncharged	Serine	Ser (S)	Hydroxyl (-OH), involved in phosphorylation
	Threonine	Thr (T)	Hydroxyl (-OH), involved in phosphorylation
	Cysteine	Cys (C)	Thiol (-SH) forms disulfide bonds
	Asparagine	Asn (N)	Amide (-$CONH_2$)
	Glutamine	Gln (Q)	Amide (-$CONH_2$), involved in nitrogen metabolism
Polar, Positively Charged (Basic)	Lysine	Lys (K)	Long-chain with amino (-NH_3^+), strong positive charge
	Arginine	Arg (R)	Guanidinium group (-$C{=}NH_2^+$), strongest base
	Histidine	His (H)	Imidazole ring, involved in enzyme catalysis and pH sensing
Polar, Negatively Charged (Acidic)	Aspartic Acid (Aspartate)	Asp (D)	Carboxyl (-COO^-) participates in enzyme catalysis
	Glutamic Acid (Glutamate)	Glu (E)	Carboxyl (-COO^-), neurotransmitter precursor
Aromatic	Phenylalanine	Phe (F)	Benzyl (-C_6H_5-CH_2), highly hydrophobic
	Tyrosine	Tyr (Y)	Phenol (-C_6H_4-OH), involved in phosphorylation and signaling
	Tryptophan	Trp (W)	Indole (-C_8H_7N), the most considerable amino acid, a precursor to serotonin

The relevance of DNA-modifying enzymes extends beyond their natural biological roles. In biosensor technologies, these enzymes are essential components for detecting nucleic acids, especially in the context of electrochemical and QCM (*Quartz Crystal Microbalance*) sensors. Their catalytic properties enable the amplification of DNA, which can be detected by using these sensors, thereby enhancing the sensitivity and selectivity of biosensing platforms. For instance, DNA polymerases are involved in enzymatic amplification techniques, such as PCR, which is central to DNA sensors' ability to detect minute quantities of DNA in biological samples.

DNA-modifying enzymes are characterized by their reliance on a set of highly conserved residues that play pivotal roles in their functions. Charged residues, including aspartic acid (Asp), glutamic acid (Glu), lysine (Lys), and arginine (Arg), contribute to the structural integrity of enzymes and interactions with other molecules. Nucleophilic residues such as cysteine (Cys) and tyrosine (Tyr) facilitate chemical reactions. In contrast, the catalytic residue, histidine (His), is often critical in the enzymatic reaction process. These essential residues work together to enable the enzymes to bind specifically to DNA, catalyze biochemical reactions effectively, coordinate metal ions necessary for their activity, and maintain the overall enzymatic stability. The intricate functions of these residues underscore their indispensable role in both fundamental genetic processes and cutting-edge biotechnological applications, such as in electrochemical and QCM-based sensors [10,11].

DNA-modifying enzyme size can range from tens to several hundred amino acids linked by peptide bonds, while non-covalent interactions, such as hydrogen bonds, disulfide bridges (specific to cysteine residues), and Van der Waals forces, stabilize their three-dimensional conformation. DNA-modifying enzymes are described in the literature as adopting well-conserved structural motifs that have evolved to support their catalytic precision and substrate specificity [12]. A hallmark description that is commonly used is the 'right-hand' configuration, which includes three distinct subunits: the fingers, the palm, and the thumb. This structural analogy highlights their mechanistic efficiency, where the 'palm' region houses the catalytically active site, the 'fingers' region interacts with and positions the DNA substrate, and the 'thumb' region maintains DNA binding and processivity [13]. In addition to the 'right-hand' structure, many DNA-modifying enzymes share common structural domains with conserved motifs critical for their function. For instance, motifs such as the Exonuclease I, II, and III domains are frequently observed in DNA polymerases with proofreading activity, enabling them to correct mismatched nucleotides. Similarly, the *Helix-Turn-Helix* (HTH) motif is often found in DNA-binding enzymes, such as endonucleases, which facilitate sequence-specific DNA recognition. Other structural similarities include OB-fold domains (oligonucleotide/oligosaccharide-binding) found in both polymerases and exonucleases, which contribute to DNA or RNA substrate binding.

The versatility of DNA-modifying enzymes lies not only in their conserved structures but also in their dynamic adaptability. These enzymes exhibit modular architectures, often comprising separate domains for catalysis, DNA binding, and additional enzymatic activities. For example, T7 DNA polymerase integrates a polymerase domain with exonuclease functionality, ensuring high fidelity during DNA synthesis. Similarly, restriction endonucleases, such as EcoRI, possess domains for recognizing specific DNA sequences and cleaving them with remarkable precision [14,15].

Beyond their structural features, DNA-modifying enzymes are often classified based on their evolutionary relationships and shared structural motifs [16]. Despite differing biological roles, many enzymes exhibit high structural and functional homology. For instance, DNA polymerases from families A, B, and C share a conserved catalytic core,

underscoring their common evolutionary origin [17]. Likewise, enzymes such as DNA ligases and helicases share ATPase domains, reflecting their reliance on ATP hydrolysis for DNA manipulation tasks [18]. Each group has distinct roles and is further classified into families based on sequence homology, structure, and functional characteristics [19]. Among these, DNA polymerases are the most frequently studied category; they are subdivided into six major families [20]:

1. *Family A*: Found in bacteria, bacteriophages, and eukaryotes, these polymerases are involved in DNA replication and repair. Its key representatives include DNA polymerase I (*E. coli*) and T7 DNA polymerase.
2. *Family B*: Predominantly found in archaea and eukaryotes, these polymerases play a vital role in DNA replication. Its examples include DNA polymerase α, δ, and ε, which function in eukaryotic replication.
3. *Family C*: it is exclusively bacterial. This family includes DNA polymerase III, the primary replicative enzyme in prokaryotes.
4. *Family D*: Found in archaea, this family includes polymerases such as PolD, which also plays a role in archaeal replication.
5. *Family X*: This family is predominantly involved in DNA repair and includes enzymes such as DNA polymerase β in eukaryotes and terminal deoxynucleotidyl transferase (TdT), which adds nucleotides at double-stranded DNA breaks.
6. The *Reverse Transcriptase* (RT) Family: These enzymes reverse-transcribe RNA into DNA in retroviruses and retrotransposons. Its examples include HIV reverse transcriptase and telomerase, which maintain chromosomal integrity in eukaryotic cells.

Other DNA-modifying enzymes, such as endonucleases and exonucleases, play a crucial role in cleaving DNA at specific sites. Endonucleases like EcoRI and HindIII are used extensively in molecular cloning, while exonucleases, such as Exonuclease I and T7 Exonuclease, are employed in processes requiring controlled degradation of DNA ends [21]. Meanwhile, helicases like RecQ are critical for unwinding DNA during replication and repair, whereas DNA ligases, such as T4 DNA ligase, are indispensable for joining DNA strands [22]. These shared structural features enable DNA-modifying enzymes to perform overlapping functions, allowing for their use in diverse biotechnological applications, including electrochemical and QCM sensor-based diagnostics. In addition to their roles in natural cellular processes, their well-characterized structures have facilitated their engineering for various research and clinical purposes, such as gene editing and disease detection. The understanding of the conserved and divergent structural elements of DNA-modifying enzymes remains a key focus for the scientific community, as it provides insights into their mechanisms and potential applications in diagnostics, therapeutics, and synthetic biology. Recent advancements have underscored the diagnostic potential of these enzymes. They are integral to molecular techniques such as PCR, qPCR, and RT-qPCR, and they are widely used for detecting genetic disorders, viral infections, and bacterial pathogens. The future of DNA-modifying enzymes lies in expanding their applications, including genome editing (e.g., CRISPR-Cas systems) [23–25], personalized medicine, and synthetic biology, leveraging their catalytic precision and diverse functionalities to address complex biological challenges.

DNA-modifying enzymes play a central role in the evolution of biosensor technologies due to their precision in catalyzing reactions involving nucleic acids. These enzymes, particularly DNA polymerases, are widely used in biosensor design to support amplification and sequence-specific recognition. Literature highlights their relevance in

high-sensitivity detection platforms used in diagnostics and genetic analysis. DNA polymerase was selected for its dual polymerization and proofreading activity in this research, with the biosensor design reflecting considerations such as enzyme orientation, structural stability, and surface compatibility. These aspects, supported by previous findings, guided the strategy for integrating the enzyme into sensor systems in a way that preserves its activity.

1.1.2. Protein biomarkers

Protein biomarkers are measurable molecules whose expression patterns reflect both physiological and pathological states. Changes in their concentration, activity, or structure provide valuable information for disease diagnosis, prognosis, and therapy monitoring. In contrast to nucleic acid biomarkers, proteins capture the integrated outcome of transcriptional, translational, and post-translational regulation, thereby serving as real-time indicators of biological activity. Their structural complexity creates particular interaction domains, which can be exploited by recognition elements such as antibodies, aptamers, or engineered receptors. These properties make proteins exceptionally attractive for biosensor development, since they can often be detected directly, without amplification, and yield precise, selective signals. This section highlights two clinically relevant protein biomarkers – BAFF (*B-cell activating factor*) and VEGF (*Vascular Endothelial Growth Factor*) – which exemplify distinct yet complementary biological processes: immune regulation and angiogenesis. Both are structurally well characterized, mechanistically important, and highly suitable as targets for advanced biosensing platforms.

1.1.2.1. BAFF protein

BAFF, also known as TNF ligand superfamily member 13B (TNFSF13B) or BLyS (B-lymphocyte stimulator), is a trimeric cytokine of the TNF-ligand family which plays a pivotal role in humoral immunity by regulating B-cell survival, maturation, and differentiation [26]. Unlike DNA-modifying enzymes, which act directly on nucleic acids to preserve genomic integrity and regulate genetic information, BAFF regulates immune system function at the cellular and molecular signaling level, specifically controlling the survival, maturation, and differentiation of B cells. BAFF is highly specific in its interactions: while enzymes recognize defined DNA motifs or structures, BAFF binds selectively to three receptors – BAFF-R, TACI, and BCMA – whose engagement activates distinct NF-κB–mediated pathways that determine the B-cell fate [27,28]. Similar to DNA-modifying enzymes, which require correct folding and orientation to retain catalytic activity, BAFF's trimeric structure (*Figure 2*) must remain intact and correctly oriented on sensor surfaces to preserve receptor-binding functionality. Synthesized as a Type II transmembrane protein and cleaved into a soluble form, BAFF functions primarily as a homotrimer (~75 kDa) [29]. However, higher-order oligomers, such as 60-mers, can form and significantly enhance receptor crosslinking and signaling potency. Physiologically, BAFF maintains B-cell homeostasis, preventing both immunodeficiency and autoimmunity. Pathologically, its overexpression promotes the survival of autoreactive B cells and autoantibody production, driving diseases such as systemic lupus erythematosus, rheumatoid arthritis, and Sjögren's syndrome [30]. Conversely, insufficient expression compromises humoral immunity and increases the risk of infection. Clinically, the therapeutic blockade of BAFF has been validated with the approval of belimumab, the first monoclonal antibody targeting BAFF, and ongoing studies explore BAFF inhibition in B-cell malignancies.

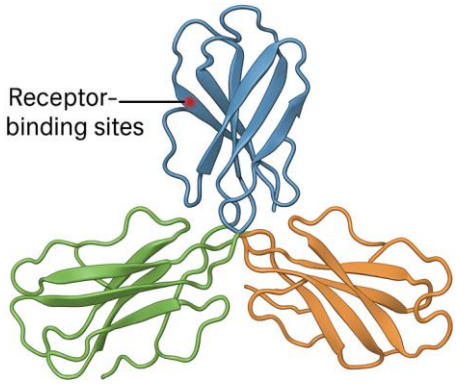


Figure 2. BAFF's trimeric structure

From a biosensing perspective, BAFF is an attractive biomarker: elevated levels in serum can be diagnostic of autoimmune disease or therapeutic efficacy, while its multivalent structure provides opportunities for signal amplification in QCM, SPR (surface plasmon resonance), or electrochemical biosensors. Effective immobilization strategies – particularly those using self-assembled monolayers – must maintain trimer integrity and avoid steric hindrance to ensure that binding epitopes remain exposed, paralleling the same structural preservation considerations applied to DNA-modifying enzymes [31]. Collectively, BAFF illustrates how cytokines, although mechanistically distinct from DNA-modifying enzymes, share critical structural and functional requirements that make them equally valuable as targets for advanced biosensing applications.

1.1.2.2. VEGF protein

VEGF, a member of the platelet-derived growth factor/vascular endothelial growth factor (PDGF/VEGF) family, is a dimeric glycoprotein which plays a central role in angiogenesis and vascular homeostasis. Each VEGF monomer (~19–23 kDa) contains a cystine-knot fold stabilized by multiple disulfide bonds, and two monomers assemble into a homodimer (~38–45 kDa) that exposes receptor-binding loops required for signaling. Unlike DNA-modifying enzymes, which catalyze chemical alterations of nucleic acids to preserve genetic stability, VEGF acts at the tissue and vascular level by stimulating endothelial cell proliferation, migration, and survival. VEGF functions through particular molecular recognition events: it binds selectively to three tyrosine kinase receptors – VEGFR-1, VEGFR-2, and VEGFR-3 – whose dimerization and trans-phosphorylation activate downstream signaling cascades. Similar to enzymes whose catalytic activity depends on correct three-dimensional folding, VEGF's dimeric architecture and conformational integrity are essential for maintaining its biological function and for enabling reliable biosensor detection [32,33].

Physiologically, VEGF is indispensable for embryonic development, wound healing, and tissue regeneration, but its dysregulated overexpression drives pathological angiogenesis in cancer, diabetic retinopathy, and chronic inflammatory diseases. Elevated VEGF levels are therefore strongly associated with tumor progression, metastasis, and poor prognosis. Therapeutically, VEGF signaling has been targeted by monoclonal antibodies (e.g., bevacizumab) and engineered biologics (ranibizumab, aflibercept) that neutralize

VEGF activity or block receptor engagement, forming the basis of modern anti-angiogenic therapies in oncology and ophthalmology [34,35].

In biosensing applications, VEGF serves as a clinically significant biomarker whose quantification provides diagnostic and prognostic insights into angiogenesis-related disorders. Traditional assays such as ELISA and Western blotting are reliable but labor-intensive, requiring labeling and multiple steps. Advanced approaches employ aptamers or antibodies immobilized on *Self-Assembled Monolayers* (SAMs) or nanostructured surfaces, enabling label-free detection via electrochemical impedance spectroscopy, differential pulse voltammetry, quartz crystal microbalance, or optical platforms such as surface plasmon resonance and ellipsometry. These designs exploit VEGF's structural dimerization and receptor-binding domains to achieve picomolar sensitivity and high specificity. As with DNA-modifying enzymes, preserving structural conformation and the correct orientation of the immobilized protein or its recognition element is essential for reliable signal generation [34,35].

Taken together, VEGF exemplifies a biomarker that, although mechanistically distinct from DNA-modifying enzymes, shares the fundamental principle that the structure dictates the function: its disulfide-stabilized dimer must remain intact to engage receptors or recognition probes effectively. This structural dependence, coupled with its pathological relevance, makes VEGF not only a key therapeutic target but also an ideal analyte for biosensor development aimed at an early cancer detection, vascular disease monitoring, and therapy evaluation [36–38].

1.2. Self-Assembled Monolayers (SAM) Strategies for Biosensor Applications

SAMs have become a cornerstone in developing biosensors because they can precisely control surface properties and facilitate specific interactions between biomolecules and sensor surfaces [39]. SAM is widely used for immobilizing various biomolecules, including proteins, DNA, antibodies, and enzymes, onto sensor surfaces. This is achieved by modifying the functional groups of the SAM with reactive groups (such as carboxyl, amino, or thiol groups) that specifically bind to biomolecules [40]. For example, in immunosensors, antibodies are covalently attached to gold surfaces via SAM, thus providing a stable surface for antigen detection. Precise control over the density and orientation of immobilized biomolecules enables high sensitivity and specificity in detecting the target analytes. SAM is also used to detect specific DNA sequences, where DNA probes are immobilized on the surface to hybridize with complementary target sequences, offering a reliable method for gene detection.

One of the key advantages of SAM in biosensor applications is its ability to minimize nonspecific binding. SAM can be functionalized with blocking agents, such as 6-mercaptohexanol (MCH), in DNA hybridization assays to prevent unreacted surface sites from adsorbing unrelated biomolecules. This strategy ensures that the sensor only responds to the target DNA sequence. SAM with tailored blocking agents is also used in protein biosensors to avoid the adsorption of proteins that could lead to false positives or interfere with sensor performance. In addition to preventing nonspecific interactions, SAM can enhance the sensitivity of biosensors through signal amplification strategies. For instance, combining SAM with gold nanoparticles increases the surface area for biomolecule interactions, resulting in stronger signals [41] upon detection of the target analytes. AuNPs functionalized with DNA, antibodies, or enzymes can be used in conjunction with SAM for enhanced electrochemical or optical detection, thereby significantly improving the sensor's detection limits. The large surface area of the nanoparticles enables a high density of target

biomolecules to be captured, thereby facilitating stronger sensor responses. SAM also allows the creation of complex nanostructures for biosensors [42]. These nanostructures can include nanoparticle arrays, nanosensors, and nanowires, which are integrated into biosensors for advanced detection capabilities. In electrochemical sensors, SAM is used to control the assembly of nanoparticles into ordered arrays, creating nanostructures that improve the efficiency of electron transfer processes. In optical biosensors, SAM can be used to functionalize gold nanoparticles, thereby enhancing *Surface Plasmon Resonance* (SPR) signals and enabling real-time monitoring of biomolecular interactions. Moreover, SAM can be modified for multiplexed sensing, incorporating different functional groups into various monolayer regions. This allows the simultaneous detection of multiple analytes within a single sensor system. For example, SAM can be modified with numerous capture molecules, such as antibodies, aptamers, or nucleic acids, each targeting different analytes. This capability is crucial in medical diagnostics, where detecting multiple biomarkers simultaneously is essential for early disease diagnosis. SAM has been applied in multiplexed immunoassays for cancer biomarker detection, where multiple antibodies targeting different tumor markers are immobilized on the same sensor surface, allowing for the detection of various biomarkers in a single sample. SAM is also widely used in electrochemical biosensors to detect multiple molecules, such as glucose, DNA, and proteins. In glucose sensors, for example, glucose oxidase is immobilized onto a gold surface via SAM, catalyzing glucose oxidation and producing a measurable electrochemical signal. Similarly, SAM is used in DNA sensors to immobilize DNA probes, enabling the detection of specific DNA sequences through hybridization-based methods.

These strategies demonstrate the versatility and importance of SAM in biosensor applications, providing a stable surface for biomolecule immobilization and enhancing selectivity, sensitivity, and the ability to detect multiple analytes simultaneously. By carefully designing and functionalizing SAM, significant advancements can be made in medical diagnostics, environmental monitoring, and food safety.

1.2.1. SAM on gold nanoparticles

SAM on AuNPs is a highly effective platform for immobilizing biomolecules, offering exceptional physicochemical properties and versatility [43]. SAMs are organized molecular one-molecule-thick layers that form spontaneously on a substrate through strong interactions between the substrate and the headgroup of the assembling molecule. These monolayers are formed through self-assembly processes, where molecules with specific functional groups – such as thiols, silanes, or phosphines – adhere to surfaces like metals (e.g., gold, silver), semiconductors, or other materials [44]. For AuNPs, SAM are typically generated by using thiol-containing compounds (–SH groups), which chemisorb onto the gold surface, forming a highly stable gold-thiol bond. This bond ensures a durable and reliable surface coating. The alkane chains of the thiol molecules promote close molecular packing, while the terminal functional groups (e.g., carboxyl, hydroxyl, or amine) [45] can be easily customized for subsequent chemical modifications or targeted biomolecular interactions.

SAM offers numerous advantages for nanotechnology and bioanalytical applications [46]. They facilitate the immobilization of biomolecules, such as proteins and DNA, enabling the precise detection of specific analytes in biosensors. The functional groups on SAM reduce nonspecific binding, improving the selectivity and sensitivity of bioanalytical devices. SAM also enhances the biocompatibility of AuNPs, making them suitable for biological and medical applications. Additionally, they create organized active sites that enhance catalytic reactions, prevent nonspecific adsorption, and support the construction

of complex nanostructures for use in electronics, photonics, and nanomedicine [47]. AuNPs, as a substrate for SAM, are highly favored due to their easy synthesis, a large surface area, and a high surface-to-volume ratio. Their strong optical absorbance, excellent thermal and mechanical stability, and superior electrical conductivity further expand their application in biosensing, bioelectronics, and redox-based processes. These combined properties make SAM-functionalized AuNPs a cornerstone of modern nanotechnology and biotechnological innovation.

SAM on AuNPs can be formed by using several methods, each offering unique advantages and limitations depending on the intended application. The solution-based process is the most used approach, where AuNPs are incubated in a solution containing thiol molecules such as 11-*Mercaptoundecanoic Acid* (MUA) or 6-*Mercaptohexanol* (MCH) [48]. The thiols spontaneously chemisorb onto the gold surface, thus creating a uniform and stable monolayer. This method is straightforward and efficient, which makes it suitable for high-throughput functionalization. However, it may result in variability in the monolayer packing density depending on the incubation conditions and thiol concentration.

Microcontact printing [49] is another technique used to create patterned SAM. A stamp coated with thiol compounds is applied to the AuNP surface to transfer the SAM in a specific pattern. This method is particularly advantageous for microarray fabrication and surface patterning in biosensing applications. However, precise control of the stamping process is required, and the scalability for large-area patterning can be challenging.

Vapor deposition [50] involves vaporizing thiol compounds, condensing onto the gold surface to form a monolayer. This technique is highly effective for achieving a uniform monolayer thickness and precise control over the surface coverage, making it suitable for optoelectronic applications. However, vapor deposition requires specialized equipment and can be less effective for functionalizing colloidal AuNPs in suspension.

Electrochemical deposition [51] enhances SAM formation by applying an electric field, which promotes the adsorption of thiol molecules onto the gold surface. This method allows for fine control over the density and orientation of the SAM and is commonly used in the development of electrochemical biosensors. Despite its precision, this approach can be limited by the complexity of the setup and the potential for electrode surface fouling during the process.

1.2.2. SAM for DNA-modifying enzymes

Historically, the first enzyme adsorption method was developed by Nelson and Griffin [52] in 1916, marking a pivotal milestone in enzyme immobilization. Their work introduced charcoal as a carrier material for immobilizing enzymes, which provided a simple yet effective method to stabilize enzymes outside their natural biological context. While their study primarily sought to demonstrate the feasibility of enzyme immobilization, it laid the foundation for the subsequent research into immobilizing a wide range of enzymes, including proteases, amylases, lipases, and oxidoreductases. The study conducted in 1916, however, focused more on establishing the concept of enzyme immobilization rather than on targeting a specific enzyme for practical applications. This early approach involved physically adsorbing enzymes onto the surface of charcoal particles via non-covalent interactions, such as hydrogen bonding and Van der Waals forces, thus marking the beginning of a broader exploration into the potential of immobilized enzymes in biotechnological processes. Charcoal, by virtue of being a widely available and cost-effective material, also demonstrated its potential of natural, inexpensive support for enzyme immobilization. Although Nelson and Griffin's method was relatively rudimentary compared to the modern techniques, it laid the foundation for subsequent developments in

enzyme immobilization. Their work inspired further exploration into other materials and immobilization techniques, paving the way for more sophisticated methods, such as covalent attachment, cross-linking, and the use of nanomaterials [53].

In subsequent decades, enzyme immobilization evolved, with researchers discovering that various carriers from inorganic supports (such as silica and glass) [54] to organic materials (such as cellulose and synthetic polymers) could be used to immobilize enzymes effectively [55]. Moreover, the realization that enzyme activity could be enhanced or stabilized through specific chemical modifications to the carrier surfaces further refined immobilization methods, leading to more efficient and versatile biosensors and biocatalysts. Today, enzyme immobilization is a well-established field with a range of carrier materials and techniques tailored to meet the specific needs of various applications [56–60]. Immobilizing DNA-modifying enzymes is essential for advancing DNA sensors and other bio-based devices. It enables their use for targeting detection or reusing these often-expensive enzymes across multiple analytical cycles. This innovation was groundbreaking at the time because it offered a method to reuse enzymes in a repetitive cycle of catalytic reactions, eliminating the need to constantly replenish the enzymes. This reduced the cost of enzyme-based responses, thus opening the door to various industrial and analytical applications.

To design effective DNA biosensors, it is crucial to understand the structural characteristics (polypeptide chains) and functional mechanisms of DNA-modifying enzymes, along with the various methodologies currently employed for their immobilization. Several techniques are available for immobilizing enzymes onto carriers, including chemical adsorption, physical adsorption, cross-linking, and covalent attachment. The enzyme-carrier interaction relies on both physical and chemical forces, facilitating the binding of DNA-modifying enzymes to the carrier. Physical adsorption typically occurs through hydrogen bonds or Van der Waals interactions [61], but this method is prone to enzyme leaching. On the other hand, covalent attachment, mainly through cross-linking, offers a more stable solution. These immobilization methods do not require expensive equipment and can be easily implemented under standard laboratory conditions.

Table 2. Residue functions in DNA-modifying enzyme structure

Residue	Common Enzyme Type	Functional Properties
Aspartate (Asp, D)	DNA polymerases, Nucleases	- Negatively charged at physiological pH; - Coordinates Mg^{2+} or Mn^{2+} ions in catalytic sites; - Facilitates nucleotide incorporation and cleavage.
Glutamate (Glu, E)	DNA polymerases, Topoisomerases	- Similar to aspartate, involved in metal ion coordination; - Participates in acid-base catalysis.
Lysine (Lys, K)	DNA ligases, Methyltransferases	- Positively charged, interacts with the negatively charged DNA backbone; - Stabilizes transition states during reactions.

Arginine (Arg, R)	DNA-binding proteins, Helicases	- Highly positive charge, enhances DNA binding affinity; - Forms hydrogen bonds with phosphate groups.
Tyrosine (Tyr, Y)	Topoisomerases, DNA endonucleases	- Participates in covalent intermediates (e.g., DNA cleavage-ligation cycle in topoisomerases); - Provides nucleophilic attack during strand cleavage.
Histidine (His, H)	Nucleases, DNA repair enzymes	- Functions as a proton donor/acceptor in acid-base catalysis; - Helps in cleaving phosphodiester bonds.
Cysteine (Cys, C)	Methyltransferases, Redox enzymes	- Forms disulfide bonds for structural stability; - Participates in S-adenosylmethionine (SAM)-dependent methylation.

DNA-modifying enzymes naturally interact with various functional groups (*Table 2*) present on active carriers due to the diversity of amino acid side chains: carboxyl (e.g., Asp – aspartic acid), hydroxyl (e.g., Ser – serine), amino (e.g., Lys – lysine, Arg – arginine), and, occasionally, sulfide (e.g., Cys – cysteine) groups. Notably, Arg and Lys residues, which are positively charged at physiological pH, can enhance enzyme-carrier binding, especially in the presence of serum [62]. DNA-modifying enzymes readily participate in alkylation, disulfide bond formation, and other covalent interactions, making them amenable to immobilization. However, a significant challenge arises from the structural constraints of the enzyme's active site. The active site, often formed by residues in the enzyme's tertiary or quaternary structure, includes hydroxyl and phosphoryl groups, which are essential for substrate conversion. Therefore, immobilization strategies must be designed to avoid interference with or modification of the active site, as improper immobilization can lead to a loss of enzymatic activity. In addition to incorrect enzyme orientation, factors such as the presence of inhibitors, carrier incompatibility, nonspecific binding, temperature, pH, ion concentration, and the distance between reactive groups significantly influence the enzyme's functional stability after immobilization [63–65]. To mitigate nonspecific binding and optimize immobilization, the enzyme's active site can be masked by using non-enzymatic proteins, such as antibodies or DNA fragments [66,67]. Furthermore, various strategies have been developed to enhance the enzyme stability and minimize leaching, including the formation of cross-linked enzyme aggregates, increasing the carrier-to-volume ratio, and optimizing the carrier porosity.

In contemporary research, there has been a shift toward the use of novel materials, such as carbonaceous nanomaterials (e.g., graphene, carbon nanotubes) [68], metallic nanomaterials (e.g., silver, gold, metal oxides, and hydroxides) [42,69], and organic carriers (e.g., silica and cellulose) [55]. The selection of an appropriate carrier depends on several critical factors, including the physical strength, stability, cost-effectiveness, environmental compatibility, and compatibility with the enzyme. By advancing enzyme immobilization methods, researchers continue to improve the performance, stability, and efficiency of DNA-modifying enzymes in biosensor applications, providing essential tools for a wide range of bioanalytical and diagnostic technologies [70].

Gold nanoparticles are among the most popular types of nanomaterials due to their easy synthesis [71–75]. They possess a large surface area for immobilization, a high

surface-to-volume ratio, and a high extinction coefficient. Additionally, AuNPs exhibit strong optical absorbance, good thermal and mechanical stability, and notable electrical properties. They also demonstrate sufficient biocompatibility and are applicable in redox processes.

The immobilization of biomolecules on the surface of AuNPs can be performed in many ways and is easily controlled. Due to these advantages, AuNPs can be readily modified with different biomolecules, making them suitable for various bioanalytical and other applications. Colloidal AuNPs, which can be prepared quickly, have been widely used to immobilize DNA-modifying enzymes [76]. Covalent bonding between carboxyl or amino groups pre-immobilized on the gold-based carrier and protein side chain amino or carboxyl groups is commonly used to design biosensing systems. The covalent binding force between the enzyme and the carrier is powerful, and no leakage is possible even at high ionic strengths. Various creative methods have been developed for the carrier production of AuNPs, including one-step and multi-step procedures. There are two AuNP preparation techniques: chemical reaction using Au^{3+} as a precursor and/or other gold forms as substrates [77–80]. It is of importance to note that the formation and activation of carboxylic groups are required in all cases. For example, DNA-modifying enzymes are rich in lysine residues and, therefore, can form stable amide bonds when interacting with active esters, such as one of the most used *N-hydroxysuccinimide* (NHS) esters. The same amino groups can easily interact with aldehyde groups that can be attached to or formed on the surface used for immobilization. DNA-modifying enzymes are rich in aspartate and glutamate, which can form stable carboxyl bonds with *1-Ethyl-3-(3-dimethylamoniminopropyl) carbodiimide* (EDC). However, activation of aqueous solutions is complicated due to ester and imide hydrolysis, as the reagents must be stored at -20 °C. The publications [81–84] and best practices have illustrated that DNA-modifying enzymes are rich in various groups suitable for immobilization. Still, the most suitable covalent immobilization method could be the activation of the carboxyl group on the carrier when using a mixed solution of EDC and NHS (*Figure 3*).

Due to their unique physicochemical properties, SAM on AuNPs has emerged as a versatile platform for immobilizing biomolecules, particularly DNA-modifying enzymes. Gold nanoparticles are among the most widely used nanomaterials owing to their ease of synthesis, a large surface area for immobilization, a high surface-to-volume ratio, and an exceptional optical, thermal, and mechanical stability. They also exhibit a high extinction coefficient, excellent electrical conductivity, and sufficient biocompatibility, making them highly suitable for redox processes and bioanalytical applications [85].

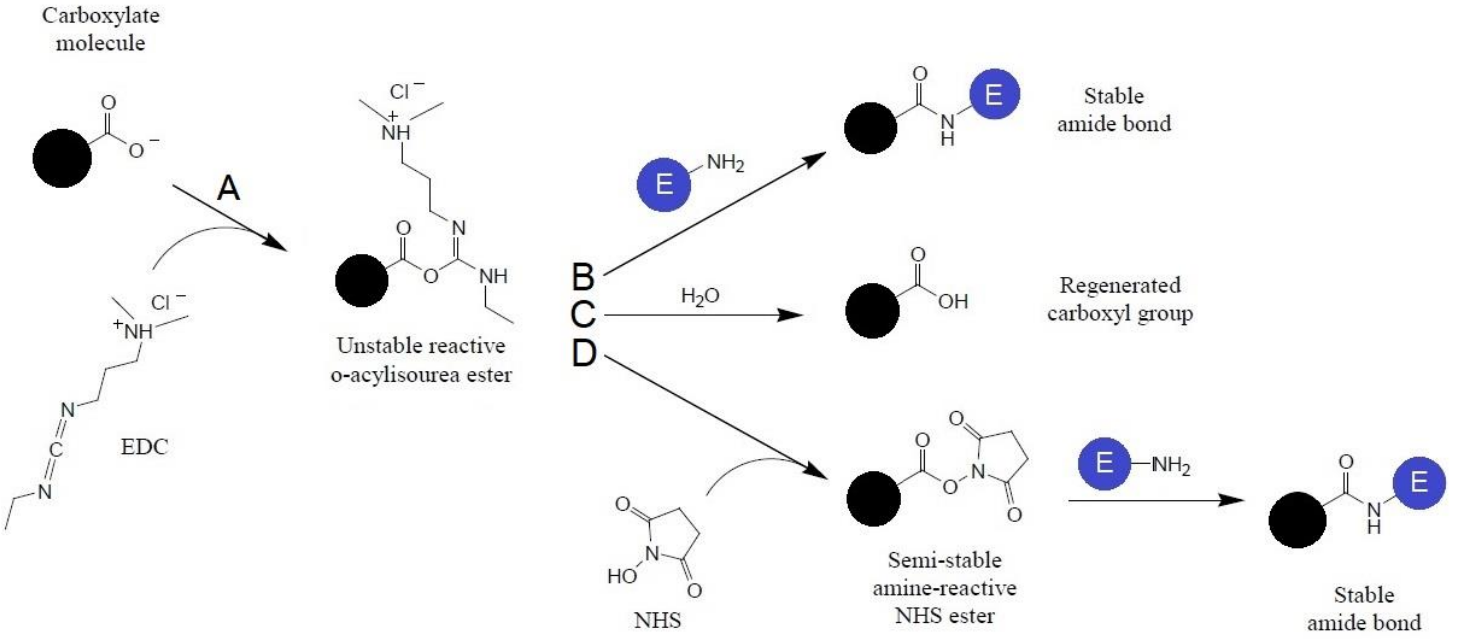


Figure 3. Sulfo-NHS and EDC (carbodiimide) crosslinking reaction scheme represents the EDC (1-ethyl-3-(3-dimethylaminopropyl) carbodiimide) coupling chemistry used for covalent attachment of molecules via carboxyl and amine groups. **A** – This is the activation step of the Carboxyl Group with EDC. EDC reacts with the molecule's carboxylate ($-COO^-$) group to form an unstable o-acylisourea ester. This intermediate is highly reactive and can respond with an amine group or hydrolyze back to the carboxylate form. **B** – This is the amide bond formation via the direct coupling step. If a primary amine ($-NH_2$) is present, it directly attacks the reactive o-acylisourea intermediate. This creates a stable amide bond, linking the two molecules covalently. The by-product, urea, is released in this reaction. **C** – Hydrolysis (Side Reaction) step. Instead of reacting with an amine, the unstable o-acylisourea ester may undergo hydrolysis, regenerating the original carboxyl group. This is an unwanted side reaction that reduces the coupling efficiency. **D** – NHS (N-Hydroxysuccinimide) Stabilization step. To increase the reaction efficiency, NHS (or Sulfo-NHS) is added. NHS reacts with the o-acylisourea intermediate to form a semi-stable NHS ester, which is more reactive and has a longer lifetime. This ester efficiently reacts with amines, leading to amide bond formation (similar to B), but with higher efficiency

The immobilization of biomolecules on AuNPs can be achieved through various approaches, including covalent bonding and physical adsorption, offering precise control over surface functionalization. This versatility makes AuNPs ideal for designing biosensing systems, as they can be readily modified with biomolecules tailored to specific applications. Colloidal AuNPs are frequently used for immobilizing DNA-modifying enzymes due to their ease of preparation and functionalization. Covalent attachment, such as the formation of amide bonds between carboxyl or amino groups on the AuNP surface and the corresponding groups on enzymes, ensures strong binding and prevents enzyme leaching, even under harsh conditions like high ionic strength. For enzyme immobilization, activating carboxyl groups on the carrier surface is crucial.

SAM, especially those used for modifying AuNPs, are based on an aqueous solution of *11-Mercaptoundecanoic acid* (MUA), which has a long alkane chain and carboxyl-containing thiols [86]. When MUA-modified small AuNPs (1.5–3.5 nm diameter) are used, they retain good fluorescence and redox-mediating properties. *6-Mercapto-1-hexanol* (MCH) is a tool used to block the active sites that remain after the immobilization of biomolecules. In this way, they prevent nonspecific absorption.

Despite these advantages, SAM-based immobilization methods are not without challenges. Hydrolysis of esters and imides during activation can complicate immobilization protocols, and the long-term stability of enzymes may be affected under certain environmental conditions. Additionally, optimization of the carrier surface chemistry to minimize nonspecific interactions remains a critical area of research. Nevertheless, the advantages of AuNP-based SAM – such as the ease of synthesis, strong enzyme binding, and compatibility with various biomolecules – make them indispensable in modern bioanalytical and biotechnological applications.

1.2.3. Limitation of SAM-based analytical systems

While SAM is a powerful tool in analytical systems, several limitations impact its performance and applicability. One of the primary challenges is the stability of SAM under varying environmental conditions. Factors such as temperature fluctuations, pH changes, and competing molecules can destabilize the monolayer, leading to desorption or degradation of the functionalized surface [87]. Another limitation is the susceptibility of SAM to nonspecific adsorption, which can interfere with the selectivity and sensitivity of the analytical system. Despite efforts to block nonspecific binding sites with compounds like *6-mercaptohexanol* (MCH), complete prevention of background interactions remains challenging, particularly in complex biological samples. The quality and uniformity of SAM formation are also critical issues. Variations in monolayer packing density and defects in the SAM can result in inconsistent analytical performance. These defects may arise during assembly due to impurities, suboptimal reaction conditions, or uneven distribution of thiol molecules.

The long-term stability and robustness of SAM pose additional concerns. Thiol-gold bonds, while strong, are not entirely immune to oxidative or photochemical degradation, especially during prolonged exposure to light or oxygen. This can limit the shelf life and reliability of SAM-based systems in practical applications. Finally, the functionalization of SAM with biomolecules often involves multistep chemical processes, which can be labor-intensive and require stringent control to achieve reproducibility. The compatibility of SAM with specific biomolecules, particularly those sensitive to the chemical environment used for assembly, can further limit its applicability. Addressing these limitations requires careful optimization of the SAM preparation protocols, surface-blocking strategies, and experimental conditions. Additionally, advancements in the SAM design, such as using mixed long- and short-chain monolayers or incorporating more robust linker molecules,

hold promise for overcoming these challenges and enhancing the performance of SAM-based analytical systems [88–90].

In conclusion, our study employed a solution-based method for SAM formation using a thiol mixture due to its simplicity, prominent efficiency, and suitability for enzyme immobilization on gold surfaces. Combining shorter, hydroxyl-terminated thiols minimizes steric hindrance and enhances enzyme accessibility, while longer carboxyl-terminated (-COOH) thiols facilitate covalent attachment via EDC/NHS coupling or electrostatic interactions. This balanced composition prevents enzyme overcrowding while maintaining a sufficiently high density for efficient immobilization. Optimizing the hydrophilic–hydrophobic balance improves enzyme orientation and reduces nonspecific adsorption, ensuring robust and reproducible functionalization. The method enables the formation of well-ordered SAMs with tunable surface properties while requiring minimal specialized equipment. Furthermore, it allows the functionalization of large batches of AuNPs under controlled conditions, providing flexibility in adjusting surface coverage and packing density by optimizing incubation parameters. These advantages establish the solution-based method as a practical and effective approach for achieving the desired functionality in biosensing applications.

Self-Assembled Monolayers (SAMs) are well-documented in the literature for their versatility in biosensor surface engineering. The chemical functionality, molecular packing, and ratio of terminal groups in SAMs influence the efficiency and specificity of biomolecule immobilization. Research consistently shows that fine-tuning SAM composition is critical to balancing accessibility with stability. In this study, SAM preparation and functionalization were guided by these principles, with particular attention to optimizing conditions for enzyme and protein binding. Literature-informed adjustments to surface chemistry ensured compatibility with the biomolecules used, enhancing both immobilization outcomes and biosensor responsiveness.

1.2.4. Quartz Crystal Microbalance (QCM)

QCM is a highly sensitive technique used to measure mass changes at the surface of a quartz crystal in real time [91]. It operates based on the piezoelectric properties of quartz, where the application of alternating current causes the crystal to oscillate at its natural resonant frequency. When a material, such as a thin film or a biomolecule, is adsorbed onto the crystal surface, the added mass induces a measurable decrease in the resonant frequency. This makes QCM an invaluable tool for studying adsorption, thin-film deposition, molecular binding, and surface interactions. The sensitivity of QCM arises from the linear relationship between the frequency shift and the mass change, described by the Sauerbrey equation, which relates the change in frequency (Δf) to the change in mass per unit area (Δm) of the crystal's surface:

$$\Delta f = -\frac{2f_0^2}{A\sqrt{\rho_q \mu_q}}\Delta m \qquad (1)$$

where: Δf – frequency shift (Hz); f_0 – fundamental resonant frequency of the quartz crystal (Hz); Δm – mass change per unit area (g/cm²); A – active area of the electrode-coated surface of the quartz crystal (cm^2); ρ_q – density of quartz (2.648 g/cm^3); μ_q – shear modulus of quartz (2.947×10^{11} g/cm^2).

This equation is valid for rigid, thin, and uniform layers, where the added mass does not affect the viscoelastic properties of the system. The negative sign indicates that an increase in mass reduces the resonant frequency. This equation calculates the mass change per unit area based on the observed frequency shift. The QCM sensor, typically a gold-coated quartz crystal, is often functionalized with self-assembled monolayers or other chemical coatings to enable specific molecular interactions. This surface preparation enhances the sensor's selectivity for target analytes. In liquid environments or when studying viscoelastic layers, the interpretation of QCM data becomes more complex. Frequency changes are accompanied by shifts (Δf) in energy dissipation (ΔD), reflecting the mechanical properties of the adsorbed layer. This provides additional insights into the layer's softness, rigidity, or hydration state. These viscoelastic properties are analyzed by using advanced models to distinguish between mass changes and mechanical effects. QCM measures at the nanoscale, with a detection range of approximately 1 Å to 1 µm, depending on the properties of the analyzed layer. Typical study subjects include biomolecules, surfactants, polymers, nanoparticles, cells, and other structures within the exact size range detailed in *Figure 4*.

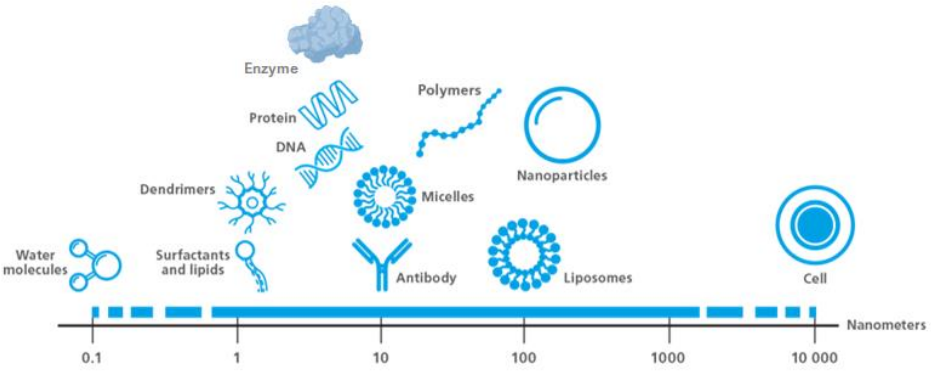


Figure 4. The appropriate molecular size range of objects and film thicknesses for Quartz Crystal Microbalance measurements

This study used Quartz Crystal Microbalance with Resistance monitoring (*QCM-R*, Maxtek Inc., Switzerland) to monitor biomolecular adsorption on functionalized gold surfaces. The primary signal the system measures is the resonance frequency shift (Δf), which correlates with changes in the surface mass according to the Sauerbrey equation under rigid, thin film assumptions. In addition to frequency, the instrument measures changes in the crystal's equivalent series resistance (R). While R is not identical to dissipation (D), as measured in other QCM-D systems (e.g., *QSense*), it reflects similar physical properties, such as energy loss per oscillation cycle and the viscoelastic behavior of the adsorbed layer. An increase in R typically indicates a softer or more hydrated layer, whereas lower resistance is characteristic of more rigid, compact films.

Due to its high sensitivity and real-time monitoring capabilities, QCM has become a powerful tool in scientific research, particularly for studying proteins and enzymes. Researchers have widely employed QCM to explore various aspects of protein and enzyme interactions, including adsorption kinetics, conformational changes, and activity assays. For example, QCM is frequently used to measure how proteins adsorb onto different surfaces in protein adsorption studies. This is crucial for understanding biocompatibility and the initial stages of cellular responses to biomaterials. These studies [92,93] provide

valuable insights into designing materials that either promote or resist protein adsorption, helping to improve biomaterial design for enhanced implant acceptance. In enzyme research, QCM has been utilized to monitor enzymatic hydrolysis processes, including the study of cellulase enzyme adsorption and activity on cellulose substrates. By observing changes in frequency and dissipation, studies can assess the binding dynamics and quantify the rate and extent of cellulose degradation, thereby providing critical insights into biofuel production processes. Additionally, QCM is crucial in peptide- and protein-based drug development and biosensing for monitoring molecular interactions, such as antigen-antibody binding, DNA hybridization, and protein adsorption. It also studies enzymatic activity, drug delivery systems, and cell adhesion, where its high sensitivity allows for the precise evaluation of protein and peptide interactions with various surfaces. This helps optimize the formulation and packaging design, while ensuring the stability and efficacy of biopharmaceuticals. The technique's ability to provide real-time, label-free measurements makes it an essential tool in biophysics, surface chemistry, and biomedical research. Integration of QCM with other analytical methods, such as electrochemical or optical techniques, further enhances its versatility, allowing for a deeper understanding of the surface phenomena and molecular interactions. Several factors need careful consideration when using QCM to study proteins and enzymes to ensure accurate results. Surface functionalization is crucial for promoting specific interactions between the QCM sensor and the target protein or enzyme, enhancing selectivity and sensitivity. Environmental conditions, such as pH, temperature, and ionic strength, must be precisely controlled as these factors can significantly influence protein conformation and activity, thus impacting the reliability of QCM measurements. Additionally, proteins and enzymes often form viscoelastic layers upon adsorption, which means that the frequency and energy dissipation data must be analyzed to distinguish between mass changes and alterations in mechanical properties. Finally, advanced modeling techniques may be necessary to interpret QCM data, mainly when working with complex biological samples or evaluating conformational changes and binding kinetics.

Literature supports its effectiveness in detecting changes in surface-bound mass with high sensitivity, making it suitable for studying enzyme immobilization, protein adsorption, and molecular recognition events. In this work, QCM was employed to monitor each phase of sensor development, from surface functionalization to biomolecule interactions. As recommended in recent studies, kinetic modeling helped interpret the dynamic behavior of biomolecules on surfaces. This methodological approach was informed by prior research into adsorption kinetics and surface interaction mechanisms, which provided a solid foundation for analyzing and validating sensor performance.

1.2.5. Fourier Transform Infrared Spectroscopy (FTIR)

FTIR is a widely used analytical technique which identifies chemical functional groups by measuring the absorption of *infrared* (IR) radiation. Molecules absorb infrared light at specific wavelengths corresponding to their vibrational modes, resulting in characteristic absorption peaks in the infrared spectrum. When IR radiation interacts with a molecule, it can induce various vibrational modes, such as:

- Stretching vibrations – bond length changes (e.g., C=O, C-H, O-H); or
- Bending vibrations – bond angles change (e.g., scissoring, rocking, twisting).

For a vibration to be IR-active, it must result in a change in the molecular dipole moment. The frequency of absorption depends on the bond strength and atomic masses, following Hooke's Law:

$$\nu = \frac{1}{2\pi c}\sqrt{\frac{k}{\mu}} \qquad (2)$$

where: ν – the vibrational frequency (cm^{-1}); c – the speed of light (cm/s); k – the bond force constant (N/m); μ – the reduced mass $\mu = \frac{m_1 m_2}{m_1 + m_2}$, where m_1 m_2 are atomic masses.

Instead of scanning individual wavelengths, FTIR uses an interferometer to simultaneously collect all wavelengths and convert the time-domain signal into a frequency-domain spectrum via the Fourier Transform. FTIR confirms the successful immobilization of biomolecules (e.g., T7 DNA polymerase) on modified surfaces. The key spectral features include:

- Carboxyl (-COOH) stretching (~1700 cm^{-1}) – indicates surface functionalization;
- Hydroxyl (-OH) stretching (~3300 cm^{-1}) – represents the hydration state and hydrogen bonding;
- Amide I and Amide II bands (~1650 cm^{-1}, ~1550 cm^{-1}) – confirm protein secondary structure and attachment stability.

Comparing FTIR spectra across different COOH:OH ratios in SAM is key to optimizing enzyme retention, stability, and activity. When combined with QCM, FTIR offers a powerful approach to correlate mass adsorption (QCM) with chemical modifications (FTIR), providing detailed insights into the enzyme-surface binding efficiency, structural changes during enzyme immobilization, and long-term stability under experimental conditions. FTIR spectroscopy is essential for characterizing biomolecule immobilization, SAM formation, and enzyme-surface interactions. By analyzing specific vibrational bands and applying quantitative models, FTIR enables the optimization of functionalized surfaces for an enhanced biosensor performance, an improved enzyme stability, and catalytic activity. FTIR is a powerful analytical technique for studying proteins and enzymes, by virtue of providing valuable insights into their structure, function, and interactions. FTIR allows us to analyze the chemical composition and conformational changes of biomolecules by measuring the absorption of infrared light by molecular bonds. In our research, FTIR has been crucial in examining the secondary structure of proteins, mainly through the Amide I band (1600–1700 cm^{-1}), which helps determine the content of α-helices, β-sheets, and random coils, while offering important information about protein folding, stability, and function. Several aspects were carefully considered when utilizing FTIR for protein and enzyme analyses. Sample preparation has been a crucial factor in ensuring high-quality spectra, particularly with the use of proper buffers and optimal concentrations. To address the strong absorption of water in the infrared region, the samples were dehydrated, and deuterated solvents were used as needed. Interpretation of FTIR spectra can be complex, and therefore advanced data processing techniques, such as curve fitting and multivariate analysis, were applied to extract meaningful insights. Moreover, the controlled environmental conditions, including pH, temperature, and ionic strength, have been maintained to ensure reproducibility and accuracy in our measurements. By addressing these aspects, FTIR has provided valuable insights into the structural and functional characteristics of proteins and enzymes, thereby advancing our understanding of biophysics, biochemistry, and biomedical applications.

FTIR spectroscopy is widely used to characterize the immobilization of biomolecules on functionalized surfaces. Literature sources emphasize its ability to confirm protein

attachment and retention of the secondary structure by analyzing vibrational modes. The technique is particularly valued for its non-destructive nature and capacity to provide structural information without labeling. In this research, FTIR was applied to assess surface-bound biomolecules, and methodological decisions were shaped by reported best practices, such as careful background correction, appropriate sample preparation, and minimizing the interference from hydration layers. These considerations ensured reliable spectral interpretation and structural verification of immobilized proteins.

2. EXPERIMENTAL SECTION

This chapter presents experimental work aimed at achieving the research objectives outlined in the introduction. The focus was on developing biosensors by immobilizing T7 DNA polymerase and protein biomarkers on gold-coated surfaces functionalized with various SAM mix compositions. The experimental design was informed by a comprehensive literature review, with specific attention paid to enzyme orientation, surface chemistry, and molecular interaction dynamics. A combination of surface-sensitive and structural techniques was employed to assess the biomolecular activity and immobilization efficiency accurately. QCM was used for real-time monitoring of surface interactions, while FTIR confirmed chemical modifications and structural retention of proteins. Each stage of biosensor development – ranging from surface functionalization to molecular interaction studies – was designed to systematically investigate the functionality and stability of the immobilized components.

2.1. Materials and Equipment

12-mercaptododecanoic acid [$HS(CH_2)_{11}COOH$ (12-MUA, CAS# 82001-53-4, purity 96%), 6-mercapto-1-hexanol [$HS(CH_2)_6OH$] (6-MCH, CAS# 1633-78-9, purity 97%), N-hydroxysuccinimide (NHS, CAS# 6066-82-6, purity 98%), N-(3-Dimethylaminopropyl)-N′-ethylcarbodiimide hydrochloride (EDC, CAS# 25952-53-8, purity 98%), and ethanol (99.5%) were purchased from *Sigma-Aldrich* (Steinheim, Germany). Agarose (R0491), TAE Buffer (Tris-acetate-EDTA) (50X) (B49), 10X Phosphate buffered saline (PBS) (pH 7.4) (AM9625), nuclease-free water (AM9906), Low DNA Mass Ladder (10068013), T7 DNA Polymerase (10 U/µL, EP0081) and 10X Reaction buffer for T7 DNA polymerase, Human BAFF (BLyS) Recombinant Protein, BAFF, 310-13-50UG and GeneJET Gel Extraction Kit (K0691) were purchased from *Thermo Scientific*. Ethidium bromide solution 1% (2218.1) was obtained from *Carl Roth*, Germany. H_2SO_4 (>96.0%, CAS# 7664-93-9) was purchased from *Lachner* (Neratovice, Czech Republic). Desalted unmodified and 3'-Thiol-Modifier C6 S-S DNA oligonucleotides and DL-dithiothreitol (DTT, CAS# 3483-12-3) were obtained from *Sigma-Aldrich* and used without further purification. Recombinant human $VEGF_{165}$ protein, expressed in HEK293 cells, was purchased from *Sigma-Aldrich*, Steinheim, Germany. All reagents were analytical grade and were used without additional purification. All aqueous solutions were prepared in deionized water. One-side QSense® (QSX 301 Gold, gold electrode ~50 nm thick) was purchased from *Biolin Scientific*. All experiments were performed by using the E-QCM system (RQCM, *Maxtek, Inc*., Switzerland), the Spectramax spectrophotometer, and the Nanodrop spectrophotometer (*Analytik Jena*, Germany), which were utilized for DNA detection in agarose gels.

2.2. T7 DNA Polymerase Studies

2.2.1. Free T7 DNA polymerase studies

The behavior of free (i.e., non-immobilized) T7 DNA polymerase was examined in solution to establish a reliable baseline for enzymatic activity. These preliminary studies aimed to characterize the enzyme's natural 3'→5' exonuclease activity and evaluate its interaction with different DNA fragments under controlled conditions. Understanding the enzyme's behavior in its native form is critical for assessing the effects of the subsequent immobilization steps and ensuring that any observed changes in performance are due to

surface interactions rather than intrinsic enzyme variability. The findings from this section served as a reference for comparison in later stages involving immobilized enzyme systems.

2.2.1.1. DNA fragments extraction from agarose gel protocol

DNA was extracted from a Low DNA Mass Ladder by using agarose gel electrophoresis to prepare specific-length DNA fragments for exonuclease activity testing. The separation was performed on a 2% TAE agarose gel, and the bands corresponding to target fragment lengths (100–2000 bp) were visualized under UV illumination. The selected DNA bands were carefully excised and purified by using a *GeneJET Gel Extraction Kit*, while following the manufacturer's protocol. The absorbance of each fragment (100 bp, 200 bp, 400 bp, 800 bp, 1200 bp, and 2000 bp) was measured by using a Nanodrop spectrophotometer at 260 nm, allowing for concentration determination and calculation of the A260/A280 ratio for assessing purity. The fragments were prepared with a final concentration of 0.25 mg/mL for each 100 bp, 200 bp, 400 bp, 800 bp, 1200 bp, and 2000 bp. This step was crucial for obtaining clean DNA substrates of a defined length, thereby ensuring reproducibility in enzymatic degradation assays.

2.2.1.2. Free T7 DNA polymerase 3'→5' exonuclease activity study

The exonuclease activity of free (non-immobilized) T7 DNA polymerase was investigated to establish a reference baseline for its exonuclease activity performance in solution. This step was critical for distinguishing intrinsic enzymatic behavior from any effects introduced by surface immobilization in later experiments. The primary objective was to assess the enzyme's natural 3′→5′ (*Figure 5*) exonuclease activity toward double-stranded DNA fragments of various lengths, concentrations, and reaction times.

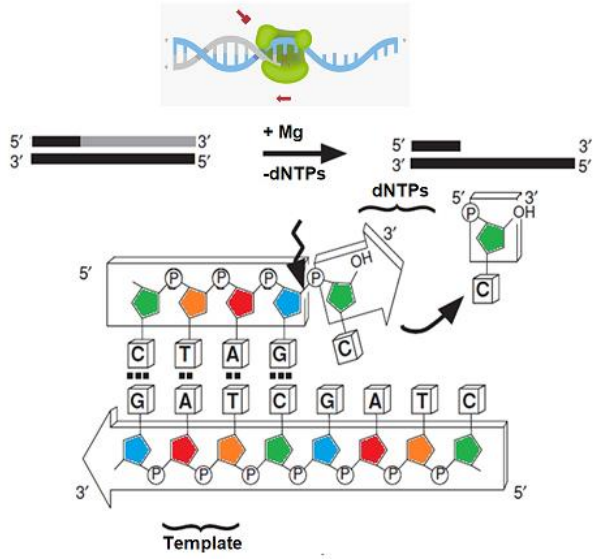


Figure 5. Schematic representation of exonuclease activity. The exonuclease activity of T7 DNA polymerase is used to remove a mismatched or terminal nucleotide from the DNA strand. The enzyme removes nucleotides one by one from the 3' end of the DNA strand, moving in the 3'-to-5' direction

Gain-purifying specific bands from a DNA ladder obtained double-stranded DNA fragments ranging from 100 to 2000 base pairs. DNA concentrations were adjusted to 25 ng and 12.5 ng per reaction. At the same time, T7 DNA polymerase was used at a final concentration of 10 U per reaction. These concentrations were selected to simulate conditions comparable to those applied during immobilized enzyme assays, thus ensuring compatibility and comparability between the formats involved. The reactions were carried out in a 96-well microplate format under the standard for T7 DNA polymerase buffer conditions (400 mM Tris-HCl (pH 7.5 at 25 °C), 100 mM $MgCl_2$, 10 mM DTT), supplemented with Mg^{2+} as a cofactor essential in nucleophilic attack for exonuclease activity. During exonucleolytic degradation, the 3′ terminal nucleotide of DNA is aligned into the exonuclease active site of the enzyme. Two coordinated Mg^{2+} ions play essential roles in catalyzing the hydrolysis reaction. The first metal ion activates a water molecule, converting it into a nucleophile. In contrast, the second metal ion stabilizes the negative charge that develops on the leaving phosphate group during the cleavage process. The nucleophilic water then attacks the phosphodiester bond at the 3′ end of the DNA, leading to hydrolysis of the terminal nucleotide and the release of a deoxynucleoside monophosphate (dNMP). Following the cleavage, the product is released, and the enzyme advances to the next nucleotide if degradation continues.

The enzyme and DNA substrates were incubated at room temperature (22–25 °C) for defined time intervals ranging from 1 hour to overnight, allowing for time-resolved kinetic analysis of DNA degradation.

DNA hydrolysis was monitored by measuring the absorbance at 260 nm, which is due to the aromatic rings in the nucleotides, while using a microplate reader. Residual DNA concentration at each time point was calculated to quantify the rate and extent of degradation. These experiments were conducted under temperature and timing conditions that mirrored those used in the immobilized enzyme studies, thus ensuring that any future comparison would reflect the influence of surface immobilization rather than differences in the reaction setup. This investigation provided essential insights into the 3′→5′ exonuclease efficiency of T7 DNA polymerase in its native state, verifying its suitability for biosensor applications where surface confinement may influence enzyme-substrate interactions.

2.2.2. T7 DNA polymerase-based sensor study

A series of experiments using gold-coated *QSense*® sensors was conducted to investigate the behavior of T7 DNA polymerase upon surface attachment. This section outlines the protocols developed for preparing biosensor surfaces by forming SAM mixtures modified with carboxyl- and hydroxyl-terminated alkanethiols, which protect the enzyme's active site, immobilize the enzyme, and assess its exonuclease activity and stability after immobilization. Immobilizing masked T7 DNA polymerase is a crucial step in developing enzyme-based biosensors. These protocols are designed to retain enzymatic functionality while enabling surface confinement that is suitable for repeated use and kinetic monitoring.

2.2.2.1. Cleaning protocol for gold QSense®

Before SAM formation, gold-coated *QSense*® electrodes were cleaned while using a standardized electrochemical procedure to ensure reproducibility and remove any surface contaminants. The electrode cleaning procedure involves *Cyclic Voltammetry* (CV) scans in 0.1 M H_2SO_4 within a potential window of -0.25 V to 1.25 V (vs. Ag/AgCl reference electrode), which facilitates the oxidation and reduction of the gold surface. During the anodic sweep, gold oxidation occurs, effectively removing organic residues, while the

cathodic sweep facilitates gold oxide reduction, due to eliminating inorganic contaminants and restoring a clean metallic surface. This controlled electrochemical activation enhances surface smoothness and reactivity, promoting the formation of stable and well-ordered SAM structures through strong Au–S bonding. Electrochemical cleaning and surface preparation were performed by using a *Gamry Reference 600* potentiostat/galvanostat, ensuring precise control over potential cycling and reproducibility across experiments. Typically, three successive CV cycles are performed, with distinct oxidation and reduction peaks confirming the removal of impurities and the successful regeneration of the surface. This standardized electrochemical cleaning protocol is crucial for achieving consistent surface chemistry, optimizing biomolecule immobilization efficiency, and enhancing the reliability of biosensing applications.

2.2.2.2. SAM formation study

Functionalized surfaces were created by forming a mixed SAM using thiol-modified alkanes: 12-mercaptododecanoic acid (12-MUA, -COOH terminated) and 6-mercapto-1-hexanol (6-MCH, -OH terminated). SAM mixtures with varying molar ratios (from 1:9 to 9:1 MUA: MCH) were prepared in ethanol (*Figure 6*). Gold-coated *QSense*® sensors were immersed in the 1 mM thiol mix solutions (0.1 mM 12-MUA and 0.9 mM 6-MCH (1:9 ratio), 0.2 mM 12-MUA and 0.8 mM 6-MCH (2:8 ratio), etc.) and incubated overnight at room temperature in the dark to allow the spontaneous formation of the SAM layer via gold-thiol bonding (Au/12-MUA+6-MCH). The concentration ratios varied across the solutions, enabling the systematic study of how the molar ratio of 12-MUA to 6-MCH affects the monolayer structure and functionality.

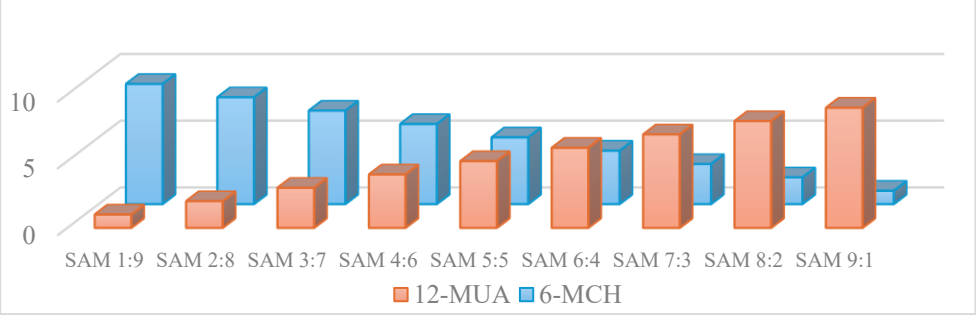


Figure 6. SAM mixtures composition visualization. 12-MUA in figure is 12-mercaptododecanoic acid [$HS(CH_2)11COOH$ (12-MUA) and 6-MCM in this Figure is 6-mercapto-1-hexanol [HS(CH2)6OH] with a different molar ratio proportion

After incubation, the surfaces were rinsed with ethanol to remove unbound molecules, and the functionalized gold electrodes (Au/12-MUA+6-MCH) were transferred into a custom-designed electrochemical QCM cell, which was integrated with a Gamry Reference 600 potentiostat/galvanostat. This setup enabled electrochemical cleaning and qualitative evaluation of electrode surface cleanliness in real-time during the modification process. The prepared electrodes were then subjected to SAM activation while using EDC/NHS coupling chemistry, thus facilitating the covalent immobilization of T7 DNA polymerase onto the functionalized surface.

2.2.2.3. T7 DNA polymerase masking study

The enzyme's active site was temporarily masked to preserve the enzymatic activity of T7 DNA polymerase during immobilization. This was achieved by pre-incubating the 0.69 μM enzyme with double-stranded DNA (dsDNA) fragments for 30 minutes at room temperature with gentle stirring to ensure thorough mixing, allowing them to bind to the polymerase's 3′→5′ exonuclease domain. The masking step prevents direct covalent coupling of the active site during SAM attachment, ensuring correct orientation and activity post-immobilization.

2.2.2.4. SAM activation and T7 DNA polymerase immobilization study

SAM activation is vital for enzyme immobilization. It enhances surface reactivity for stable enzyme attachment through strong covalent bonds created by carboxyl functional groups. This ensures specific immobilization and controls the enzyme orientation, preserving access to the active site for optimal activity. Additionally, SAM activation minimizes non-specific adsorption, improving reproducibility and system performance. It also enhances enzyme stability against variations in pH, temperature, and buffer conditions, ensuring uniform enzyme distribution in biosensing applications for an improved signal response and detection efficiency.

A series of experiments using a functionalized gold electrode (Au/12-MUA+6-MCH) was mounted in a custom-designed small-volume (0.1 mL) flow-through QCM cell. QCM measurements were carried out by using a *Maxtek QCM-R* system (5 MHz). Integration of a real-time flow setup enabled continuous monitoring of the frequency and resistance changes, allowing for precise characterization of the surface functionalization and the subsequent biomolecular interactions. Before the SAM activation on the gold-coated electrode (Au/12-MUA+6-MCH), an electrode washing step was performed by using nuclease-free water at a constant flow rate of 1 mL/min for 30 minutes at room temperature in a closed QCM cell. The carboxyl group activation on the gold electrode (Au/12-MUA+6-MCH) was performed while using a solution of 0.6 mg/mL NHS and 0.4 mg/mL EDC in 1× PBS at pH 7.4 at a flow rate of 0.5 mL/min for 20 minutes at room temperature. Following activation, 0.69 μM of masked T7 DNA polymerase in 1× PBS was introduced at a flow rate of 0.1 mL/min for 2 hours at room temperature. Real-time QCM monitoring tracked the enzyme's adsorption, and post-immobilization rinsing with PBS was performed to remove any unbound material. Immobilization was repeated in triplicate to ensure reproducibility, and the process was analyzed via Sauerbrey equation-based mass changes and kinetic (first-, second-, and n-order) modeling.

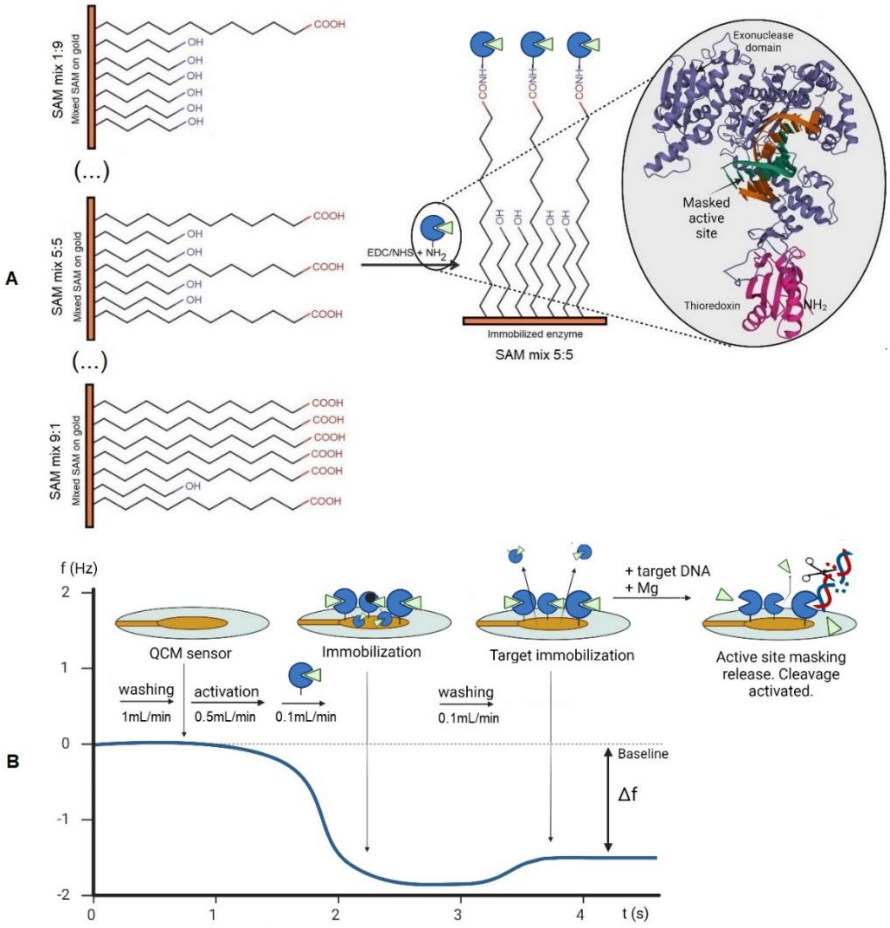


Figure 7. Schematic representation of T7 DNA Polymerase sensor development. (**A**) This section illustrates the detailed structure of the SAM mixtures and the masked T7 DNA polymerase during the immobilization process. The schematic highlights the molecular arrangement and the interaction of the enzyme with the functionalized surface. (**B**) QCM monitoring process. This section illustrates the real-time QCM assessment of the sensor fabrication process, including the immobilization of T7 DNA polymerase and the subsequent washing steps. QCM expected signal variations indicate changes in mass loading, thereby confirming successful enzyme attachment and surface cleaning

Frequent shifts in both frequency (Δf) and resistance (ΔR) provided quantitative insights into the binding kinetics and the overall performance of the biosensor. The average frequency shifts were calculated to ensure the reproducibility of the results, thus confirming the reliability of the sensor responses throughout the experiment. The general schematic representation of the SAM mixture's structure and activation process, involving the immobilization of T7 DNA polymerase, along with the general variations in the QCM signal, is illustrated in *Figure 7*. The functionalized sensor was subsequently exposed to the target DNA substrate in the presence of Mg^{2+} ions, which are essential for activating the catalytic site of T7 DNA polymerase.

2.2.2.5. T7 DNA polymerase-based sensor 3'→5' exonuclease activity study

The catalytic activity of immobilized T7 DNA polymerase was assessed to determine whether its 3′→5′ exonuclease function was preserved after covalent attachment to the gold-coated electrode (Au/12-MUA+6-MCH) SAM-modified surface. This step was essential to confirm the functionality of the surface-bound enzyme and to compare its performance with that of the free enzyme under identical buffer and substrate conditions. Following successful enzyme immobilization on a series of experiments using a functionalized gold-coated electrode (Au/12-MUA+6-MCH), the surface was exposed to 15 ng dsDNA in T7 DNA polymerase buffer conditions (400 mM Tris-HCl [pH 7.5 at 25 °C], 100 mM $MgCl_2$, 10 mM DTT) containing Mg^{2+} as a cofactor for 18 hours at room temperature to initiate exonuclease reactions. The exonuclease reaction products were visualized by using 2% TAE agarose gel electrophoresis, thus revealing the changes in the degradation of the substrate fragments.

The experiment was designed to reflect the solution-phase reaction conditions as closely as possible. A consistent dsDNA fragment length and concentration were used to minimize the variation and ensure comparability between surface-bound and free enzyme activities. This timing was chosen based on the optimal activity range identified in solution-based experiments.

2.2.2.6. T7 DNA polymerase-based sensor re-usage study

To evaluate the practical applicability and stability of the developed biosensor, a reuse protocol was established to investigate the enzymatic performance of immobilized T7 DNA polymerase over multiple cycles of exonuclease activity. The experiments aimed to determine whether the biosensor maintained its 3′→5′ exonuclease activity across repeated uses and to identify those conditions that optimize enzymatic retention. The studies were conducted while using a gold-coated electrode (Au/12-MUA+6-MCH) functionalized with a 6:4 molar ratio SAM-modified surface, onto which, T7 DNA polymerase was covalently immobilized by using a custom-designed small-volume (0.1 mL) flow-through QCM cell system, as previously described. The surface-bound enzyme concentration was determined to be approximately 427.95 ± 0.60 ng. dsDNA fragments, serving as substrates, were introduced into the flow-through QCM cell in T7 DNA polymerase buffer conditions (400 mM Tris-HCl (pH 7.5 at 25 °C), 100 mM $MgCl_2$, 10 mM DTT) with Mg^{2+}, a necessary cofactor for enzymatic activity. To simulate the conditions relevant to rapid biosensing applications, each cycle used 1 ng of the dsDNA substrate and was incubated at room temperature for 45 minutes and 90 minutes. After each reaction, the surface was gently rinsed with the buffer to remove degradation products, and the same enzymatic surface was reused for the subsequent cycle without regeneration. The degradation efficiency of DNA substrates in each cycle was evaluated by running 2% TAE agarose gel electrophoresis. Band intensity changes were analyzed quantitatively by using *TotalLab* image analysis software, and optical band volumes were utilized to assess residual DNA concentrations following the enzymatic exonuclease activity reaction.

2.2.2.7. T7 DNA polymerase-based sensor hydrolysis study

Hydrolysis experiments were performed while using Proteinase K, a broad-spectrum serine protease, to investigate the susceptibility of surface-bound T7 DNA polymerase to proteolytic degradation. These studies aimed to characterize the enzymatic stability of immobilized T7 DNA polymerase and to evaluate the effectiveness of QCM for monitoring

real-time surface protein degradation. Following successful enzyme immobilization in a series of experiments using a functionalized gold-coated electrode (Au/12-MUA+6-MCH) with a SAM-modified surface, the surface was exposed to a 1.4 μM solution of Proteinase K in 1× PBS buffer (pH 7.4) introduced into the system at a constant flow rate of 0.1 mL/min for 2 hours at room temperature. Real-time QCM monitoring was employed to track experiments conducted while using functionalized gold-coated electrodes (Au/12-MUA+6-MCH) and the hydrolysis of the T7 DNA polymerase enzyme. The primary reaction involves the enzymatic hydrolysis of T7 DNA polymerase by Proteinase K:

T7 DNA Polymerase + Proteinase K → Hydrolyzed Peptides + Amino Acids

This hydrolysis study aimed to evaluate the performance and stability of immobilized T7 DNA polymerase in various surface environments modified with different SAMs. It analyzed the hydrolysis efficiency in order to determine the optimal SAM mixture composition that would provide the highest stability of T7 DNA polymerase. A quantitative analysis of the kinetic (first-, second-, and n-order) data was also performed in an attempt to understand the interaction between the enzyme and the immobilization matrix, which affects the enzyme's susceptibility to hydrolysis. This provides insights into the design of more robust and efficient enzyme-based biosensors for various applications.

2.3. BAFF Protein Study

2.3.1. Free BAFF protein study

Recombinant human BAFF (BLyS) protein was reconstituted in sterile 1× phosphate-buffered saline (PBS, pH 7.4) according to the manufacturer's instructions to obtain a working stock of 1 mM. The reconstituted protein solution was aliquoted into low-binding microtubes and stored at –20 °C to prevent activity loss due to repeated freeze–thaw cycles. For each experiment, a fresh aliquot was thawed on ice and diluted to the required concentration with PBS immediately before use.

The structural integrity and purity of the recombinant BAFF were verified by SDS-PAGE (15% polyacrylamide gel, reducing conditions), followed by Coomassie Brilliant Blue staining. A single prominent band was observed slightly above the theoretical 17 kDa, consistent with the predicted molecular weight of the soluble BAFF monomer. This confirmed that the recombinant protein preparation was of high purity (≥ 95% by SDS-PAGE and HPLC, as specified by the supplier) and suitable for subsequent experiments.

2.3.2. BAFF protein-based sensor study

2.3.2.1. SAM activation and BAFF immobilization study

The cleaning protocol for the gold-coated *QSense*® sensor, along with the preparation of the SAM mixture, activation of the SAM, and the BAFF immobilization process using a custom-designed small-volume (0.1 mL) flow-through QCM cell system, was executed with precision, as detailed in the previous sections, while using T7 DNA polymerase. All parameters and process conditions were consistently maintained. The 3:7 SAM mixture composition on the gold-coated electrodes (Au/12-MUA+6-MCH) was specifically chosen to ensure successful BAFF protein immobilization studies.

2.3.2.2. SAM deactivation study

Following successful BAFF immobilization in a series of experiments using a functionalized gold-coated electrode (Au/12-MUA+6-MCH) with a 3:7 SAM-modified surface, the unabsorbed surface was deactivated by applying a 1 mg/mL BSA solution in 1X PBS (pH 7.4). This step was performed to block non-specific binding sites while using a custom-designed small-volume (0.1 mL) flow-through QCM cell system at a constant rate of 0.1 mL/min for 20 minutes at room temperature and in the dark with real-time frequency shift (Δf) monitoring to confirm surface saturation. Following deactivation, the electrode was washed with 1X PBS (pH 7.4) under identical flow conditions to remove unbound BSA.

Bovine Serum Albumin (BSA) is commonly used as a blocking agent in biosensor applications due to its advantageous physicochemical properties. BSA is a stable, water-soluble protein abundant in serum with a relatively high molecular weight (approximately 66.5 kDa), which makes it practical for saturating the available binding sites on sensor surfaces. Its high content of charged amino acids and hydrophilic nature allows it to adsorb onto surfaces through electrostatic and Van der Waals interactions, which leads to forming a stable, non-specific protein layer that prevents the binding of non-target molecules. Importantly, BSA does not contain any functional groups that would interfere with the specific interaction between the target analyte and the sensor, thereby ensuring that only particular interactions are detected. This makes it ideal for preventing non-specific protein adsorption, which could otherwise cause background noise and false readings in biosensing experiments. Additionally, BSA is well-documented for maintaining surface passivation over extended periods, ensuring consistent and reliable sensor performance. Furthermore, BSA is cost-effective, easy to handle, and compatible with many buffer systems, including 1X PBS (pH 7.4), which makes it a go-to choice in many surface deactivation protocols.

2.3.2.3. BAFF protein-based sensor evolution study

Following SAM deactivation on the gold-coated electrode (Au/12-MUA+6-MCH/BAFF/BSA), the BAFF biosensor was functionalized by introducing a specific single-stranded DNA (ssDNA) fragment. This step was performed for targeting detection by using a custom-designed small-volume (0.1 mL) flow-through QCM cell system at a constant rate of 0.1 mL/min for 20 minutes at room temperature and in the dark with real-time frequency shift (Δf) monitoring to confirm ssDNA binding. After the targeting step, the biosensor surface was rinsed with 1X PBS (pH 7.4) under identical flow conditions to remove unbound ssDNA.

Real-time QCM monitoring tracked the BAFF adsorption and post-immobilization rinsing with PBS, and surface deactivation with BSA was performed, followed by targeting DNA adsorption to develop a functional BAFF biosensor. The entire process was repeated in triplicate to ensure reproducibility, and the results were analyzed by using the Sauerbrey equation-based mass changes and kinetic modeling. A quantitative analysis of the kinetic (first-, second-, and n-order) data was also performed to understand the interaction between the enzyme and the immobilization matrix, which affects the enzyme's susceptibility to hydrolysis. This provides insights into the design of more robust and efficient enzyme-based biosensors for various applications.

2.4. VEGF Protein Study

Gold-coated sensor discs were used as substrates for aptamer immobilization. The surfaces were first cleaned and then incubated overnight with a solution of the assembled anti-VEGF DNA aptamer, consisting of three oligonucleotides (combSL2B, stalkGTG, r_stalkGTG). The aptamer structure was formed by hybridization of three complementary oligonucleotides: the combSL2B recognition strand, a thiol-modified stalkGTG oligonucleotide, and its complementary reverse r_stalkGTG sequence. The thiol group at the 3′-end of the stalk oligonucleotide was first reduced by using 100 mM dithiothreitol (DTT) in 10 mM sodium phosphate buffer (pH 8.3) for 1 h at room temperature. The reduced oligonucleotide was purified by size-exclusion chromatography (*Sephadex G-25* column) to remove excess reagents. The three oligonucleotides were then mixed in an equimolar ratio (30 pmol/µL each) in PBS and subjected to thermal annealing: heating in a water bath for 5 min at 95 °C, followed by gradual cooling to room temperature. This procedure yielded a stable self-assembled anti-VEGF aptamer structure, in which, the stalk domains provide the anchoring capacity, whereas the combSL2B domain ensures specific recognition of VEGF. The aptamer structure ensured the correct folding and surface orientation, thereby facilitating VEGF recognition. Functionalization was confirmed by spectroscopic ellipsometry.

To minimize nonspecific adsorption, the modified sensor surface was blocked with 1% BSA in PBS (30 min). After blocking, the sensing chamber was rinsed with PBS (pH 7.4) to establish a stable baseline. VEGF detection was performed by injecting 260 nM VEGF into the chamber, while monitoring changes in ellipsometric parameters in real time. Regeneration of the surface was achieved by treatment with 50 mM NaOH / 17.34 mM SDS (5 min), which disrupted the VEGF/aptamer complex and partially disassembled the aptamer, leaving only the covalently surface-bound stalkGTG strand.

3. RESULTS AND DISCUSSION

This study explores the interaction between free and immobilized T7 DNA polymerase and examines its 3'→5' exonuclease activity. This section presents a detailed analysis of experiments on a gold-coated electrode (Au/12-MUA+6-MCH) functionalized with various molar ratios of SAM surfaces. The experimental studies utilized gold-coated QCM sensors, while focusing on T7 DNA polymerase and protein biomarkers, to demonstrate the feasibility of constructing label-free DNA-modifying enzyme biosensors. By employing these sensors, the study illustrates how enzyme and protein immobilization on gold-coated surfaces can be effectively achieved and monitored in real-time. The interaction kinetics were evaluated through detailed calculations to assess the binding behavior of the immobilized T7 DNA polymerase and protein biomarkers. These calculations were critical for understanding how surface-bound enzymes interact with their substrates and how the presence of a solid surface influences the enzyme's catalytic activity. The results provided important insights into the functional stability and performance of the biosensors, as well as their potential application in real-world diagnostic settings.

3.1. T7 DNA Polymerase Study Results

3.1.1. Free T7 DNA polymerase study results

To study the behavior of free T7 DNA polymerase, DNA (Low DNA Mass Ladder) fragment hydrolysis was conducted while using varying concentrations of DNA substrates. The Low DNA Mass Ladder consists of DNA fragments ranging from 100 bp to 2000 bp. The DNA fragments are double-stranded and typically blunt-ended. Both strands of each DNA fragment terminate at the same nucleotide, resulting in no overhangs [94,95]. Blunt-ended DNA fragments are generally more stable, but they can be less efficient for specific enzymatic reactions, such as ligation. T7 DNA polymerase binds to the blunt-ended DNA fragment. The blunt end provides a straightforward substrate for the enzyme's 3' → 5' exonuclease activity. The 3'→5' exonuclease activity of T7 DNA polymerase removes nucleotides from the 3' end of the DNA strand [96]. This activity is typically used to correct the misincorporated nucleotides during DNA synthesis, and it could effectively hydrolyze DNA fragments when no polymerization synthesis occurs. The exonuclease activity removes nucleotides from the 3' end, progressively shortening the DNA fragment. This process will continue until the enzyme dissociates from the DNA or the fragment has been completely degraded. The enzyme cleaves the phosphodiester bonds between the nucleotides, releasing the nucleotides one by one from the 3' end [10,97].

This part of the study examined the use of 1 µg of Low DNA Mass Ladder as a double-stranded DNA (dsDNA) substrate following a 21-hour reaction under the conditions of the T7 DNA polymerase buffer (400 mM Tris-HCl (pH 7.5 at 25 °C), 100 mM $MgCl_2$, and 10 mM DTT). The results confirmed the complete hydrolysis of the 1 µg Low DNA Mass Ladder over the 21 hours *in vitro* reaction, while using 12.5 U of T7 DNA polymerase. Results were obtained for both responses, with and without the enzyme, as shown in *Figure 8*.

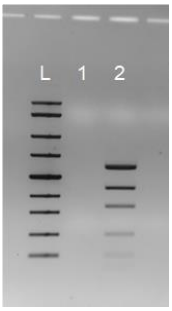


Figure 8. 1 µg of DNA is hydrolyzed over 21 hours with 12.5 U of T7 DNA polymerase. **L** – DNA ladder, **1** – 1ug of Low DNA Mass Ladder after the hydrolysis with the T7 DNA polymerase over 21 hours. **2** – 1ug of Low DNA Mass Ladder as control reaction without the T7 DNA polymerase over 21 hours

To study the behavior of free T7 DNA polymerase, the hydrolysis of different DNA length fragments was conducted while using varying concentrations of DNA substrates. The degradation of different DNA length fragments during the enzymatic reaction was monitored by measuring absorbance at 260 nm at regular intervals (at every 30 seconds for 1 hour). These absorbance values were converted into the remaining DNA concentration (*Figure 9*) at each time point. To investigate the kinetics of DNA degradation, the DNA hydrolysis reaction was initially analyzed while using a first-order kinetic model.

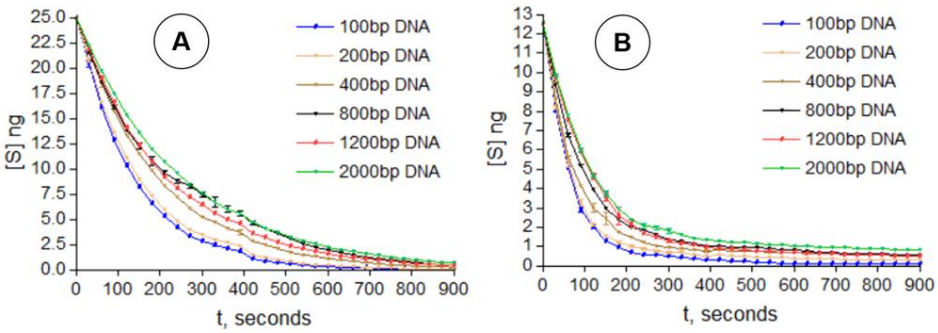


Figure 9. Hydrolysis of various DNA fragment lengths using primary substrate concentration of 25 ng (A) and 12.5 ng (B) in the T7 DNA polymerase 3'→5' exonuclease activity reaction

In order to determine whether the reaction follows first-order kinetics, a plot of time *(t)* versus the natural logarithm of the remaining DNA concentration, *ln([S])*, was created. Here, *[S]* represents the remaining DNA concentration at each time interval. The linear regression analysis was conducted for the DNA hydrolysis reaction over the initial 200 seconds, testing various DNA fragment lengths and primary substrate concentrations of 25 ng and 12.5 ng. This analysis calculated the slope, intercept, and R^2 value. The presence of a linear relationship in this plot confirms that the reaction follows first-order kinetics, as illustrated in the accompanying *Figure 10* and *Figure 11*.

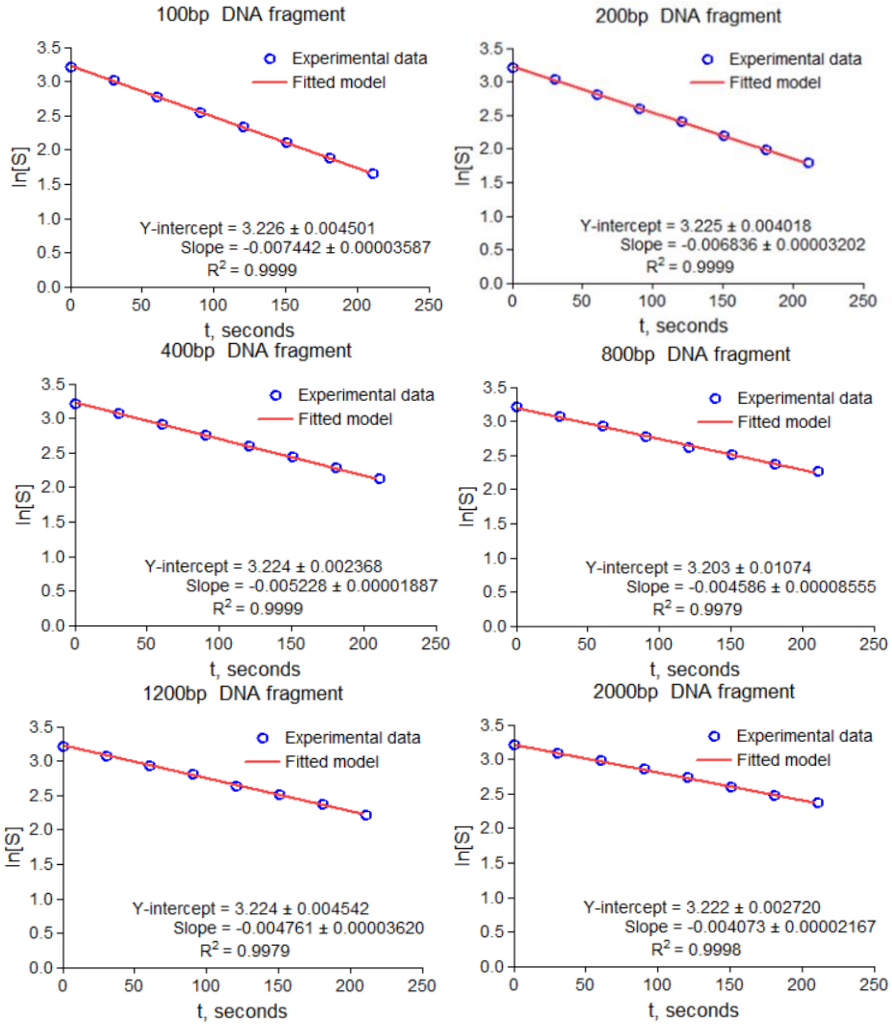


Figure 10. Comparison of linear regression analysis of experimental data for T7 DNA polymerase 3'→5' exonuclease activity reaction on various DNA fragment lengths using a primary substrate concentration of 25 ng. The experimental data points, represented by the blue circles, were fitted to the linear regression model, indicated by the solid red lines, for each DNA fragment length

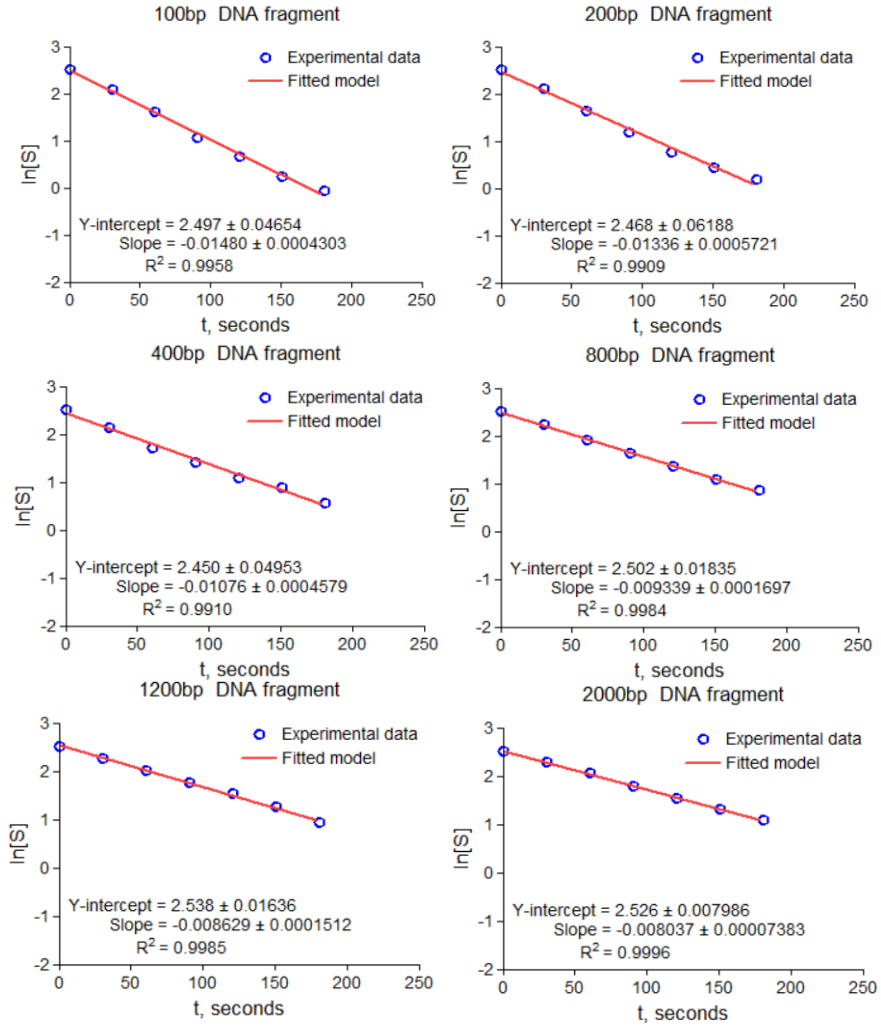


Figure 11. Comparison of linear regression analysis of experimental data for T7 DNA polymerase 3'→5' exonuclease activity reaction on various DNA fragment lengths, using a primary substrate concentration of 12.5 ng. The experimental data points, represented by the blue circles, were fitted to the linear regression model, indicated by the solid red lines, for each DNA fragment length

To further evaluate the applicability of the first-order kinetic model, the experimental data were compared with the theoretical model derived from the first-order kinetic equation to assess the accuracy of the fit. The reaction velocity V_0 rate is directly proportional to the substrate *[S]* concentration, represented by the velocity and the First-order kinetic equation:

$$V_0 = k \times [S] \qquad (3)$$

$$[S] = [S_0]e^{-kt} \qquad (4)$$

where *[S]* represents the remaining DNA substrate concentration in ng at a given time, $[S_0]$ is the initial DNA concentration in ng, k is the rate constant determined from the linear regression slope, and t is the reaction time in seconds.

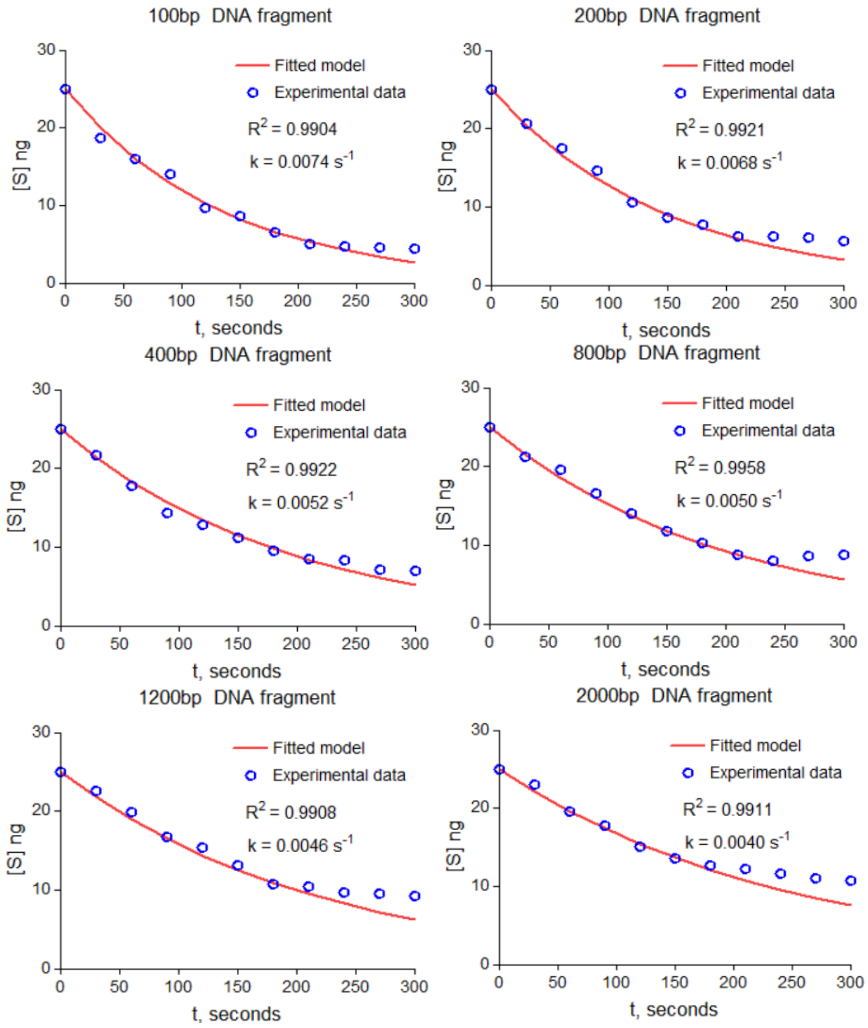


Figure 12. Comparison of experimental and First-Order Kinetics Plots for T7 DNA Polymerase 3'→5' exonuclease activity reaction on various DNA fragment lengths using a primary substrate concentration of 25 ng. The experimental data points, represented by the blue circles, were fitted to the linear regression model, indicated by the solid red lines, for each DNA fragment length

Finally, the remaining DNA concentration of various DNA fragment lengths was recalculated by using the slope and intercept derived from the experimental data as a fitted model. The experimental and modeling of various DNA fragment lengths concentration *[S]* data were plotted alongside the predicted curve over a 300-second reaction period to assess how well the first-order kinetic model fit the observed DNA degradation (see *Figure 12* and *Figure 13*). The comparison between the experimental data and the first-order kinetic model revealed a strong alignment across the entire reaction time range. No significant deviations were observed, which indicates that the DNA degradation process consistently followed first-order kinetics. This suggests that factors such as enzyme saturation, secondary interactions, or diffusion limitations did not significantly influence the reaction under the tested conditions. The quality of the fit was further supported by high correlation

coefficients (R^2 values >0.99), thereby confirming that the first-order kinetic model accurately describes the system's behavior and reliably reflects the underlying reaction mechanism.

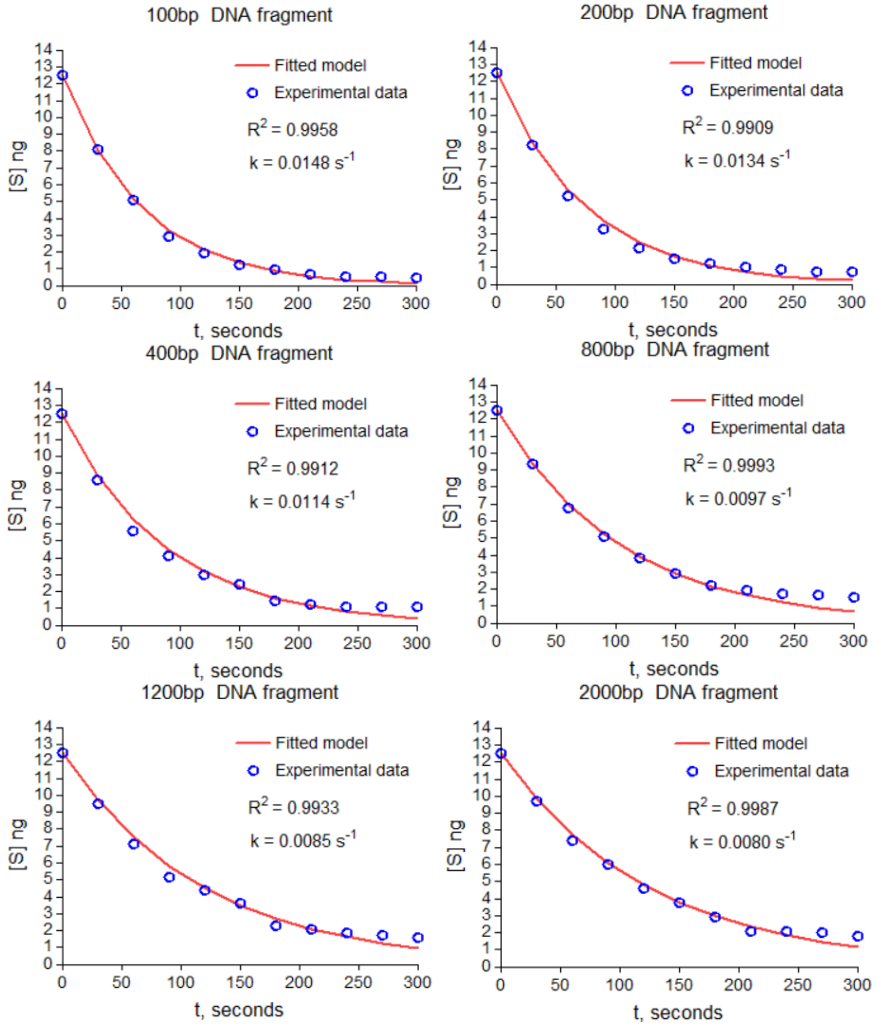


Figure 13. Comparison of experimental and First-Order Kinetics Plots for T7 DNA Polymerase 3'→5' exonuclease activity reaction on various DNA fragment lengths using a primary substrate concentration of 12.5 ng. The experimental data points, represented by the blue circles, were fitted to the linear regression model, indicated by the solid red lines, for each DNA fragment length

To study the Michaelis-Menten kinetics for T7 DNA Polymerase 3'→5' exonuclease activity reaction on various DNA fragment lengths, the initial reaction velocity (V_0) was recalculated following the appropriate kinetic equations:

$$V_0 = \frac{\Delta[S]}{\Delta t} \qquad (5)$$

$$V_0 = \frac{V_{max}[S]}{K_m + [S]} \qquad (6)$$

where: V_0 – reaction velocity, ng/s; V_{max} is the maximum velocity, ng/s; $\Delta[S]$ – substrate concentration, ng; Δt – time, seconds; and K_m is the Michaelis-Menten constant

To determine whether the reaction follows Michaelis-Menten kinetics, a plot of recalculated reaction velocity V_0 versus the remaining DNA substrate concentration *[S]* during the entire reaction time (1 hour) was created (see *Figure 14* and *Figure 15*). The relationship between the initial reaction velocity V_0 and varying substrate concentrations *[S]* was analyzed. Experimental data were collected and plotted to evaluate how the enzyme's catalytic activity responds to increasing DNA concentrations. The data were fitted to the Michaelis-Menten equation by using non-linear regression methods with the objective to estimate the key kinetic parameters: the maximum reaction velocity V_{max} and the Michaelis constant K_m. This approach enabled a detailed assessment of the enzyme's substrate affinity and catalytic efficiency while revealing the saturation behavior at higher substrate concentrations, characteristic of enzyme-limited reactions.

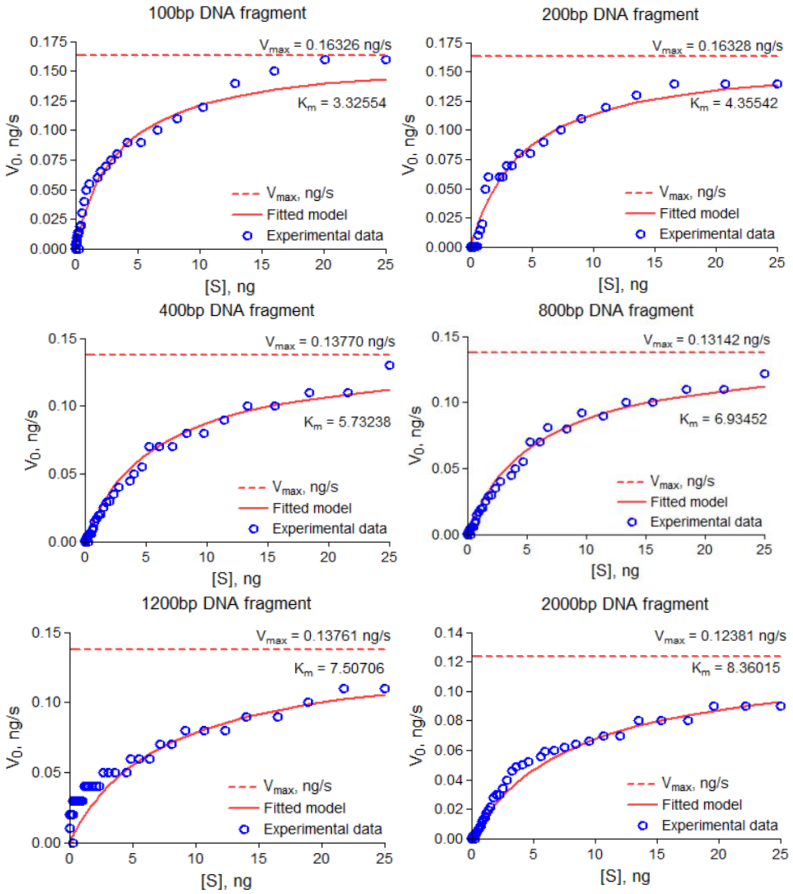


Figure 14. Comparison of experimental and modeled Michaelis-Menten Kinetics for T7 DNA Polymerase 3'→5' exonuclease activity reaction on various DNA fragment lengths using a primary substrate concentration of 25 ng. The experimental data points (the blue circles) were fitted to the Michaelis-Menten model (the red solid lines) for each fragment length. The dashed red lines indicate the V_{max} values obtained from the fitted models

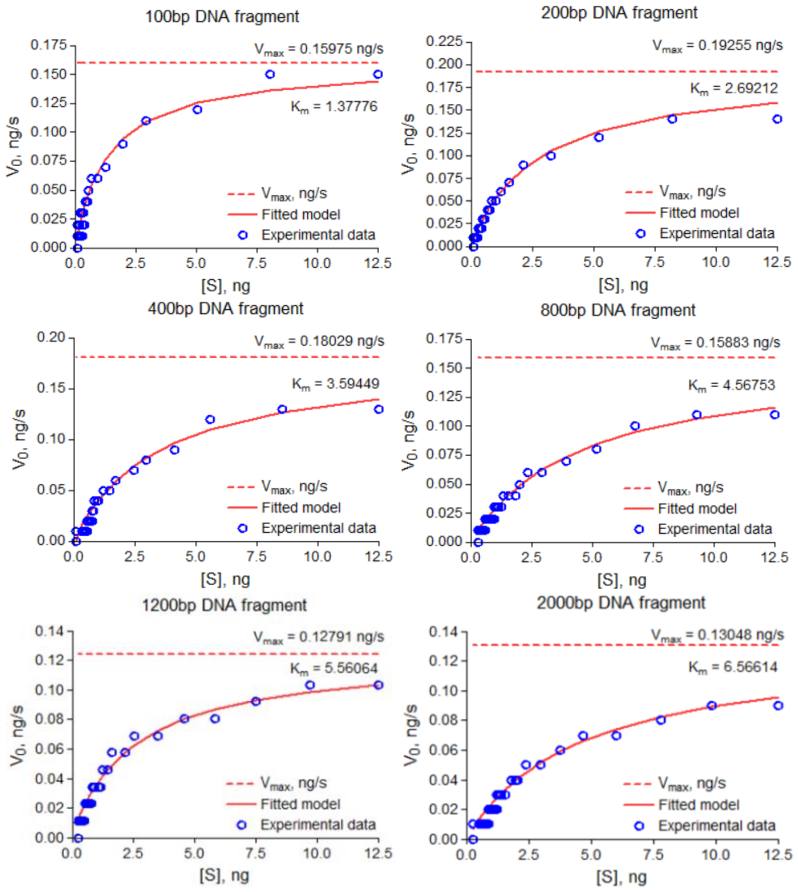


Figure 15. Comparison of experimental and modeled Michaelis-Menten Kinetics for T7 DNA Polymerase 3'→5' exonuclease activity reaction on various DNA fragment lengths using a primary substrate concentration of 12.5 ng. The experimental data points (the blue circles) were fitted to the Michaelis-Menten model (the red solid lines) for each fragment length. The dashed red lines indicate the V_{max} values obtained from the fitted models

The Michaelis-Menten kinetics model enabled us to gain a better understanding of the dynamics of the enzymatic reaction and the influence of the substrate concentration on the reaction rate. The experimental data and the fitted model illustrate the Michaelis-Menten kinetics of T7 DNA Polymerase *3′→5′* exonuclease activity reaction across different DNA fragment lengths at two substrate concentrations (25 ng and 12.5 ng). The data were analyzed by using the Michaelis-Menten model, confirming that enzymatic activity adheres to the classical enzyme kinetics. The plots illustrate how V_{max} and K_m change with varying fragment lengths, thereby providing insight into how the DNA length influences the enzyme exonuclease activity. V_{max} values vary with the fragment length, thus suggesting that the substrate size impacts the catalytic efficiency of T7 DNA polymerase. K_m increases with the DNA length, implying that longer DNA fragments have a lower binding affinity to the enzyme. Whereas, shorter DNA fragments exhibit lower K_m values, indicating a stronger enzyme-substrate affinity. In this context, longer fragments exhibit increased K_m values, suggesting a reduced binding affinity – but with comparable V_{max} values. At a 25 ng DNA concentration, the V_{max} values slightly increase (compared to 12.5 ng), thus

confirming that the enzyme maintains high activity levels across a range of substrate concentrations. Increasing K_m at higher concentrations suggests substrate competition or a potential shift in the enzyme-substrate interaction dynamics. The well-fitted curves confirm that the enzyme exhibits a predictable kinetic behavior across the investigated DNA lengths.

The nonlinear hyperbolic trend of Michaelis-Menten kinetics data was linearized by using the Lineweaver-Burk transformation to analyze the kinetic parameters and validate the estimated values. The double-reciprocal plot $\frac{1}{V_0}$ versus $\frac{1}{[S]}$ was generated, allowing for the determination of V_{max} and K_m from the slope and the y-intercept of the fitted regression line. This linear representation facilitated the comparison of kinetic parameters across different DNA fragment lengths despite its sensitivity to errors at low substrate concentrations. The data were also plotted by using the Lineweaver-Burk transformation:

$$\frac{1}{V_0} = \frac{K_m}{V_{max}} \times \frac{1}{[S]} + \frac{1}{V_{max}} \quad (7)$$

$$y = \frac{1}{V_0} \quad (8)$$

$$x \frac{1}{[S]} \quad (9)$$

$$m = \frac{K_m}{V_{max}} \quad (10)$$

$$b = \frac{1}{V_{max}} \quad (11)$$

Lineweaver-Burk plots for T7 DNA polymerase *3′→5′* exonuclease reaction activity were analyzed on various DNA fragment lengths and different concentrations of 25 ng 12.5 ng (see *Figure 16* and *Figure 17*). The data confirmed that the enzyme kinetics followed the expected theoretical models. The Michaelis-Menten plot exhibits a nonlinear hyperbolic trend, as expected (cf. *Figure 14* and *Figure 15*), whereas the Lineweaver-Burk exhibits linear regression (*Figure 16* and *Figure 17*) in the form of y = mx + b.

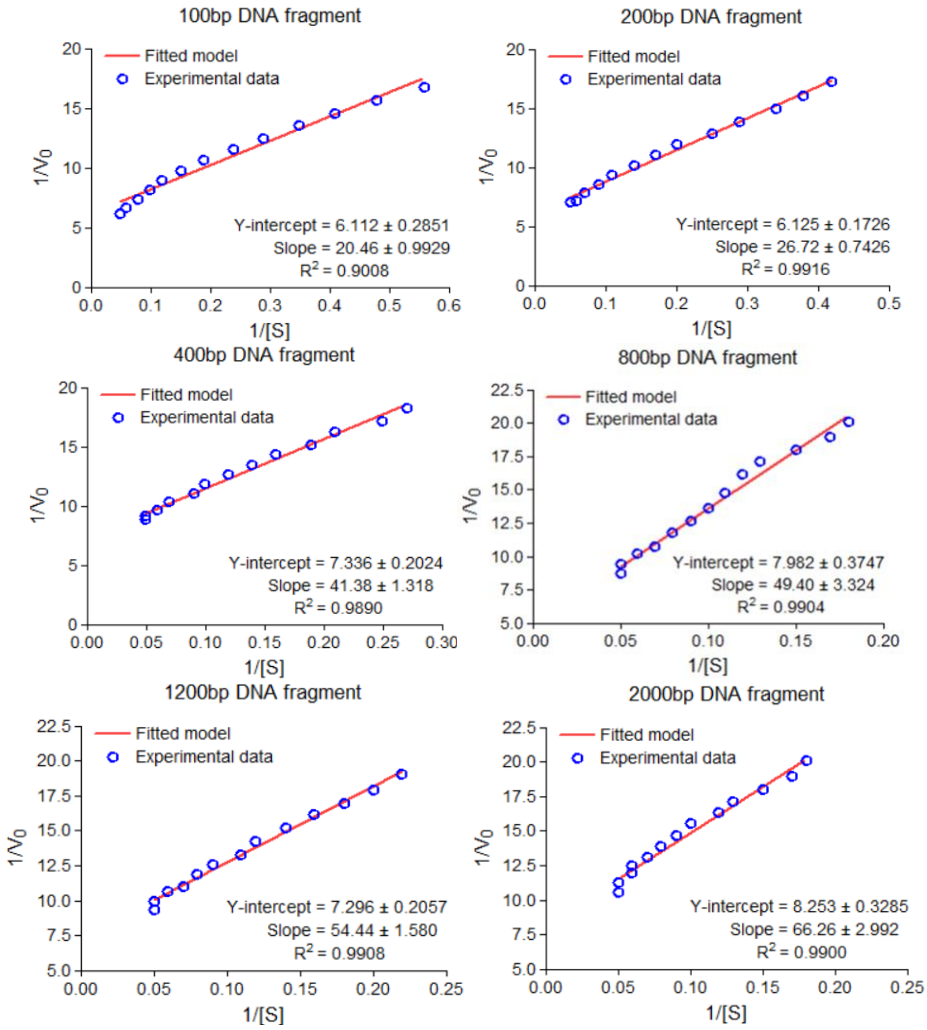


Figure 16. Comparison of experimental and modeled Lineweaver-Burk Plots for T7 DNA Polymerase 3'→5' exonuclease activity reaction on various DNA fragment lengths using a primary substrate concentration of 25 ng. The experimental data points (the blue circles) were fitted to the Lineweaver-Burk model (the red solid lines) for each DNA fragment length

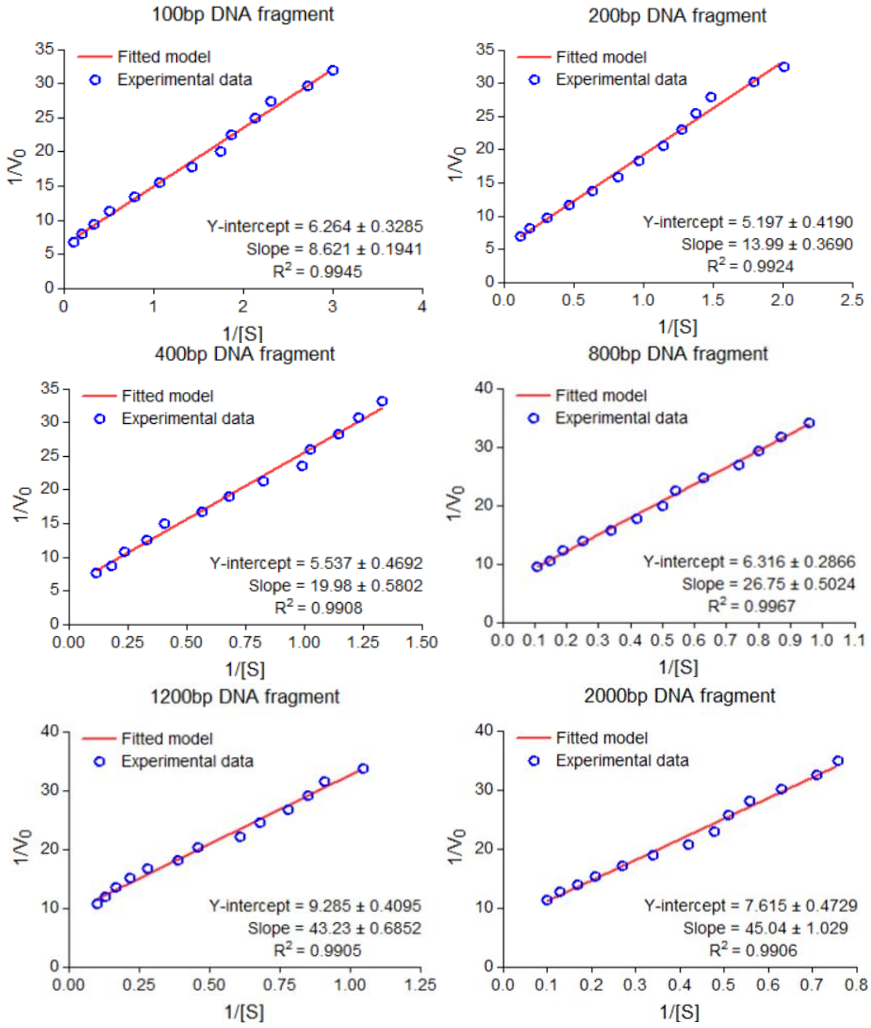


Figure 17. A comparison of experimental and modeled Lineweaver-Burk Plots for T7 DNA Polymerase 3'→5' exonuclease activity reaction on various DNA fragment lengths using a primary substrate concentration of 12.5 ng. The experimental data points (the blue circles) were fitted to the Lineweaver-Burk model (the red solid lines) for each DNA fragment length

Since the observed K_m values from Michaelis-Menten Kinetics are lower than the substrate concentrations (*[S]* = 12.5 ng, K_m =1.37776–6.56614 ng; *[S]* = 25 ng, K_m =3.32554–8.36015 ng), the reaction predominantly occurs under conditions approaching enzyme saturation, where zero-order kinetics are expected. Therefore, detailed zero-order kinetic modeling was not necessary, although saturation effects were noted. However, in order to further investigate the kinetic behavior at low substrate concentrations $[S] << K_m$, the reaction was analyzed by using First-Order decay kinetics. By plotting $ln(V_0)$ against *ln([S])* (*Figure 18*), the linear relationship should confirm First-Order decay kinetics in this substrate range.

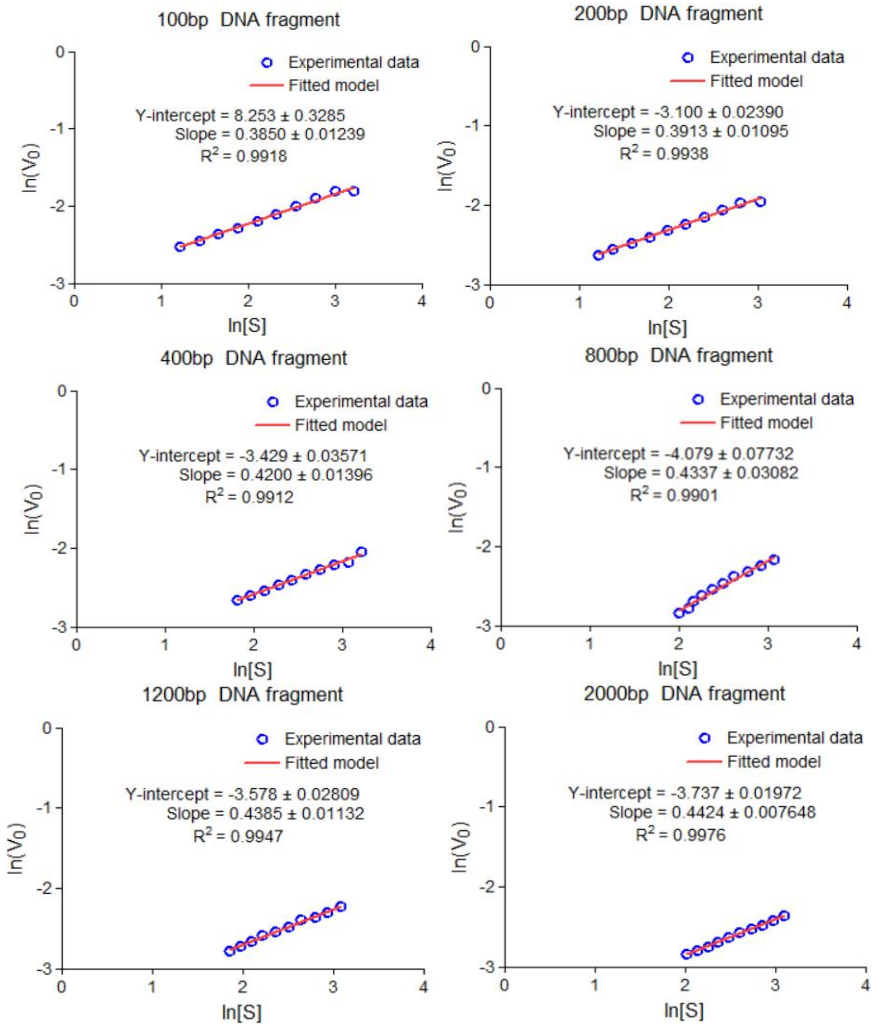


Figure 18. Comparison of experimental and modeled First-Order decay kinetics for T7 DNA Polymerase 3'→5' exonuclease activity reaction on various DNA fragment lengths using a primary substrate concentration of 25 ng. The experimental data points (the blue circles) were fitted to the First-Order decay kinetics (the red solid lines) for each DNA fragment length

The plot of $ln(V_0)$ versus $ln([S])$ produced a linear relationship described by the Equation:

$$ln(V_0) = m\ ln([S]) - b \qquad (12)$$

where: the slope (m) represents the reaction order. The obtained slope value confirms that the reaction follows first-order kinetics with respect to the substrate concentration, thus indicating a direct proportionality between V_0 and $[S]$ under the tested conditions. If m (slope) ≈ 1, the reaction follows first-order kinetics concerning $[S]$. If m (slope) ≈ 0, the reaction follows zero-order kinetics, which means that V_0 does not depend on $[S]$. If m is

between 0 and 1, the reaction has a fractional order (e.g., diffusion-limited kinetics). Finally, if $m > 1$, it suggests cooperative binding or a complex reaction mechanism.

Since the $ln(V_0)$ vs. $ln([S])$ plot shows a linear relationship with a slope of 0.4, this indicates that the reaction follows fractional-order kinetics rather than first-order kinetics. This suggests that the reaction rate is directly proportional to substrate concentration in a non-integer manner, which may be influenced by factors such as enzyme-substrate binding dynamics, steric effects, or limitations in reaction-diffusion. However, as the experimental data align with the classical Michaelis-Menten kinetics, this fractional-order behavior likely reflects the enzyme's interaction with the substrate rather than a deviation from the standard enzymatic kinetics. Therefore, no additional kinetic model fitting or higher-order calculations were performed beyond the Michaelis-Menten analysis, as the existing model was sufficient to describe the observed behavior within the tested concentration range.

Table 3. Summary kinetics table of T7 DNA Polymerase 3'→5' exonuclease activity on various DNA fragment lengths using a primary substrate concentration of 25 ng

25 ng DNA length	First-order rate	Michaelis-Menten Kinetics			Lineweaver-Burk Plots	
	K (s^{-1})	V_{max} (ng/s^{-1})	K_{cat} (s^{-1})	K_m (ng)	V_{max} (ng/s^{-1})	K_m (ng)
100bp	0.0074	0.15975	0.012780	3.32554	0.16361257	3.34751309
200bp	0.0068	0.19255	0.015404	4.35542	0.16326531	4.36244898
400bp	0.0052	0.18029	0.014423	5.73238	0.13631407	5.64067612
800bp	0.0050	0.15883	0.012706	6.93452	0.12528188	6.18892508
1200bp	0.0046	0.12791	0.010233	7.50706	0.13706140	7.46162281
2000bp	0.0040	0.13048	0.010438	8.36015	0.12116806	8.02859566

Table 4. Summary kinetics table of T7 DNA Polymerase 3'→5' exonuclease activity on various DNA fragment lengths using a primary substrate concentration of 12.5 ng

12.5 ng DNA length	first-order rate	Michaelis-Menten Kinetics			Lineweaver-Burk Plots	
	K (s^{-1})	V_{max} (ng/s^{-1})	K_{cat} (s^{-1})	K_m (ng)	V_{max} (ng/s^{-1})	K_m (ng)
100bp	0.0148	0.16326	0.00653	1.37776	0.15964240	1.37627714
200bp	0.0134	0.16328	0.00653	2.69212	0.19241870	2.69193766
400bp	0.0114	0.13770	0.00551	3.59449	0.18060322	3.60845223
800bp	0.0097	0.13142	0.00526	4.56753	0.15832806	4.23527549
1200bp	0.0085	0.13761	0.00550	5.56064	0.10770059	4.65589661
2000bp	0.0080	0.12381	0.00495	6.56614	0.13131976	5.91464215

The similar pseudo first-order rate constants (k_{cat}) of 0.026 s^{-1} and 0.023 s^{-1} were determined at 25 °C and pH 8.0 for T7 DNA polymerase [98], respectively. The rate of hydrolysis of pNP-TMP catalyzed by T7 DNA polymerase is significantly lower than that for polynucleotide substrates. Lehman et al. measured the rate of hydrolysis of pNP-TMP catalyzed by the Klenow fragment, finding a k_{cat} of 0.065 s^{-1} at 37 °C and pH 9.0 [99]. In the literature, T7 DNA polymerase is typically used at a concentration of 1 μM. At the same time, the current studies utilize 10 U of enzymes, approximately equivalent to 1.6 μM (if

assuming 1 U equals 1 nmol of enzyme activity). This suggests that the enzyme concentrations in both studies are similar, though slightly higher in the present experiment. Additionally, the literature reports the use of a FAM-labeled DNA substrate, whereas our studies utilize 100–2000 bp DNA fragments. The fluorophore-labeled substrate in the literature could potentially result in different interaction dynamics, which may influence the rate of polymerase activity. Moreover, the literature conditions include additional components, such as thioredoxin, BSA, and Mg^{2+}, which are known to enhance the polymerase activity and could account for some of the observed differences. The rate constants reported in the literature for T7 DNA polymerase are in the range of 0.2 s^{-1}, measured under substrate concentration conditions of 200–250 nM. In contrast, our studies report a lower rate constant, ranging from 0.004 to 0.0148 s^{-1}, depending on the various DNA lengths and concentrations. This difference can be attributed to variations in substrate concentration and the length of the DNA fragments. The lower substrate concentration (25 ng – 7.58 nM and 12.5 ng – 3.79 nM in our study) and the potentially longer DNA fragment (100–2000 bp vs. smaller DNA in the literature) will likely reduce the overall reaction rate. Therefore, these experimental differences can explain the slower rate observed in this study.

The initial experiments focused on evaluating the reaction rates and the substrate composition while using free enzyme systems. These studies involved varying substrate concentrations (of various DNA fragments) in order to establish baseline kinetic parameters, including the reaction rate constants and the enzyme's affinity for the substrate. The free enzyme approach allowed for a thorough investigation of enzyme activity under controlled conditions, providing a clear understanding of the enzyme's catalytic behavior in solutions. Building on these initial findings, subsequent experiments were conducted while using immobilized enzyme systems to explore the effects of enzyme attachment on surface-modified substrates. The immobilization process introduces several factors that can influence the enzyme kinetics, including changes in the enzyme accessibility, conformational constraints, and the local concentration of the substrate near the enzyme's active site. By comparing the reaction rates and substrate binding affinities of free and immobilized enzyme systems, the study aimed to determine how immobilization affects the enzyme's efficiency and specificity in biosensing applications. These further studies were crucial for understanding the potential limitations and advantages of enzyme immobilization in real-world sensing devices. This version elaborates on the methodology of free and immobilized enzyme systems, connects them logically, and highlights the importance of the transition for our dissertation's argument.

3.1.2. T7 DNA polymerase-based sensor study results

3.1.2.1. QSense® sensor after cleaning characterization

Cyclic Voltammetry (CV) measurements were conducted within a potential range of -0.25 V to 1.25 V (vs. Ag/AgCl) in 0.1 M H_2SO_4 and at a scan rate of 100 mV/s. The CV measurements were performed in triplicate to ensure reproducibility. The typical voltammograms for the gold electrode are shown in *Figure 19*.

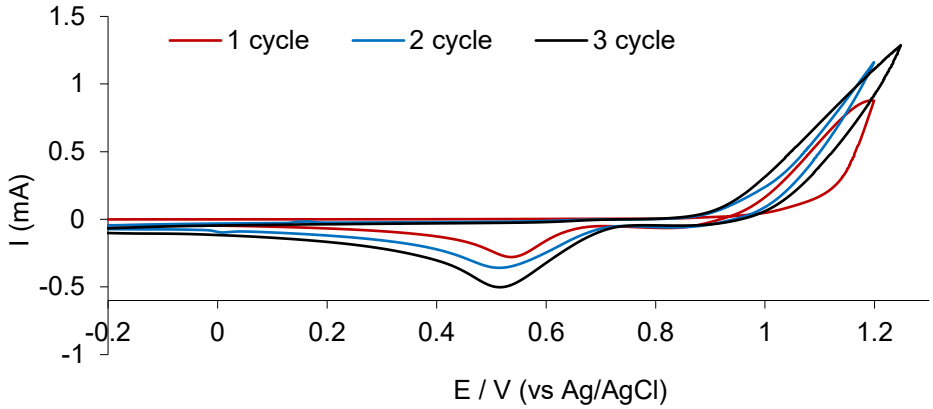


Figure 19. Cyclic voltammetry data over three cycles of gold *QSense*® sensor cleaning

A visual inspection of the curves reveals noticeable differences, providing preliminary insights into the quality of the gold surface. Notably, an oxygen desorption peak is observed at approximately 0.5 V, which is characteristic of clean gold surfaces. This peak indicates that the gold surface has been appropriately cleaned and activated, thereby confirming its readiness for subsequent biofunctionalization.

3.1.2.2. SAM surface characterization

Fourier Transform Infrared Spectroscopy (FTIR) is a powerful analytical technique used to investigate molecular bonding, chemical modifications, and biomolecular interactions with surfaces. FTIR spectra illustrate the effect of varying 12-MUA and 6-MCH ratios on the SAM surface with immobilized T7 DNA polymerase enzyme (*Figure 20*). This study examines the fundamental principles, chemical bond alterations, and their impact on enzyme activity and stability, aiming to establish a scientific basis for the conducted sequence of experiments.

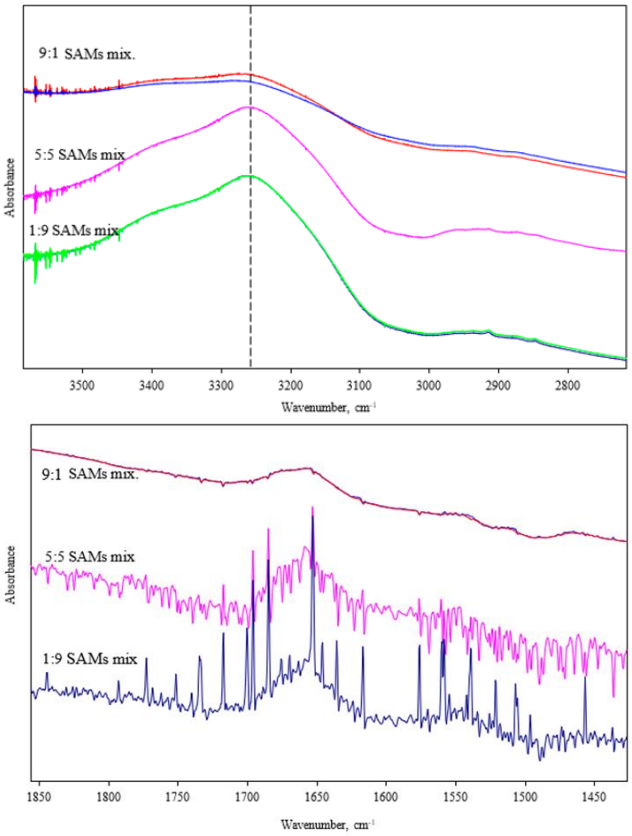


Figure 20. Immobilized T7 DNA polymerase on SAM mix with FTIR analysis

FTIR analysis reveals that the COOH/OH ratio has a significant impact on enzyme binding and catalytic performance. A balanced 5:5 SAM mix composition optimally supports stable enzyme attachment. The data indicate that enzyme efficiency depends on the binding strength, surface chemistry, and structural organization. Enzymes perform best on hydrophilic surfaces that maintain hydration while allowing sufficient attachment. The 5:5 SAM mix composition promotes electrostatic interactions and flexibility, while balancing stability and activity in order to prevent constrained mobility that hinders substrate interaction.

Carboxyl groups (COOH, ~1700 cm^{-1}) play a crucial role in enzyme attachment, forming covalent or electrostatic interactions with amino groups (-NH_2) via amidation reactions or charge-based interactions. A high COOH content (9:1 SAM mix) exhibits a pronounced C=O absorption band (~1700 cm^{-1}), indicating active COOH participation in enzyme interactions. The mode of interaction – electrostatic or covalent – depends on the experimental conditions. An increased COOH content enhances electrostatic interactions and enzyme immobilization, with a strong C=O band signifying an active COOH involvement, while weaker O-H and C-O bands suggest reduced hydroxyl participation. In contrast, a low COOH content (1:9 SAM mix) reduces the carbonyl absorption band, thus reflecting a reduced COOH-mediated enzyme attachment. Meanwhile, an elevated OH content produces a hydrophilic surface, favoring enzyme activity through hydrogen bonding but providing weaker chemisorption. In such cases, the FTIR spectrum exhibits a

strong O-H stretching band (~3300 cm^{-1}) and prominent C-O vibrations (~1000–1200 cm^{-1}).

A balanced COOH and OH ratio (5:5 SAM mix) generates a mixed interfacial environment, stabilizing enzyme attachment through electrostatic interactions with COOH and hydrogen bonding with OH. FTIR spectra display a moderate-intensity carbonyl band (~1700 cm^{-1}) and proportional C-O/C-OH vibrations (~1000–1200 cm^{-1}), confirming this balanced interaction. Stronger attachment correlates with more excellent stability but it may reduce enzyme flexibility and catalytic efficiency.

Hydroxyl groups (OH, ~3300 cm^{-1}) influence hydrophilicity and the enzyme structural stabilization through hydrogen bonding with water and biomolecules. A high OH content (1:9 SAM mix) results in a pronounced O-H stretching band (~3300 cm^{-1}), thus indicating a more hydrophilic surface that can enhance the enzyme activity when the catalytic center functions in an aqueous environment. Conversely, a low OH content (9:1 SAM mix) weakens the O-H band, thereby indicating a less hydrophilic surface, potentially reducing enzyme-solvent interactions. Excess hydroxyl groups may hinder strong enzyme-surface interactions, while an insufficient OH content can lead to enzyme aggregation or denaturation on a hydrophobic surface.

C-O and C-OH vibrations (~1000–1200 cm^{-1}) provide insight into surface functionalization and the structural integrity of SAMs. The 1:9 SAM mix exhibits strong C-O/C-OH absorption, reflecting active hydroxyl interactions. However, excessive hydroxyl interactions may result in a weak enzyme attachment, leading to instability and desorption under experimental conditions. Conversely, the 9:1 SAM mix shows weaker C-O absorption, indicating a more significant COOH influence on surface interactions. A reduced hydroxyl participation leads to stronger enzyme binding, which may impose structural constraints and a lower catalytic activity. These variations underscore the crucial role of SAM composition in regulating the surface properties and the enzyme adsorption behavior.

The FTIR spectral analysis elucidates the effects of COOH- and OH-terminated alkanethiol molar ratios on the SAM formation and the subsequent enzyme immobilization. The spectral feature around 3300 cm^{-1}, indicative of hydrogen-bonded O-H stretching, varies significantly with the composition. The 9:1 SAM mixture, enriched in carboxylic acid (COOH) groups, exhibits a broad absorption band, suggesting strong hydrogen bonding that facilitates enzyme attachment via covalent or electrostatic interactions. The 5:5 SAM mixture exhibits a moderate absorption intensity, indicating a balanced distribution of COOH and OH groups that supports enzyme immobilization through combined interactions. In contrast, the 1:9 SAM mixture, dominated by OH-terminated alkanethiols, exhibits a reduced absorption around 3300 cm^{-1}, implying weaker hydrogen bonding and a limited enzyme attachment due to a lower COOH content. These findings confirm that an increased COOH content enhances the enzyme immobilization efficiency, thus influencing the stability and the catalytic activity of the immobilized enzyme on the SAM surface.

The molar ratio of *12-Mercaptoundecanoic Acid* (12-MUA) to *6-Mercaptohexanol* (6-MCH) in the SAM plays a crucial role in determining the surface properties that influence enzyme immobilization. A higher proportion of 12-MUA increases the density of carboxyl functional groups available for covalent coupling via the EDC/NHS chemistry, thereby potentially enhancing the efficiency of enzyme immobilization. However, excessive 12-MUA can lead to steric hindrance and a reduced accessibility for biomolecular interactions. The inclusion of 6-MCH modulates the hydrophilicity and the packing density of the *Self-Assembled Monolayer* (SAM). A balanced ratio of 12-MUA to 6-MCH optimizes surface hydration and minimizes non-specific adsorption, while promoting proper enzyme

orientation and activity. An optimal molar ratio [100,101] ensures a well-ordered monolayer with minimal defects, reducing non-specific binding and improving the sensor reproducibility. A 12-MUA content that is too high may lead to irregular packing due to electrostatic repulsion between carboxyl groups, whereas excessive 6-MCH may reduce the functionalization efficiency by limiting the available binding sites. The molar ratio also influences the microenvironment surrounding the immobilized enzyme. A well-tuned SAM composition supports the enzyme conformational stability as well as the functional activity, whereas an imbalanced ratio may lead to enzyme denaturation or a restricted substrate access. The influence of T7 polymerase immobilization on different molar ratios of SAM shall be investigated in the next section of our study.

3.1.2.3. Characterization of enzyme-based sensor QCM data

QCM registers a change in resonance frequency proportional to the mass deposited on the surface [102,103]. The experimental T7 DNA polymerase immobilization/adsorption kinetic and layer thickness investigation scheme is shown in *Figure 21*. Each point of the frequency change represents the meaning of triplicated measurements carried out under stable conditions while using different SAM mixture surfaces at room temperature. At physiological conditions (pH 7.4), the peptide bond formation and the T7 DNA polymerase adsorption process on the gold-coated electrode with the QCM system indicate changes in Δf during the process. The real-time QCM profile refers to the adsorption process of T7 DNA polymerase.

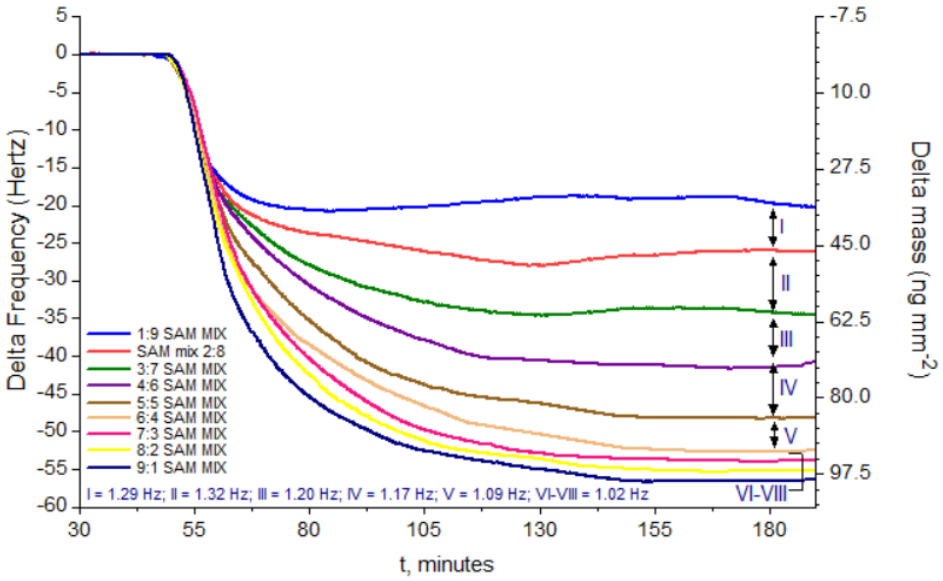


Figure 21. Experimental QCM profile and recorded data of T7 DNA polymerase immobilization on the gold surface of this study. The frequency signal and time profile during the experiment. Measurements were taken after the initial equilibrium phase (<30 min) while using pure 1X PBS (pH 7.4) buffer at room temperature. With the introduction of EDC/NHS for self-assembled monolayers and carboxyl group activation, the frequency shift signals remain stable at 30–50 min intervals. These 'no changes' indicate that, before kinetic measurements, Au/12-MUA+6-MCH surface washing in nuclease-free water for 30 min at room temperature at a rate of 1 ml/min in a closed cell is sufficient to remove non-

specifically absorbed 12-MUA, 6-MCH, and other molecules. Within the 50–150 min interval, the introduction of the 0.69 μM T7 DNA polymerase solution caused a sudden drop in the frequency signal, followed by a slight decrease in frequency. The significant frequency shift changes indicated that the covalent attachment of 0.69 μM T7 DNA polymerase occurs efficiently and proportionally on all SAM mixture (i.e., from 1:9 to 9:1) surfaces. The formation of T7 DNA polymerase layers on Au/12-MUA+6-MCH after enzyme injection occurs on the surface, dependent on the molar number of active carboxyl groups. As the number of carboxyl groups on the surface increases, the adsorption efficiency increases. The 150–200 min interval shows a stably formed Au/12-MUA+6-MCH/T7 DNA polymerase monolayer

During the T7 DNA polymerase adsorption process, a sudden drop in the resonance frequency (Δf) signal was observed after the QCM sensor had been incubated with all evaluated gold-coated electrodes and various SAM mixtures. The resonance frequency shift (Δf) values decrease proportionally with the increasing number of carboxyl groups on the surface (see *Figure 21*). The first abrupt signal change is associated with the rapid adsorption of T7 DNA polymerase over the surface of the SAM mixture. As a result of (i) maximum mass transport rate through the boundary layer above the self-assembled monolayer surface, the enzyme concentration in contact with the surface is zero at the beginning of the loading step; and (ii) complete availability of the sensor surface to bind the enzyme molecules. After the stabilization of the resonance frequency by 1X PBS (pH 7.4) solution at room temperature, the steady-state frequency shifts were obtained after 30–100 min (time interval from 50 min to 80 min for 1:9 SAM mixture, and from 50 min to 150 min for 9:1 SAM mixture composition), respectively. The subsequent washing step with 1X PBS (pH 7.4) was performed in order to desorb unabsorbed T7 DNA polymerase molecules from the gold surface and/or to rearrange the enzyme to achieve lower energy configurations and alter its local conformation. The dynamic changes that occurred made additional adsorption sites available on the surface, resulting in slow but steady adsorption necessary to increase the concentration of the adsorbed enzyme, and ultimately to reach the saturation stage. At this final condition, a dynamic equilibrium is reached between the new T7 DNA polymerase molecules adsorbing on the surface and the same molecules leaving the SAM-modified QCM-sensor surface. The lack of significant frequency change during T7 DNA polymerase adsorption on the 7:3, 8:2, and 9:1 SAM mixture surfaces demonstrates that the entire electrode surface of the QCM sensor was covered and saturated by T7 DNA polymerase molecules at room temperature. It is worth noting that approximately 80% of all molecules are immobilized within the initial 30 minutes at room temperature during the immobilization stage. Because of the QCM flow chamber design and the chosen flow rate (0.1 ml minute^{-1}), such primary covalent attachment is likely limited by enzyme diffusion through the boundary layer rather than by the surface reaction itself. The data indicate that the amount of T7 DNA polymerase immobilized on the surface increases if the concentration of the SAM mixtures is increased.

Assuming that the immobilization process is kinetically controlled, the adsorbed layer is rigidly connected to the sensor, and the viscoelastic effects are negligible (in this study, a value of <10 was established), we attempted to fit the change in the resonant frequency of all measurements to the Sauerbrey [104] equation in order to evaluate the T7 DNA polymerase masses accumulated on the surface, respectively:

$$\Delta m = -\frac{C}{n}\Delta f_n \qquad (13)$$

where: Δf_n is the frequency change (Hz); C is the mass sensitivity constant (17.7 ng cm^{-2} Hz^{-1} at a 5 MHz system); and n is the number of harmonics or the frequency overtone number [105]. In this study, the covalently attached T7 DNA polymerase on surfaces does not behave as a viscous layer (the dissipation shift observed for the frequency change is small, $\Delta D/(-\Delta f/n) < 4\times10^{-7}$ Hz^{-1}), hence, energy dissipation does not affect the changes in the measured resistance frequency. The Sauerbrey model sufficiently estimates the actual mass of the adsorbed layer. By inserting the resonance frequency change, Δf_n, that results from Δm of the addition of the Au/12-MUA+6-MCH/T7 DNA polymerase layer. We applied regression analysis to each step in order to determine the thickness of the formed Au/12-MUA+6-MCH/T7 DNA polymerase monolayer modification, following a detailed procedure described below.

3.1.2.4. Characterization of enzyme-based sensor kinetic models

This study employs pseudo-first-order, pseudo-second-order, and n-rate law kinetic models of an arbitrary order to investigate the covalent attachment kinetics of T7 DNA polymerase on different SAM mixtures. The following equations are used, assuming that the measured concentrations correspond to Au/12-MUA+6-MCH/T7 DNA polymerase surface concentrations. These three rate equations are among the most widely applied for enzyme and protein immobilization from liquid solutions:

$$m(t) = m_{max}[1 - e^{-k_1 \times t}] \qquad (14)$$

$$m(t) = m_{max}\frac{k_2 \times m_{max} \times t}{1 + k_2 \times m_{max} \times t} \qquad (15)$$

$$m(t) = m_{max} - [m_{max}^{1-n} + (n-1) \times k_n \times t]^{\frac{1}{1-n}} \qquad (16)$$

where: m_{max} and $m(t)$ denote the amounts of the adsorbed T7 DNA polymerase (ng) at equilibrium and at any time t (min), respectively; k_1 (min $^{-1}$); k_2 (ng min $^{-1}$) and k_n represent the immobilization rate constant of the pseudo-first, pseudo-second, and rate law of arbitrary orders (for n≠1, the solution to this equation with m (t=0) = 0) models, respectively. The fitting curves (see *Figure 22*) represent the pseudo-first, pseudo-second, and rate law of arbitrary order equations, and the extracted parameters for each SAM mixture are reported. The correlation coefficients (R^2) of the fitted lines for first, second, and rate law of arbitrary order models are higher than 0.93 (except for pseudo-second order determined for 1:9 ratio-based SAM), thus indicating the agreeable fitting of the kinetic models on the experimental data. The pseudo first- and second-order equations fitted well with the experimental data. A comparison of the experimental adsorption capacity and the theoretical value is presented in *Figure 22*. The theoretical m_{max} value estimated from the rate law of the arbitrary order kinetic model gave a significantly different value than the experimental value. However, the correlation coefficient was found to be higher. These results showed that the first- and second-order kinetic models are proper for this T7 DNA polymerase immobilization system study. However, the theoretical m_{max} value for the immobilization was very close to the experimental m_{max} value in the case of first-order kinetics. The first-order kinetics best described these study data.

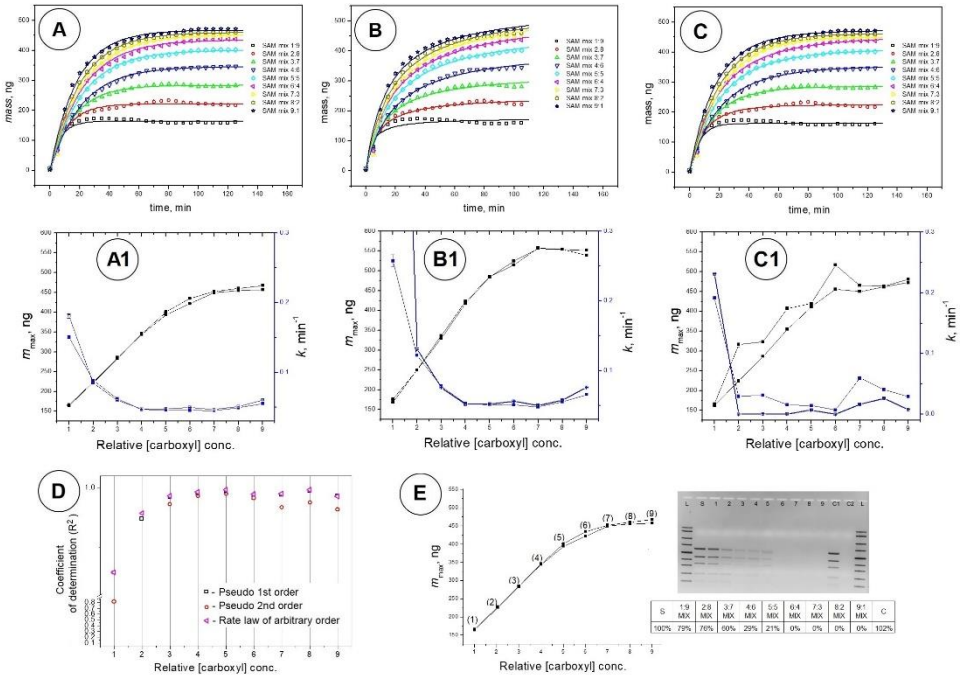


Figure 22. Experimental kinetic data. The amounts of immobilized T7 DNA polymerase on different SAM mixture surfaces were incorporated in the gold sensor for 120 min. The dependence of the maximum adsorbed mass of T7 DNA polymerase and reaction rate at different SAM mixtures by (**A1**) – pseudo-first, (**B1**) – pseudo-second, and (**C1**) – rate law of arbitrary order models. **D** – Assessment of data correlation quality. **E** – Au/12-MUA+6-MCH/T7 DNA polymerase monolayer surface saturation is achieved at a 6:4 SAM mixture composition. Agarose gel electrophoresis shows immobilized T7 DNA polymerase activity after 18 hours of enzymatic activity at room temperature. L – DNA fragment ladder. S – substrate of response. C1 – negative control, substrate on gold Q-sense without enzyme. C2 – positive control, 400 ng enzyme with 15 ng of the substrate in an *in vitro* reaction. 1 (1:9 SAM mixture) – 9 (9:1 SAM mixture) on different surfaces and T7 DNA polymerase exonuclease activity results. The DNA fragment degradation shows that the total enzymatic activity is retained from a 6:4 to a 9:1 ratio-based SAM

Revellame et al. [106] comprehensively reviewed adsorption kinetic modeling while using pseudo-first-order and pseudo-second-order rate laws. They discussed the utility of these models in studying the immobilization kinetics of enzymes and proteins from liquid solutions onto solid surfaces. Similarly, Ezzati et al. [107] derived pseudo-first-order and pseudo-second-order rate equations from Langmuir and the Freundlich isotherms for adsorption studies. In our study, similar kinetic models were employed to analyze the immobilization of masked T7 DNA polymerase. The pseudo-first-order and pseudo-second-order models used in our research align with those reviewed by Revellame et al. and Ezzati et al. Our study's calculated results from different kinetic models showed that the pseudo-first-order model provided the highest equilibrium amount of an adsorbed enzyme (m_{max} = 427.95 ng) with a high correlation coefficient (R^2 = 0.992). Furthermore, the experimental data in our study (436.34 ng) closely matched the calculated results from the kinetic models, particularly the pseudo-first-order. This agreement between the

experimental and the modeled data reinforces the validity of using these kinetic models for enzyme immobilization studies, as suggested by Revellame et al. and Ezzati et al.

This study section investigated the functionality of immobilized T7 DNA polymerase on electrodes. The preservation of the T7 DNA polymerase activity after immobilization was achieved by protecting the enzyme's active site with partial DNA. This approach ensures that the active sites are excluded from the immobilization reaction, thus allowing the enzyme to maintain the correct orientation after immobilization. A cofactor, such as magnesium, is sufficient to restore the enzyme activity in the system. We measured the specificity of the immobilized enzyme to evaluate the performance of the T7 DNA polymerase sensor. The amount of the immobilized enzyme was calculated, and the double-stranded DNA substrate suitable for measuring 3'→5' exonuclease activity concentration, according to the T7 DNA polymerase processivity, was selected [108–110]. After 18 hours of enzymatic reaction with the buffer solution containing magnesium and 15 ng of the double-stranded DNA fragment at room temperature, the reaction products were visualized by agarose gel electrophoresis, and the change in the degradation of the substrate fragments was observed in *Figure 22*. The results show that the QCM sensor with immobilized 427.95 ± 0.60 ng of T7 DNA polymerase could specifically cleave 15 ng of double-stranded DNA fragments during overnight incubation at room temperature. These results demonstrate that the immobilized 10 ng of T7 DNA polymerase corresponds to a 1.20 Hz frequency change. In particular, the results indicate that immobilized T7 DNA polymerase is fully functional on all surfaces of the evaluated SAM mixtures, and the enzyme's active site was well protected from inactivation.

Table 5. Parameters extracted from the fitting curves

Equation	SAM mixture	m_{max} , ng	k	Reaction order	R^2
Pseudo 1st order; Equation (2)	1:9	166.09 ± 0.29	$1.46\times10^{-1} \pm 1.88\times10^{-3}$	1	0.939
	2:8	223.16 ± 0.32	$8.66\times10^{-2} \pm 6.56\times10^{-4}$	1	0.975
	3:7	284.72 ± 0.30	$6.13\times10^{-2} \pm 2.79\times10^{-4}$	1	0.992
	4:6	344.47 ± 0.38	$4.73\times10^{-2} \pm 1.88\times10^{-4}$	1	0.995
	5:5	396.50 ± 0.33	$4.71\times10^{-2} \pm 1.40\times10^{-4}$	1	0.997
	6:4	427.95 ± 0.60	$4.74\times10^{-2} \pm 2.42\times10^{-4}$	1	0.992
	7:3	452.95 ± 0.56	$4.50\times10^{-2} \pm 1.96\times10^{-4}$	1	0.994
	8:2	457.87 ± 0.33	$4.97\times10^{-2} \pm 1.36\times10^{-4}$	1	0.998
	9:1	462.87 ± 0.55	$1.46\times10^{-1} \pm 1.88\times10^{-3}$	1	0.992
Pseudo 2nd order; Equation (3)	1:9	178.30 ± 0.76	$2.45\times10^{-1} \pm 8.35\times10^{-3}$	2	0.827
	2:8	252.95 ± 0.49	$1.17\times10^{-1} \pm 1.21\times10^{-3}$	2	0.981
	3:7	335.65 ± 0.63	$7.40\times10^{-2} \pm 5.87\times10^{-4}$	2	0.990
	4:6	423.49 ± 0.79	$5.09\times10^{-2} \pm 3.27\times10^{-4}$	2	0.994
	5:5	488.80 ± 0.89	$5.01\times10^{-2} \pm 3.13\times10^{-4}$	2	0.995
	6:4	528.30 ± 1.29	$5.02\times10^{-2} \pm 4.18\times10^{-4}$	2	0.991
	7:3	566.57 ± 1.94	$4.59\times10^{-2} \pm 5.13\times10^{-4}$	2	0.985
	8:2	561.38 ± 1.49	$5.34\times10^{-2} \pm 5.00\times10^{-4}$	2	0.989
	9:1	556.32 ± 1.66	$6.41\times10^{-2} \pm 7.43\times10^{-4}$	2	0.982
Rate law of arbitrary order; Equation (4)	1:9	163.79 ± 0.28	$2.04\times10^{-1} \pm 2.17\times10^{-5}$	$0.93 \pm 2.77\times10^{-3}$	0.943
	2:8	233.72 ± 0.76	$8.97\times10^{-3} \pm 1.05\times10^{-3}$	$1.45 \pm 2.25\times10^{-2}$	0.985
	3:7	296.36 ± 0.76	$1.25\times10^{-2} \pm 9.72\times10^{-4}$	$1.30 \pm 1.41\times10^{-2}$	0.995
	4:6	365.80 ± 1.29	$7.50\times10^{-3} \pm 6.58\times10^{-4}$	$1.32 \pm 1.49\times10^{-2}$	0.997
	5:5	412.34 ± 0.92	$1.35\times10^{-2} \pm 7.79\times10^{-4}$	$1.21 \pm 9.68\times10^{-3}$	0.998
	6:4	453.66 ± 2.19	$7.63\times10^{-3} \pm 9.43\times10^{-4}$	$1.31 \pm 2.02\times10^{-2}$	0.994

	7:3	448.20 ± 0.99	6.48×10^{-2} ± 4.14×10^{-3}	0.94 ± 1.10×10^{-2}	0.994
	8:2	457.73 ± 0.64	5.03×10^{-2} ± 2.17×10^{-3}	1.00 ± 7.39×10^{-3}	0.998
	9:1	465.81 ± 1.06	4.32×10^{-2} ± 3.34×10^{-3}	1.05 ± 1.33×10^{-2}	0.992

Using a structure-based, well-engineered T7 DNA polymerase enables the system to analyze the possibilities and properties of the effective immobilization of this enzyme on QCM resonators. The QCM technique represents a fundamental and innovative approach to improving DNA-modifying enzyme-based biosensors. The results confirm that QCM-based determination of DNA is highly sensitive [111–113], offers a fast response [114,115], is suitable for real-time measurements [116,117], is inexpensive [118], and can be used out of the lab [119,120]. When using QCM probes, no additional markers, labels, or mediators are required to determine the analytical signal effectively. The quantitative results demonstrate that T7 DNA polymerase with a masked active site can be almost completely immobilized on various SAM mixture composition surfaces without losing functionality. A robust QCM assay has confirmed that T7 DNA polymerase is specific, and surface saturation is achieved on a 6:4 ratio-based SAM with an immobilized enzyme surface concentration.

As shown in free *T7* DNA polymerase studies, 1 µg (1000 ng) of DNA was fully hydrolyzed by 12.5 U of free T7 DNA polymerase over 21 hours, demonstrating the enzyme's capability to degrade a large amount of DNA in a prolonged reaction. In immobilized enzyme studies, 3 U (or 427.95 ± 0.60 ng) of T7 DNA polymerase hydrolyzed only 15 ng of DNA, thus highlighting a difference in the catalytic efficiency between free and immobilized enzyme systems. The immobilized enzyme shows a ~6.25% (immobilized enzyme cleaves ~0.000066 ng of DNA fragment per 1 U T7 DNA polymerase per second; free – ~0.00106 ng of DNA fragment per 1 U T7 DNA polymerase per second) as an efficient degradation capacity per unit over the same reaction time, likely due to restricted diffusion, steric hindrance, or altered enzyme dynamics when immobilized.

3.1.2.5. Characterization of enzyme-based sensor re-usage

In order to characterize the reusability of immobilized T7 DNA polymerase, the enzyme-functionalized QCM sensors prepared with a 6:4 ratio of Au/12-MUA+6-MCH were subjected to multiple cycles of DNA hydrolysis. The study aimed to evaluate the extent to which the enzyme retained its 3'→5' exonuclease activity after repeated use, which is critical for determining its applicability in long-term biosensing platforms. The time-series data from the QCM and the immobilization efficiency of masked T7 DNA polymerase on a 6:4 ratio SAM mixture sensor surface are presented in *Figure 23*. The sharp decline observed in our frequency of investigation after 40 minutes indicates a rapid binding of masked T7 DNA polymerase to the sensor surface, reflecting an efficient initial immobilization phase. The magnitude of this frequency shift (Δf) correlates with the mass of masked T7 DNA polymerase immobilized on the surface. Following the initial binding, the frequency stabilizes, which signifies that the system has reached equilibrium with minimal further changes in mass on the surface. The tightly clustered Δf_{max} values across the three experimental runs (-52.06 Hz, -52.37 Hz, and -52.59 Hz) indicate a high reproducibility and a consistent immobilization efficiency of masked T7 DNA polymerase on the Au/12-MUA+6-MCH layer. The minimal variability between the runs suggests that the immobilization conditions are optimized for stable attachment of the enzyme, thus providing a reliable platform for further analysis of applications involving masked T7 DNA polymerase on sensor surfaces.

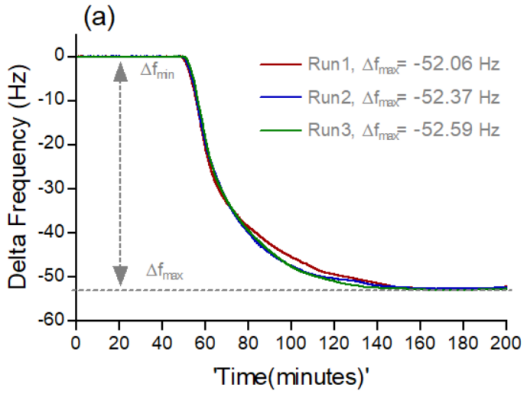


Figure 23. Experimental QCM profile and recorded data of masked T7 DNA polymerase immobilization (**a**) and saturation (**b)** on the gold surface covered with 6:4 ratio SAM mixture

Two different incubation durations, 45 and 90 minutes, were used to examine how the reaction time influences the functional stability and reusability of the immobilized enzyme on 6:4 ratio Au/12-MUA+6-MCH functionalized electrodes (see *Figure 24*). After each reaction cycle, the electrode surface was washed and reused under identical conditions in order to simulate the practical regeneration of the sensor. The reuse stability and exonuclease activity efficiency of immobilized masked T7 DNA polymerase were analyzed by using 2% TAE agarose gel electrophoresis and optical band volume analysis. The experimental setup, including control lanes ('K') – the reaction without an enzyme and incremental reuse cycles (1–5) – allows for the assessment of the exonuclease function and the potential degradation of the double-stranded DNA fragment over successive cycles. The 2% TAE agarose gel electrophoresis image reveals changes in the DNA band intensity, indicating a reduction in the hydrolysis efficiency of the DNA substrate after multiple runs. Reaction times of 45 minutes (a) and 90 minutes (b) were used to simulate different substrate processing conditions. The electrophoresis data were converted to the optical band volume by using the *TotalLab* system to quantify the changes in the band intensity, thus providing objective insights into the enzyme's reusability and relative activity. Further analysis aims to correlate the optical band volume with the exonuclease activity for each reuse cycle, mainly if a decline is observed with successive cycles.

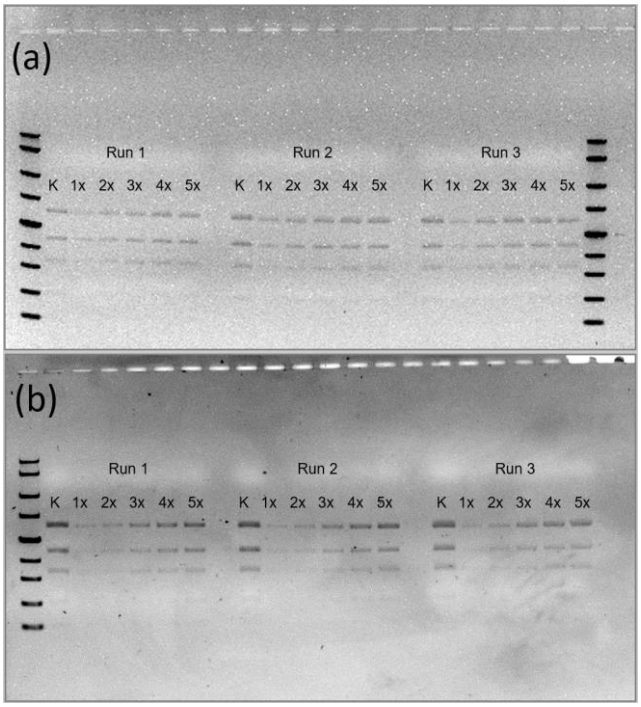


Figure 24. Reuse Study of Au/12-MUA+6-MCH/T7 DNA Polymerase Monolayer via Agarose Gel Electrophoresis. Agarose gel (2% TAE+SYBR Safe) electrophoresis demonstrates the reuse of immobilized, masked T7 DNA polymerase on an Au/12-MUA+6-MCH monolayer, specifically examining its exonuclease activity across multiple cycles (1–5). Agarose gel electrophoresis was used to assess the enzyme function after each cycle, with two reaction times – 45 minutes (**a**) and 90 minutes (**b**) – at room temperature, using a 1 ng double-stranded DNA fragment as the substrate

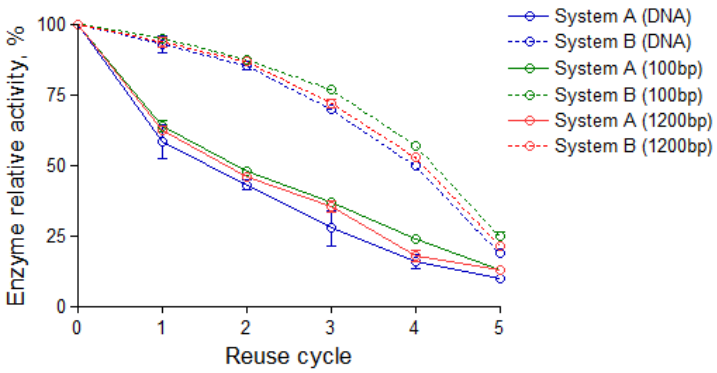


Figure 25. Reuse efficiency of immobilized masked T7 DNA polymerase under two conditions: System A (the solid line), a 45-minute reaction, and System B (the dashed line), a 90-minute response, with the same concentration of 1 ng of double-stranded DNA fragment. The y-axis shows the enzyme's relative activity in percentage values, while the x-axis represents the number of reuse cycles (0 to 5). In the image, DNA represents the Low DNA Mass Ladder, where 100 bp indicates the hydrolysis of 100 bp DNA length fragments, whereas 1200 bp indicates the hydrolysis of 1200 bp DNA length fragments

Reuse studies of the optical band volume that quantify changes in the band intensity show (as presented in *Figure 25*) that the enzyme activity declines significantly with each reuse cycle in a 45-minute reaction system with a 1 ng double-stranded DNA fragment (System A), dropping to approximately 25% by the third cycle and nearly depleting by the fifth cycle. In contrast, the enzyme activity is more stable over multiple cycles in a 90-minute reaction system with one ng double-stranded DNA fragment (System B). By the third reuse cycle, System B retains about 50% of its initial activity, whereas, by the fifth cycle, it maintains around 20%, thus indicating an improved stability, if compared to System A.

Kumar et al. [108] explored the structural and functional aspects of T7 DNA polymerase, emphasizing its high processivity [108–110] and fidelity during DNA synthesis. Wuite et al. [109] investigated the mechanical properties of T7 DNA polymerase, highlighting its ability to unwind DNA and perform the exonuclease functions efficiently. This study immobilized masked T7 DNA polymerase on a gold surface and achieved saturation when using a 6:4 SAM mixture ratio of thiolated linkers. This approach likely contributed to the enzyme's stability by creating an environment conducive to its activity. Our results demonstrate that immobilization significantly influences the reuse efficiency observed between the 45-minute and 90-minute reaction times. When enzymes are immobilized, their movement – and thus their ability to access the substrate – can be restricted, thus impacting their activity and the overall efficiency depending on the reaction duration [121], leading to changes in the enzyme structure. In shorter reaction times, such as 45 minutes, immobilized enzymes may require more time to interact with the substrate fully. A restricted accessibility to the active site can lead to incomplete substrate processing and a more rapid decline in activity across reuse cycles, potentially due to minor denaturation or limitations of the active site. On the other hand, the 90-minute reaction time provides the immobilized enzyme with more time to process the substrate thoroughly, even under conditions of spatial restrictions. This extended duration may facilitate a more vital substrate-enzyme interaction, allowing for more efficient turnover and reducing the adverse effects of immobilization. As our results indicate, the 90-minute setup enables the immobilized enzyme to retain its effectiveness better across successive reuse cycles, thus enhancing the overall stability. These findings highlight the crucial role of the reaction time and immobilization conditions in optimizing the enzyme reuse in practical applications. The 90-minute reaction time may be ideal for applications requiring enzyme stability and efficiency over multiple cycles, allowing the enzyme to perform at a high level despite immobilization constraints.

The successful immobilization and stability of masked T7 DNA polymerase indicate that similar approaches could be employed for other enzymes used in industrial biocatalysis. Industries can achieve reusable and stable catalysts by immobilizing enzymes on suitable surfaces, reducing costs, and improving the process efficiency. This is particularly relevant for large-scale production processes where enzyme reusability is crucial. Similarly, in the pharmaceutical industry, immobilized enzymes can be used for the synthesis of complex molecules, drug development, and biotransformation processes [122]. The demonstrated stability and reusability of immobilized T7 DNA polymerase can be leveraged to develop more efficient and cost-effective enzymatic processes for drug synthesis and production. The food industry can benefit from immobilized enzymes for various applications, including an improved product shelf life, enhanced flavors, and processing ingredients [123]. Usage of immobilized enzymes in biofuel production can improve the efficiency of biomass conversion processes [124]. The stability and reusability of the immobilized T7 DNA polymerase demonstrated in this study can be applied to enzymes involved in breaking down biomass into fermentable sugars, thereby improving

the overall efficiency and sustainability of biofuel production [125]. Developing enzyme-based biosensors can significantly benefit from the immobilization techniques demonstrated in this study. Immobilized enzymes, such as T7 DNA polymerase, can be used in biosensors for medical diagnostics, environmental monitoring, and food safety testing, providing precise and reliable analyses. To further improve immobilization techniques, future research can focus on optimizing immobilization protocols to enhance the enzyme stability and activity. Exploration of different surface materials, linker molecules, and immobilization conditions can lead to the development of more robust and efficient immobilized enzyme systems. Combining immobilization techniques with enzyme engineering approaches can enhance the properties of enzymes, including their stability, activity, and selectivity. Research can explore the synergistic effects of immobilization and genetic or chemical modifications to create tailor-made enzymes for specific applications.

3.1.2.6. Characterization of enzyme-based sensor hydrolysis

Immobilized T7 DNA polymerase hydrolysis was evaluated using QCM by monitoring real-time frequency shifts upon exposure to Proteinase K in order to characterize the enzyme-based sensor hydrolysis. As shown in *Figure 26*, the QCM data reveal distinct frequency shifts corresponding to different SAM compositions. The initial frequency drop confirms the successful immobilization of T7 DNA polymerase, as already described above. At the same time, the subsequent increase upon Proteinase K exposure indicates enzymatic hydrolysis and mass loss due to protein degradation. The hydrolysis efficiency varied among SAM compositions, with more densely packed monolayers exhibiting an excellent enzyme stability, leading to slower hydrolysis rates. The frequency shifts (Δf) change from -55 Hz to -10 Hz depending on the SAM composition, correlating with mass changes of 10–97.5 ng/mm². The data suggest that specific SAM ratios influence the enzyme's susceptibility to hydrolysis, impacting its stability and potential for biosensing applications. These findings provide insight into optimizing the surface chemistries for an improved enzyme immobilization and longevity in biosensor designs.

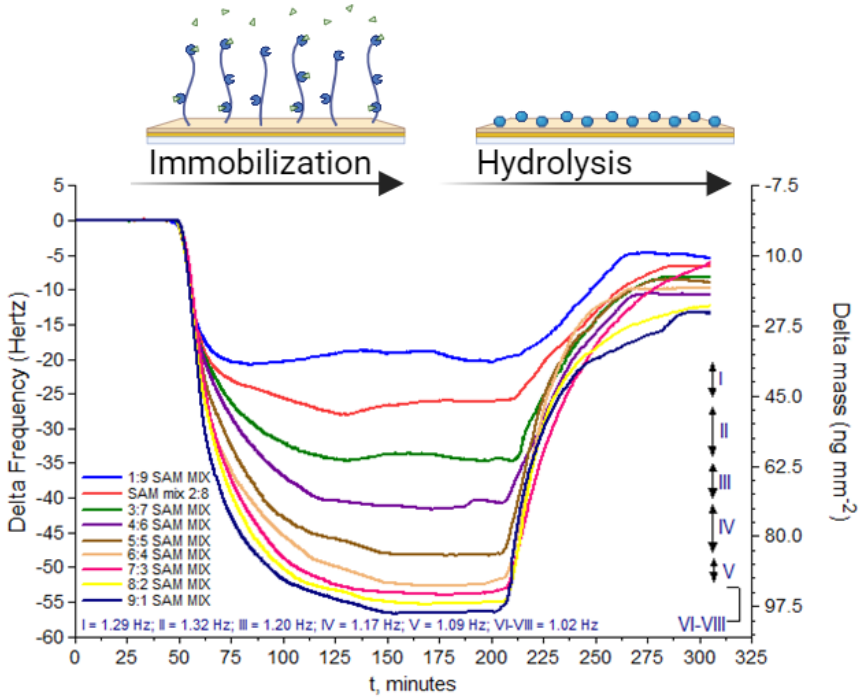


Figure 26. QCM frequency shifts during immobilization and hydrolysis of T7 DNA polymerase on various SAM-modified electrodes. The frequency signal and the time profile during the experiment. Measurements were taken after the initial equilibrium phase (<30 min) when using a pure 1X PBS (pH 7.4) buffer at room temperature. With the introduction of EDC/NHS for self-assembled monolayers and carboxyl group activation, the frequency shift signals remain stable at 30–50 min intervals. These 'no changes' show that, before kinetic measurements, Au/12-MUA+6-MCH surface washing in nuclease-free water for 30 min at room temperature, at a rate of 1 ml/min, in a closed cell, is sufficient to remove non-specifically absorbed 12-MUA, 6-MCH, and other molecules. Within the 50–150 min interval, introduction of the 0.69 µM T7 DNA polymerase solution caused a sudden drop in the frequency signal, followed by a slight decrease in frequency. The significant frequency shift changes indicated that the covalent attachment of 0.69 µM T7 DNA polymerase occurs efficiently and proportionally on all SAM mixture (from 1:9 to 9:1) surfaces. The formation of T7 DNA polymerase layers on Au/12-MUA+6-MCH after enzyme injection occurs on the surface, dependent on the molar number of active carboxyl groups. As the number of carboxyl groups on the surface increases, the adsorption efficiency increases. As shown in the insert, steady-state conditions were achieved after 150 minutes of the measurement process. The 150–200 min interval shows a stably formed Au/12-MUA+6-MCH/T7 DNA polymerase monolayer. After 200 minutes, the Proteinase K performance was introduced, resulting in the hydrolysis of polymerase from the Au/12-MUA+6-MCH/T7 DNA polymerase monolayer surface and a slight increase in frequency

When applying the classical theory of enzymatic catalysis, the reaction between the substrate (S) and the enzyme (E) proceeds through an intermediate active complex (ES), ultimately forming the product (P). This process follows a two-step mechanism:

$$S + E \underset{k_{des}}{\overset{k_{ads}}{\rightleftarrows}} ES \xrightarrow{k_{cat}} P + E \qquad (17)$$

where: the rate constant k_{ads} describes the formation of the active complex ES according to a second-order reaction mechanism; k_{des} is the first-order rate constant for dissociating ES back into the initial reactants; and k_{cat} is the first-order rate constant for product formation. The constant k_{cat} is directly related to the enzyme's catalytic activity and is, therefore, referred to as the catalytic constant of the enzymatic reaction.

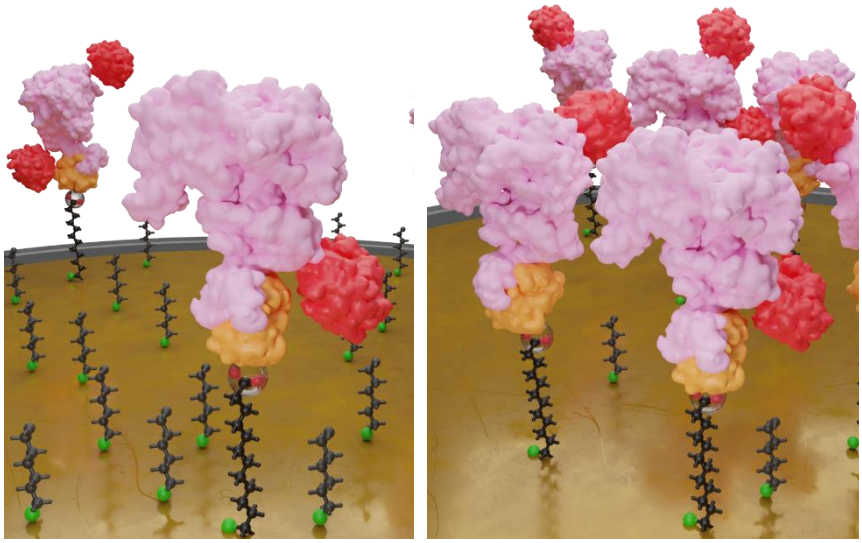


Figure 27. Immobilized T7 DNA polymerase hydrolysis with Proteinase K. The light pink color represents immobilized polymerase with the orange thioredoxin domain. The red color indicates that the Proteinase K protein is ready for hydrolysis. Both pictures depict the same information from different concentrations of T7 DNA polymerase in the sensor

In the studied system, the chemical reaction occurs at the liquid-solid interface, which means that Protease K (enzyme E) first adsorbs onto the surface and then forms an active complex (ES) with T7 DNA polymerase (substrate S). Therefore, k_{ads} is more appropriately referred to as the adsorption rate constant, while the dissociation rate k_{des} corresponds to the desorption rate of the enzyme (E). If assuming that enzyme adsorption and desorption follow a simple Langmuir model, the reaction rates for the formation of the active complex ES and product P can be described by the following differential equations:

$$\frac{\mathrm{d}\,\theta_{ES}}{\mathrm{d}\,t} = k_{ads}[E]\theta_S - (k_{des} - k_{cat})\theta_{ES} \qquad (18)$$

$$\frac{\mathrm{d}\,\theta_P}{\mathrm{d}\,t} = k_{cat}\theta_{ES} \qquad (19)$$

The parameter $\theta_X = \Gamma_X/\Gamma_{tot}$ is the relative surface coverage by a given substance. It represents the ratio of the current surface coverage Γ_X to the maximum possible coverage Γ_{tot}, corresponding to the total number of available adsorption sites. Thus, θ_S and θ_{ES} denote the relative surface coverages of the substrate S (in this study case, the immobilized T7

DNA polymerase) and the active Proteinase K/T7 DNA polymerase complex as ES, respectively. It is also of importance to note that $\theta_S + \theta_{ES} + \theta_P = 1$, where θ_P represents the relative surface coverage by the product. In the QCM experiments, only the product fraction bound to the electrode surface was detected. Therefore, P can be considered a partial product or a product fragment which remains directly attached to the electrode surface after the reaction.

The equation could be applied to describe these QCM-derived studies data, specifically, the degradation of T7 DNA polymerase (substrate S) by Proteinase K (enzyme E). However, it is also evident that the equation does not account for the diffusion limitations of the enzyme, in this case, Proteinase K (enzyme E). Similar challenges have been encountered in other studies when interpreting data obtained via SPR [126]:

$$\frac{\mathrm{d}\,\theta_{ES}}{\mathrm{d}\,t} = \frac{k_{ads}[E](1-\theta_{ES}-\theta_P) - (k_{des}-k_{cat})\theta_{ES}}{\beta(1-\theta_{ES}-\theta_P)+1} \qquad (20)$$

$$\beta = k_{ads}\,{}^{\Gamma_{tot}}/_{k_m} \qquad (21)$$

A modified enzymatic reaction rate equation was applied to better fit the experimental data, incorporating the enzyme's diffusion toward the electrode surface and the subsequent adsorption and desorption. In this equation, the term β explicitly describes the influence of adsorption and diffusion on the reaction rate. As previously mentioned, Γ_{tot} represents the maximum surface coverage, while the parameter k_m is associated with diffusion and is called the mass transfer coefficient.

In order to calculate the rate constants of the reaction stages k_{ads}, k_{des} and k_{cat} the parameter β, and the relative surface coverage by the product θ_P, in the next step of data analysis, the Equation *20* was applied. However, as can be seen, this equation, which describes the rate of the rate-limiting stage, is expressed in a differential form. Since the data of the change in electrode mass over time $\Delta m(t)$, measured by QCM, represent the integrated behavior of the reaction rate, it was decided to use a nonlinear curve fitting method instead of seeking the integral form of the equation. Therefore, a numerical method for solving differential equations and a data fitting procedure were applied to determine all the unknown quantities. The equation was solved by using the Runge-Kutta [127] method, implemented through the ***odeint***. function in the ***„SciPy" Python*** module. This solution procedure can be divided into the following stages:

- First, the changes in the electrode mass over time, $\Delta m(t)$, recorded by QCM, were converted into the relative surface coverage by the active complex, $\theta_{ES}(t)$.
- The differential equation was solved: the experimental $\theta_{ES}(t)$ data were compared with the numerical solution of the differential equation. The initial model value $\theta_{ES}^{model}(0)$, was set equal to the initial experimental data value $\theta_{ES}(0)$.
- Formulation of the objective function: The difference between the experimental θ_{ES} (t) values and the model-predicted θ_{ES}^{model} (t) values were evaluated as the sum of squared deviations:

$$Error = \sum_{i=1}^{N} (\theta_{ES,i} - \theta_{ES,i}^{model})^2 \qquad (22)$$

- Optimization: The ***scipy.optimize.minimize*** function with the "L-BFGS-B" algorithm was used to reduce the error function, aiming to find the optimal values for all unknowns, i.e., k_{ad}, k_{de}, k_{cat}, β, and θ_P. The fitting bounds were constrained by the physical requirements of the model, which means that all optimized parameters were restricted to positive values.
- Result validation: The fitting quality for the optimal unknowns, i.e., k_{ad}, k_{de}, k_{cat}, β, and θ_P, was visually assessed by comparing the experimental data with the model's solution.

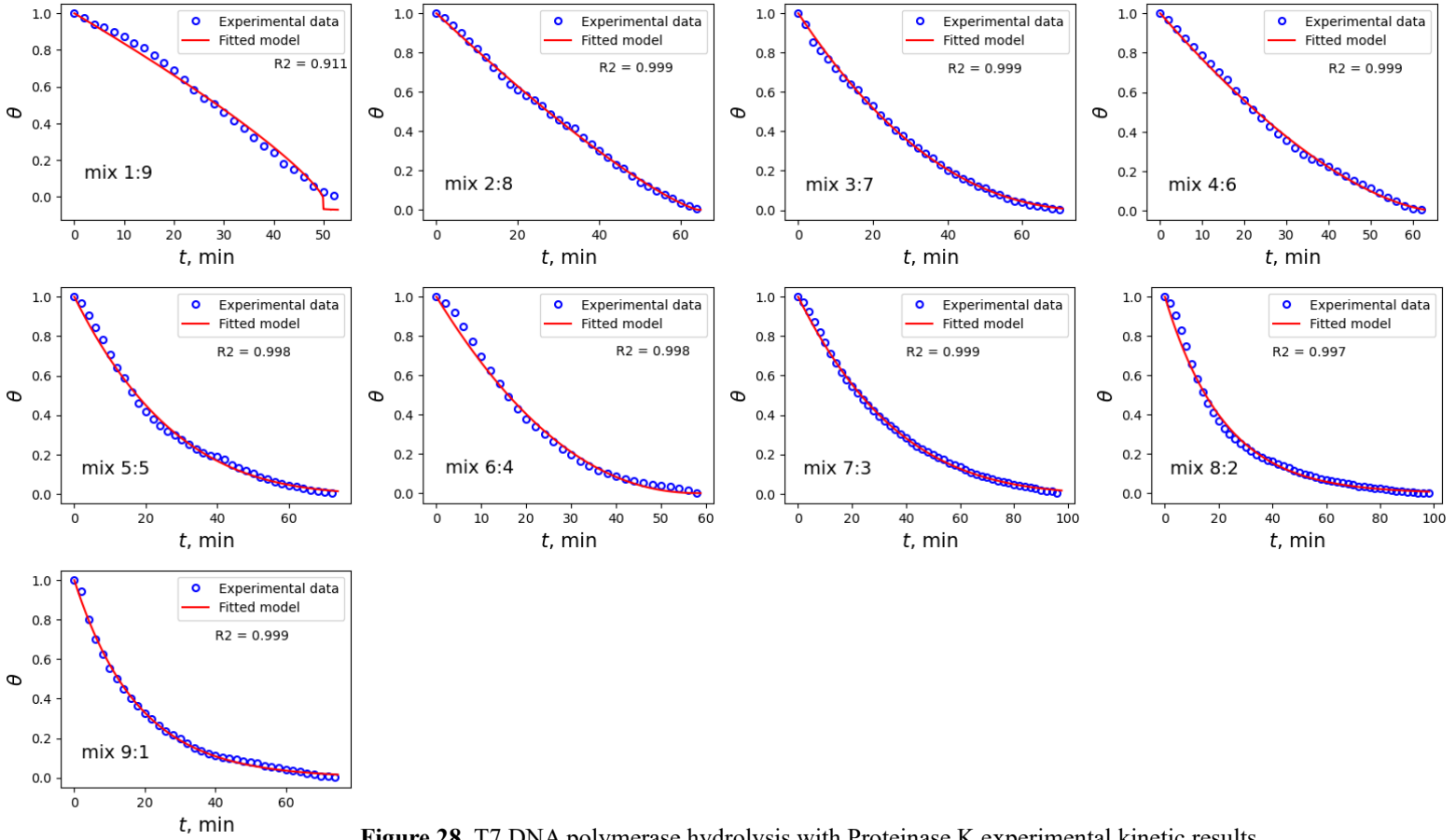


Figure 28. T7 DNA polymerase hydrolysis with Proteinase K experimental kinetic results

During data optimization, the following initial values were selected for all unknowns: k_{ad} = 2.00×10^{4} $L\cdot mol^{-1}\cdot min^{-1}$, k_{de} = 2.00×10^{-2} min^{-1}, k_{cat} = 1.70×10^{-3} min^{-1}, β = 4.50×10^{-3}, and θ_P = 2.00×10^{-2}. Since a constant flow of Proteinase K solution into the QCM cell was maintained throughout the experiment, the enzyme concentration was considered constant at [E] = 1.38×10^{-6} $mol\cdot L^{-1}$. *Figure 28* presents the immobilized T7 DNA polymerase enzyme degradation results: the blue dots represent the experimental data, while the red lines show the optimized data obtained when using the earlier-discussed method. As observed, the data optimization yielded a high correlation (~0.9). The figure illustrates the dependencies of the optimized unknowns on the surface coverage of the immobilized T7 DNA polymerase protein.

The hydrolysis of immobilized T7 DNA polymerase by Proteinase K, as monitored when using the QCM system, provided valuable insights into the kinetics of enzymatic degradation at the solid-liquid interface. The reaction followed a two-step mechanism characteristic of enzymatic catalysis, where Proteinase K first adsorbed onto the sensor surface before forming an active complex with the immobilized T7 DNA polymerase. The application of classical enzymatic kinetics, combined with a modified reaction rate equation that incorporates diffusion effects, enabled an accurate description of the degradation process. By optimizing the kinetic parameters – the adsorption rate constant (k_{ads}), the desorption rate constant (k_{des}), the catalytic rate constant (k_{cat}), the diffusion influence parameter (β), and the relative surface coverage by the degradation product (θP) – a strong correlation between the experimental and the modeled data (~0.9) was achieved. This confirms that the modified enzymatic model, which accounts for enzyme diffusion and adsorption-desorption dynamics, provides a robust framework for interpreting QCM-based proteolysis data. Moreover, the study highlights the importance of diffusion limitations in surface-bound enzymatic reactions. Unlike bulk-phase kinetics, where substrate availability is generally uniform, the observed reaction rates in this system were influenced by Proteinase K's transport to the immobilized T7 DNA polymerase layer. This aspect was successfully accounted for through numerical modeling by using the Runge-Kutta [127] method and nonlinear curve fitting, thereby ensuring precise parameter determination.

In solution-phase studies, Proteinase K demonstrates k_{cat} values in the range of ~2.7×10^{-3} min^{-1} under standard conditions, increasing up to ~12.2×10^{-3} min^{-1} when stabilized (e.g., by spermidine) [128]. In bulk protein hydrolysis assays (e.g., sarcoplasmic proteins), k_{cat} values reach ~190 s^{-1} (~1.14×10^{4} min^{-1}), thereby indicating far higher turnover rates when the substrate is in excess and freely diffusing. By comparison, our surface-bound degradation process of immobilized T7 DNA polymerase by Proteinase K yielded $k_{cat} \approx 1.70\times10^{-3}$ min^{-1} and diffusion-associated parameter $\beta \approx 4.50\times10^{-3}$, thus reflecting the combined limitations of substrate accessibility, enzyme adsorption-desorption dynamics, and a reduced turnover in heterogeneous interface conditions. The model's high fit ($R \approx 0.9$) validates our approach in capturing these diffusion-limited catalytic interactions.

These findings demonstrate that the enzymatic degradation of immobilized proteins can be effectively characterized by using QCM in conjunction with advanced kinetic modeling. This approach may be applied to further investigations of the enzyme-substrate interactions on biosensor surfaces, particularly in the protein stability, enzymatic specificity, and surface-functionalization strategies in biosensing applications.

3.2. BAFF Protein Study Results

3.2.1. Free BAFF study results

SDS-PAGE analysis confirmed the high purity of recombinant human BAFF, revealing a single predominant band without detectable contaminants. The band migrated slightly above the theoretical 17 kDa, which is characteristic of recombinant proteins, and which was used as the validated 1 mM BAFF solution stock for the subsequent QCM immobilization experiments.

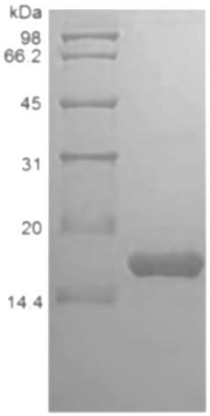


Figure 29. SDS-PAGE analysis of recombinant human BAFF**.** The protein was separated on 15% polyacrylamide gel under reducing conditions and visualized by Coomassie Brilliant Blue staining. A single dominant band was observed at ~17–20 kDa, consistent with the predicted molecular weight of the soluble BAFF monomer (152 aa). Molecular weight standards (kDa) are shown in the left lane

3.2.2. Characterization of BAFF-based sensor QCM data

The experimental BAFF protein immobilization/adsorption, SAM surface deactivation, and targeting ssDNA detection kinetic layer thickness investigation results are shown in *Figure 30*. Each point of the frequency change represents the result of triplicated measurements carried out under stable conditions using a 3:7 ratio SAM mixture surface at room temperature. At physiological conditions (pH 7.4), the peptide bond formation and the BAFF, BSA adsorption process on the gold-coated QCM sensor system indicate changes in Δf during the process.

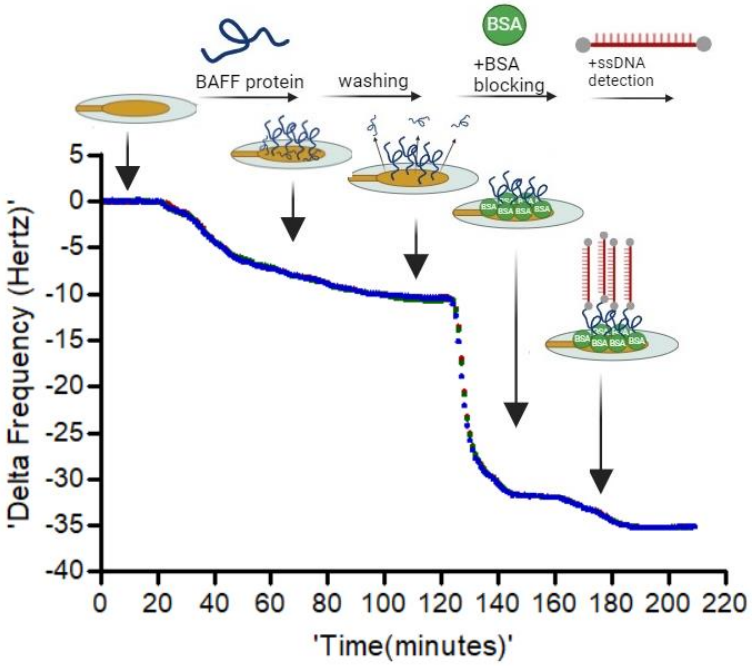


Figure 30. Experimental QCM profile and recorded data of BAFF protein immobilization on the gold surface, SAM deactivation with BSA, and targeting DNA detection of this study

During the BAFF protein adsorption process, a sudden drop (within the 20–120 min interval) in the resonance frequency (Δf) signal was observed after the QCM-resonator. The resonance frequency shift (Δf) values decrease proportionally with an increase in carboxyl groups on the surface. The first abrupt signal change is associated with the rapid adsorption of the BAFF protein over the surface of the SAM mixture. As a result of (i) the maximum mass transport rate through the boundary layer above the SAM surface, the enzyme concentration in contact with the surface is zero at the beginning of the loading step, and (ii) complete availability of the sensor surface to bind the enzyme molecules is evident. After stabilizing the resonance frequency with 1X PBS (pH 7.4) solution at room temperature, the steady-state frequency shifts were obtained after 110–120 min. The subsequent washing step with 1X PBS (pH 7.4) was performed to desorb the unabsorbed BAFF protein molecules from the gold surface and/or to rearrange the enzyme to achieve forms with lower energy configurations and alter their local conformation. The dynamic changes that occurred made additional adsorption sites available on the surface, resulting in a slow but steady adsorption, which is necessary to increase the surface concentration of the adsorbed enzyme and ultimately reach the saturation stage. At this final condition, a dynamic equilibrium is reached between the new BAFF protein molecules adsorbing on the surface and the same molecules leaving the SAM-modified QCM-sensor surface. The lack of a significant frequency change during BAFF protein adsorption on the 3:7 SAM mixtures' surfaces demonstrates that the entire electrode surface of the QCM sensor was covered and saturated by BAFF protein molecules at room temperature.

During the SAM surface inactivation, the BSA protein adsorption process was performed, and a sudden drop (see the 120–150 min interval) in the resonance frequency (Δf) signal was observed after the QCM sensor. The resonance frequency shift (Δf) values decrease proportionally with an increase in carboxyl groups on the surface. The first abrupt

signal change is associated with the rapid adsorption of the BSA protein over the surface of the SAM mixture. After stabilizing the resonance frequency with 1X PBS (pH 7.4) solution at room temperature, the steady-state frequency shifts were obtained after 150–160 min. The subsequent washing step with 1X PBS (pH 7.4) was performed to desorb unabsorbed BSA protein molecules from the gold surface and to rearrange the enzyme into forms with lower energy configurations, thereby changing their local conformation. The dynamic changes that occurred made additional adsorption sites available on the surface, resulting in slow but steady adsorption necessary to increase the surface concentration of the adsorbed protein, and ultimately reach the saturation stage. At this final condition, a dynamic equilibrium is reached between the new BSA/BAFF protein molecules adsorbing on the surface and the same molecules leaving the SAM-modified QCM-resonator surface. The lack of significant frequency change during BSA protein adsorption on the 3:7 SAM mixtures surfaces demonstrates that the whole electrode surface of the QCM-resonator was covered and saturated by BSA protein molecules at room temperature.

During the DNA targeting detection on the immobilized BAFF biosensor, the ssDNA aptamer adsorption process was performed, and the sudden drop (within the 160–210 min interval) in the resonance frequency (Δf) signal was observed after the QCM-sensor. The first abrupt signal change is associated with the rapid adsorption of the ssDNA aptamer onto the BAFF-sensor surface. After stabilizing the resonance frequency with 1X PBS (pH 7.4) solution at room temperature, the steady-state frequency shifts were obtained after 210 min. The subsequent washing step with 1X PBS (pH 7.4) was performed in order to desorb the unabsorbed ssDNA aptamer molecules from the BAFF-sensor surface and/or to rearrange the protein so that to achieve lower energy configurations and alter its local conformation. The dynamic changes that occurred made additional adsorption sites available on the surface, resulting in a slow but steady adsorption necessary to increase the surface concentration of the adsorbed ssDNA aptamer, and ultimately reach the saturation stage. At this final condition, a dynamic equilibrium is reached between the new BAFF/BSA/DNA molecules adsorbing on the surface and the same molecules leaving the SAM-modified QCM-sensor surface. The lack of a significant frequency change during the ssDNA aptamer adsorption on the BAFF-sensor surfaces demonstrates that the whole electrode surface of the QCM-sensor was covered and saturated by ssDNA molecules at room temperature.

If assuming that the immobilization process is kinetically controlled, the adsorbed layer is rigidly connected to the sensor, and the viscoelastic effects are negligible, it was made to fit the change in the resonant frequency of all measurements to the Sauerbrey equation [104] to evaluate the BAFF protein masses accumulated on the surface, respectively. By inserting the resonance frequency change, Δf_n, that results from Δm of addition Au/12-MUA+6-MCH/BAFF/BSA/DNA layer, we applied regression analysis to each step in order to determine the thickness of the formed Au/12-MUA+6-MCH/BAFF/BSA protein monolayer modification according to a detailed procedure to be described in the next section.

3.2.3. Characterization of BAFF-based sensor kinetic models

In this study, the pseudo-first-order, pseudo-second-order, and rate law of arbitrary order (n-order) kinetic models were applied to investigate the covalent attachment kinetics of BAFF protein on a 3:7 SAM mixture ratio, the BSA blocking, and DNA binding by using the following Equations *14-16*, while assuming that the measured concentrations are equal to Au/12-MUA+6-MCH/BAFF protein surface concentrations. Each equation models how the immobilized protein concentration *m(t)* changes over time, where m_{max} represents the

initial concentration of the BAFF protein, BSA is a blocking agent and DNA in the solution, and k is the rate constant. The Pseudo-First-Order Kinetics Equation *14* assumes that the immobilization rate is directly proportional to the unbound protein concentration. Pseudo-Second-Order Kinetics (Equation *15*) suggests that the reaction rate depends on the unbound protein and the available binding sites, leading to a quadratic relationship. The denominator (1+kt) accounts for the gradual saturation of the binding sites. The equation predicts a faster initial immobilization rate compared to first-order kinetics. Arbitrary n-Order Kinetics (Generalized Rate Law) Equation *16* generalizes immobilization kinetics when the reaction does not strictly follow first- or second-order kinetics.

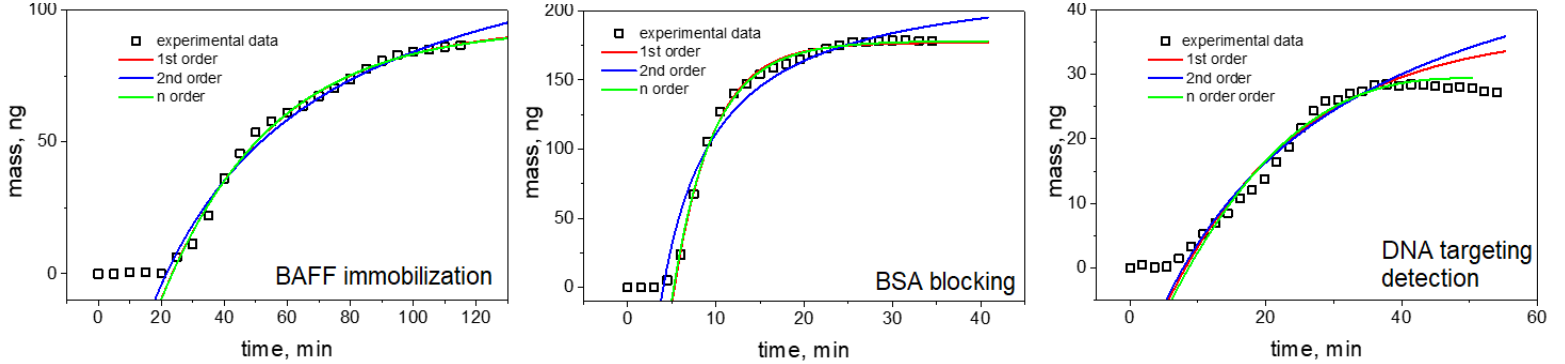


Figure 31. Comparison of experimental and modeled first-, second-, and n-order kinetics for BAFF and BSA adsorption and DNA interaction on various gold electrodes. The experimental data points (the black rectangles) were fitted to the First (the red solid lines), Second (the blue solid lines), and n-order (the green solid lines) kinetics on a gold electrode

Table 6. Summary kinetics table of BAFF and BSA adsorption and DNA interaction on gold electrode

Stage	Reaction rate model	k
BAFF immobilization	1	0.028 ± 0.0000826
	2	0.028 ± 0.000198
	n (0.978±0.012)	0.031 ± 0.001
BSA blocking	1	0.226 ± 0.000645
	2	0.444 ± 0.008
	n (1.04 ± 0.008)	0.178 ± 0.0081
ssDNA targeting binding	1	0.050 ± 0.000857
	2	0.039 ± 0.000897
	n (0.620 ± 0.025)	0.227 ± 0.020

The kinetic data for BAFF and BSA interactions were analyzed by using various kinetic models, including the pseudo-first-order, pseudo-second-order, and n-order kinetics. Among these models, the n-order kinetic model best fits most of the data, with the calculated order of the reaction being close to 1. Specifically, in the cases of BAFF and BSA, the obtained n-order values were remarkably close to 1, thereby indicating that these interactions can be described effectively by using first-order kinetics. This suggests that the interactions between BAFF and BSA, though occurring in the presence of the sensor surface, follow a relatively straightforward single-step adsorption process, where the binding rate is proportional to the concentration of the reacting species available in the system. This insight aligns with the experimental findings, where the adsorption behavior of both BAFF and BSA on SAM-functionalized surfaces exhibited characteristics typical of the first-order kinetics, with adsorption occurring rapidly at first and gradually slowing down as the available binding sites became occupied. Consequently, despite the broader applicability of n-order models for more complex interactions, the data for BAFF and BSA can be accurately described by the first-order model, thus reflecting simpler reaction dynamics and a minimal steric hindrance or surface complications in these cases.

3.3. VEGF Protein Study Results

The interaction between VEGF and the immobilized DNA aptamer on the SAM surface was modeled by using the Langmuir adsorption isotherm, which assumes a 1:1 binding stoichiometry and homogeneous surface binding sites. The normalized response (R) as a function of VEGF concentration (C) is described by:

$$R = \frac{R_{max} \times C}{K_D + C} \qquad (23)$$

where: R is the measured signal (e.g., normalized impedance or amperometric response), R_{max} is the maximum signal at saturation, and K_D is the apparent equilibrium dissociation constant.

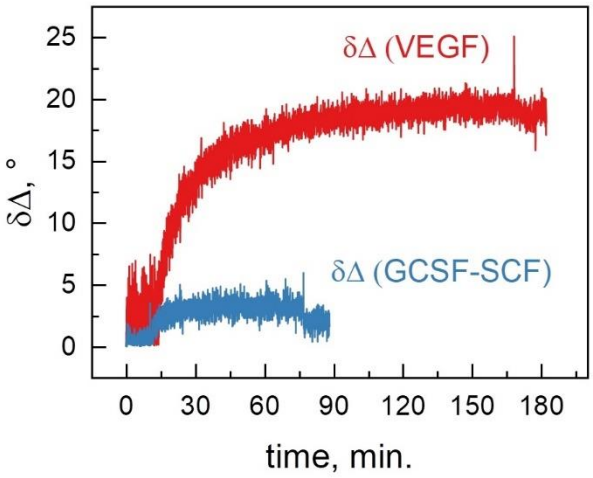


Figure 32. VEGF binding to aptamer–SAM sensogram

The experimental data were obtained by recording the sensor response at increasing VEGF concentrations (0–20 nM). Each measurement was repeated on at least three independently prepared electrodes, and the mean values were used for curve fitting. Standard deviations were calculated and plotted as error bars. The fitting procedure was carried out by nonlinear regression using least-squares minimization *GraphPad Prism*. The fit quality was evaluated by using the coefficient of determination (R^2), which exceeded 0.98 for all datasets, thus indicating a good agreement between the experimental data and the Langmuir model.

The apparent dissociation constant (K_D) obtained from the fit was approximately 0.1 nM, which is consistent with a high-affinity aptamer – VEGF interactions reported in the literature. The linear-scale plot (*Figure 33 A*) highlights the classical saturation behavior, while the logarithmic-scale plot (*Figure 33 B*) emphasizes the wide dynamic range of the sensor response at a low VEGF concentration.

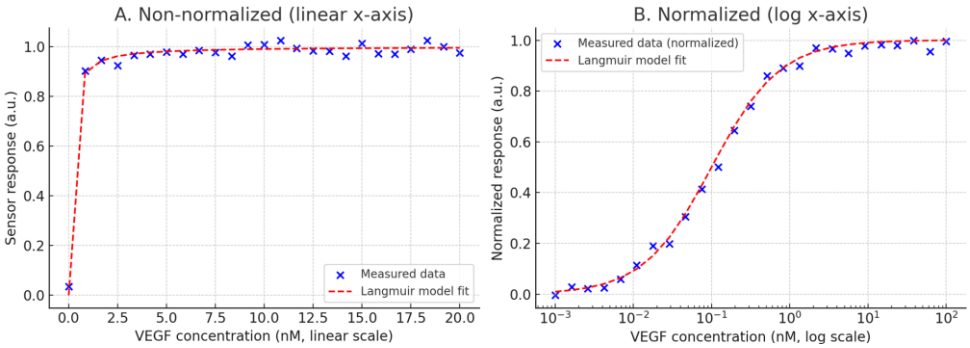


Figure 33. Langmuir isotherm analysis of VEGF binding to the aptamer–SAM biosensor. (**a**) Calibration curve of normalized sensor response vs. VEGF concentration plotted on a linear scale (0–20 nM). Experimental data (the blue crosses) were fitted with the Langmuir adsorption isotherm (the red dashed line), yielding an apparent dissociation constant ($K_D \approx$ 0.1 nM). (**b**) The same dataset was plotted on a logarithmic scale (0.01–20 nM),

emphasizing the sensor performance across a wider dynamic range. The semi-sigmoidal appearance results from the logarithmic axis transformation; however, both plots are consistent with Langmuir binding kinetics

An anti-VEGF aptamer was constructed from three self-assembling oligonucleotides (combSL2B, stalkGTG, r_stalkGTG) and immobilized on gold-coated sensor discs. After blocking with BSA, VEGF detection was performed by using Total Internal Reflection Ellipsometry (TIRE). Real-time monitoring showed a strong and specific interaction: injection of 260 nM VEGF produced a ~20° Δ shift, whereas the control dimer yielded only a minor and reversible signal, thereby confirming specificity. Optical modeling demonstrated that aptamer immobilization generated an ~11.4 nm partial layer, while VEGF binding formed a monolayer of 5.75 ± 0.16 nm thickness with a surface mass density of 62 ± 2.5 ng·cm^{-2}, and these values are consistent with VEGF165 dimensions. Kinetic analysis using a two-step binding model yielded an association rate constant (k_a) of 3.25 × 10^3 M^{-1} s^{-1}, a dissociation rate constant (K_D) of 3.43 × 10^{-7} s^{-1}, and an equilibrium dissociation constant $K_D \approx 0.1$ nM, with a Gibbs free energy of binding $\Delta G \approx -56$ kJ·mol^{-1}, indicating a thermodynamically favorable and exceptionally stable complex. Teran and Nugent reported a value of 2.91 × 106 M^{-1} s^{-1} and a K_D of 5.69 × 10-4 s^{-1} for VEGF with chimeric receptors obtained by SPR[129]. While Nonaka et al. reported DNA aptamers with different binding properties, they also reported DNA aptamers for VEGF binding with affinities from 1 nM to 20 nM [130]. Notably, the hybridized aptamer showed ~5-fold higher affinity compared to the parent SL2B sequence, thus highlighting the role of the aptamer orientation and immobilization strategy in improving the recognition efficiency.

CONCLUSION

1. The construction of T7 DNA polymerase biosensors on gold-coated QCM electrodes functionalized with various self-assembled monolayer (SAM) compositions resulted in functional, stable, and efficient enzymatic surfaces. Among the tested models, the pseudo-first-order kinetic model best described the immobilization behavior, indicating that immobilization of 10 ng of T7 DNA polymerase corresponds to a 1.20 Hz frequency change in the QCM system. This model accurately captured the rapid initial binding followed by gradual saturation, thus validating it as a reliable tool for analyzing enzyme–surface interactions and supporting the optimization of sensor sensitivity.
2. The study has confirmed that T7 DNA polymerase sensors could maintain reusability over multiple reaction cycles, with over 50% of exonuclease activity retained after three cycles. This finding highlights the long-term stability and practical application of the sensors in real-world diagnostics, where their repeated use is essential.
3. The enzymatic hydrolysis of immobilized T7 DNA polymerase by Proteinase K was successfully monitored in real-time by using the QCM system. The hydrolysis followed a surface-bound proteolysis kinetic model, with parameters optimized from the data of $k_{ads} = 2.00 \times 10^{4}$ $L \cdot mol^{-1} \cdot min^{-1}$, $k_{des} = 2.00 \times 10^{-2}$ min^{-1}, $k_{cat} = 1.70 \times 10^{-3}$ min^{-1}, $\beta = 4.50 \times 10^{-3}$, and $\theta P = 2.00 \times 10^{-2}$, which supported the modeling of protein turnover on the surface. These values indicate a well-defined enzymatic turnover process occurring on the surface, confirming that surface-bound proteolysis can be accurately modeled and quantified by using kinetic parameters derived from the QCM data.
4. A BAFF-based biosensor, developed on SAM-modified gold-coated surfaces, successfully detected specific DNA sequences with a measurable DNA adsorption of 27.9 ng. The n-order kinetic model provided the best fit for the BAFF–DNA interaction process, on the grounds of capturing the nonlinear dynamics of surface adsorption due to steric hindrance and molecular rearrangements. The calculated rate constant of 0.227 ± 0.020 min^{-1} supported the conclusion that the BAFF layer remained biologically active and capable of recognizing DNA in real-time.

FUTURE OUTLOOK

This dissertation opens several pathways for advancing electrochemical sensor technologies based on enzyme-functionalized surfaces. The successful immobilization of masked T7 DNA polymerase and its reusability have demonstrated and provided a foundation for developing cost-effective and regenerable biosensors. Future research can explore opportunities of expanding this approach to other DNA-modifying enzymes, thereby enabling broader applications in genetic diagnostics, forensic analysis, and synthetic biology. Moreover, integration with microfluidic platforms and electrochemical detection systems could lead to the development of compact, high-throughput analytical devices. Further scale-ups, kinetic modeling, and long-term stability studies under varying conditions will be essential for translating these biosensor systems into real-world clinical and environmental monitoring tools.

The investigation of BAFF immobilization and its interactions with DNA expands the potential of biosensors beyond enzymatic activity to immunologically relevant targets. This research lays the groundwork for label-free, real-time detection systems that could be applied in autoimmune disease diagnostics, therapeutic antibody screening, and immunoassay development. Future directions include further refining BAFF-based surface functionalization for an enhanced sensitivity and specificity, integrating it into multiplexed platforms for simultaneous cytokine profiling, and exploring BAFF-ligand interactions with aptamers or DNA nanostructures. These advancements could support the development of next-generation immunosensors with applications in clinical diagnostics and personalized medicine

SANTRAUKA

ĮVADAS

Apžvalgoje vertinama ankstesnių darbų pažanga bei identifikuojamos spragos, kurias šis tyrimas siekia užpildyti. Ypatingas dėmesys skiriamas genetinių ir imunologinių veiksnių integracijai, kad būtų geriau suprasti tiriamas sąveikas. Fermentai, tokie kaip T7 DNR polimerazė, atlieka esminį vaidmenį DNR replikacijoje, klaidų taisyme ir korekcijoje. Šių DNR modifikuojančių fermentų gebėjimas sąveikauti su DNR substratais yra itin svarbus kuriant biojutiklius, kur tikslumas ir jautrumas yra lemiami veiksniai. Tuo tarpu BAFF baltymas (B ląstelių aktyvavimo faktorius) yra imuninės sistemos citokinas, būtinas B ląstelių diferencijavimui ir aktyvacijai. Jo reikšmė apima ne tik pagrindines imunologines funkcijas, bet ir ryšį su autoimuninėmis ligomis, todėl jis laikomas potencialiu diagnostiniu biologiniu žymekliu.

Šioje disertacijoje sujungiamas biojutiklių technologijų genetinis ir imunologinis aspektas, tiriant T7 DNR polimerazės ir BAFF imobilizaciją bei pritaikymą biojutiklių sistemose. BAFF, dalyvaudamas imuninėse reakcijose, tampa vertingu tiksliniu taikiniu, o T7 DNR polimerazė suteikia patikimą fermentinį pagrindą molekulinei detekcijai. Šių komponentų sinergija leidžia kurti tikslesnius ir veiksmingesnius diagnostikos įrankius, atskleidžiančius genetinių ir imuninių sąveikų svarbą šiuolaikinėje biojutiklių technologijoje. T7 DNR polimerazės ir BAFF baltymo imobilizacijos tyrimai pateikia vertingas strategijas, skirtas pagerinti fermentais pagrįstų sistemų efektyvumą, ekonomiškumą ir patikimumą įvairiose pramoninėse bei mokslinėse srityse. Disertacija prisideda prie molekulinės biologijos, farmacijos, maisto pramonės ir klinikinės diagnostikos plėtros, siūlydama naujoviškus sprendimus fermentų stabilumo ir funkcionalumo gerinimui praktinėse taikymuose.

Šio tyrimo tikslas – ištirti T7 DNR polimerazės imobilizaciją, jos pakartotinį naudojimą bei fermentinį efektyvumą funkcinėse biojutiklio terpėse ir įvertinti jos potencialą taikymui molekulinėje diagnostikoje. Papildomai siekiama sukurti ir charakterizuoti BAFF pagrindu veikiantį biojutiklį, skirtą DNR sąveikų aptikimui, apimant genetinius ir imunologinius biojutiklių projektavimo aspektus.

Darbo uždaviniai

- Sukurti T7 DNR polimerazės biojutiklį, naudojant aukso elektrodus su įvairios sudėties savaime susitvarkančiais monosluoksniais (SAM), ir įvertinti jo imobilizacijos efektyvumą bei fermentinį aktyvumą.
- Įvertinti imobilizuotos T7 DNR polimerazės 3′→5′ egzonukleazės aktyvumą, sutelkiant dėmesį į fermento stabilumą ir pakartotinio naudojimo galimybes skirtingomis sąlygomis.
- Ištirti imobilizuotos T7 DNR polimerazės skaidymą naudojant Proteinazę K ir įvertinti proteolizės kinetiką ant skirtingais SAM sluoksniais modifikuotų aukso elektrodų.
- Sukurti BAFF pagrindu veikiantį biojutiklį, naudojant SAM sluoksniu modifikuotus aukso elektrodus, ir pademonstruoti jo funkcionalumą stebint DNR sąveikas naudojant QCM.
- Eksperimentinius QCM duomenis pritaikyti kinetiniams modeliams (pirmojo, antrojo ir n-laipsnio) ir nustatyti tinkamiausią adsorbcijos elgseną apibūdinantį modelį tiek BAFF, tiek T7 DNR polimerazės biojutiklių sistemose.

Mokslinis naujumas

Šis tyrimas pateikia kelis naujus aspektus:

- Sukurta nauja imobilizacijos strategija T7 DNR polimerazei, naudojant aukso elektrodus su SAM sluoksnių mišiniais, užtikrinanti fermento aktyvumo ir aktyviojo centro prieinamumo išlaikymą.
- Pirmą kartą įrodyta imobilizuotos T7 DNR polimerazės pakartotinio naudojimo galimybė, atlikus keletą egzonukleazės veiklos ciklų ir nustatytos optimalios reakcijos sąlygos.
- Proteinazės K skaidymo eksperimentuose kiekybiškai išanalizuota imobilizuotos T7 DNR polimerazės hidrolizė, pritaikant QCM pagrįstą kinetinį modeliavimą.
- Pirmą kartą pademonstruota BAFF baltymo imobilizacija ir funkcinė DNR atpažinimo galimybė aukso elektrodo SAM paviršiuje, stebint realiuoju laiku naudojant QCM.
- Pritaikyti pirmojo, antrojo ir n-laipsnio kinetiniai modeliai paviršiaus adsorbcijos duomenims, atskleidžiant sudėtingesnį sąveikų pobūdį nei klasikiniai modeliai leidžia.

Ginamieji teiginiai

1. Užmaskuota *T7* DNR polimerazė gali būti efektyviai imobilizuota ant savaime susitvarkančiais monosluoksniais (SAM) modifikuotų auksinių elektrodų, sudarydama stabilų ir funkcionalų biojutiklį.
2. Funkcionalūs *T7* DNR polimerazės biojutikliai gali būti pakartotinai naudojami.
3. Su paviršiumi susijusio fermento stabilumas gali būti įvertintas realiu laiku taikant bekontaktinį QCM metodą ir proteolizinio skaidymo kinetinę analizę.
4. BAFF, imobilizuotas ant SAM-funkcionalizuotų auksinių elektrodų, leidžia be žymenų aptikti tikslines DNR sekas, o jo sąveikos kinetika gali būti patikimai aprašyta kinetiniais modeliais, pagrindžiančiais biojutiklio jautrumą ir specifiškumą.

LITERATŪROS APŽVALGA

Šioje dalyje aptariami su tiriamais klausimais susiję darbai, ypač dėmesys skiriamas DNR modifikuojančių fermentų ir imuninei sistemai svarbių baltymų (pvz., BAFF) taikymui biojutiklių kūrime. Literatūros analizė padeda atskleisti esamus tyrimų trūkumus bei mokslinę nišą, kurią siekiama užpildyti šiuo darbu. Tuo pačiu, šioje dalyje remiamasi teoriniais ir eksperimentiniais šaltiniais, kad būtų pagrįstas tiriamos temos aktualumas ir numatoma mokslinė naujovė [1–6].

Biologinės makromolekulės

Biologinės makromolekulės yra didelės, sudėtingos molekulės, būtinos ląstelių struktūrai, funkcijai ir reguliacijai. Makromolekulė paprastai apibūdinama kaip molekulė, turinti didelę molekulinę masę, paprastai virš 1000 Daltonų (Da). Biologinėse sistemose šios makromolekulės dažniausiai svyruoja nuo 10 kDa iki kelių gigadaltonų (GDa), pavyzdžiui, ribosomos sudaro apie 2,5 MDa, o žmogaus genominė DNR – apie 3,2 GDa [7,8]. Biologinės makromolekulės, sudarytos iš pasikartojančių monomerinių vienetų, sujungtų kovalentiniais ryšiais į dideles polimerines struktūras, skiriasi nuo mažesnių biomolekulių,

tokių kaip metabolitai, hormonai ir paprastieji cukrūs, savo dideliu dydžiu ir sudėtingumu. Keturi pagrindiniai biologinių makromolekulių tipai – baltymai, nukleorūgštys, angliavandeniai ir lipidai – atlieka skirtingas funkcijas įvairiuose ląsteliniuose ir fiziologiniuose procesuose:

- Baltymai atlieka fermentinę katalizę (pvz., DNR modifikuojantys fermentai, tokie kaip DNR polimerazės), struktūrinę atramą (pvz., kolagenas), signalų perdavimą (pvz., augimo faktoriai), pernašą (pvz., hemoglobinas) ir imuninę gynybą (pvz., antikūnai).
- Nukleorūgštys saugo ir perduoda genetinę informaciją, reguliuoja genų raišką ir katalizuoja reakcijas (pvz., ribozimai).
- Angliavandeniai (polisacharidai) dalyvauja energijos kaupime (pvz., glikogenas, krakmolas), struktūrinėje atramoje (pvz., celiuliozė, chitinas), ląstelių komunikacijoje (pvz., glikoproteinai, glikolipidai) ir imuninėse reakcijose.
- Lipidai atlieka membranų formavimo funkciją (pvz., fosfolipidai), energijos kaupimą (pvz., trigliceridai) ir veikia kaip signalinės molekulės (pvz., steroidai, prostaglandinai), dalyvaujančios signalų perdavime ir molekulinių sąveikų valdyme.

DNR modifikuojantys fermentai yra didelės, sudėtingos baltyminės struktūros, kurios atlieka gyvybiškai svarbų vaidmenį biologiniuose procesuose. Priklausydami makromolekulių klasei, šie fermentai yra būtini pagrindinėms ląstelių funkcijoms, tokioms kaip DNR replikacija, taisymas ir transkripcija. Jų gebėjimas sąveikauti su DNR ir keisti jos struktūrą yra būtinas genetinio stabilumo palaikymui ir genų raiškos reguliavimui. Be svarbos ląstelių veikloje, šie fermentai taip pat yra nepakeičiami įrankiai, taikomi biojutiklių sistemose.

DNR modifikuojantys fermentai

DNR modifikuojantys fermentai yra didelės, sudėtingos baltyminės struktūros, kurios atlieka gyvybiškai svarbias funkcijas, susijusias su genetinės medžiagos apdorojimu. Jie dalyvauja:

- DNR replikacijoje – naujų DNR molekulių sintezė ląstelių dalijimosi metu.
- DNR taisyme – pažeistų DNR sričių atstatymas, siekiant išlaikyti genetinį stabilumą.
- DNR transkripcijoje – DNR informacijos perrašymas į RNR molekules.

Šie fermentai geba atpažinti specifines DNR sekas, modifikuoti jų struktūrą, katalizuoti naujų grandinių sintezę arba šalinti pažeistas vietas. Vienas iš svarbiausių DNR modifikuojančių fermentų pavyzdžių yra *T7* DNR polimerazė, kuri pasižymi aukštu specifiškumu ir turi 3'→5' egzonukleazės aktyvumą, leidžiantį koreguoti klaidas DNR sintezės metu [5,6]. 1 pav. plačiai iliustruoja polimerazių, egzonukleazių ir kitų nukleorūgščių apdorojimo fermentų sąveiką DNR sintezės, taisymo ir modifikavimo procesuose. Be savo pagrindinės biologinės reikšmės, šie fermentai plačiai naudojami ir kaip analitiniai įrankiai biojutikliuose. Jų gebėjimas sąveikauti su DNR ir katalizuoti tikslias reakcijas leidžia kurti itin jautrias ir specifiškas aptikimo sistemas, skirtas genetinių taikinių atpažinimui ir analizei [7,8].

BAFF baltymas

BAFF (B ląstelių aktyvavimo faktorius) yra naviko nekrozės faktoriaus (TNF) šeimai priklausantis citokinas, atliekantis esminį vaidmenį B limfocitų biologijoje. BAFF reguliuoja B ląstelių diferenciaciją, proliferaciją ir išgyvenimą, prisijungdamas prie trijų specifinių receptorių: BAFF-R, TACI ir BCMA [9]. BAFF vaidmuo yra ypač svarbus imuninės sistemos funkcionavimui. Normaliomis sąlygomis, BAFF padeda palaikyti tinkamą B ląstelių homeostazę ir imuninį atsaką. Per didelė BAFF ekspresija siejama su autoimuninėmis ligomis, tokiomis kaip sisteminė raudonoji vilkligė, reumatoidinis artritas ir Sjögreno sindromas [10,11]. Per maža BAFF ekspresija gali sukelti imunodeficitines būkles, mažinant B ląstelių skaičių ir imuninį atsparumą. Dėl savo gebėjimo specifiškai sąveikauti su B ląstelėmis ir dalyvauti imuninėse reakcijose, BAFF yra laikomas perspektyviu biologiniu žymekliu įvairių imuninių ligų diagnostikai ir terapijai [12,13].

Šiame darbe BAFF buvo pasirinktas kaip imuninės sąveikos modelis biojutiklio sistemai, siekiant sukurti imuniniais mechanizmais paremtą aptikimo platformą. BAFF baltymas buvo imobilizuotas ant aukso paviršiaus, padengto savitvarkiu monosluoksniu (SAM), leidžiant realiuoju laiku stebėti jo sąveiką su specifinėmis viengrandėmis DNR sekų taikiniais, naudojant QCM technologiją. Imobilizuoto BAFF stabilumas ir gebėjimas atpažinti DNR molekules buvo esminiai kriterijai vertinant jo tinkamumą biojutiklių kūrimui ir tolesniam diagnostiniam pritaikymui.

Savitvarkiai monosluoksniai (SAM) biojutiklių kūrime

Savitvarkiai monosluoksniai (SAM) yra plačiai naudojami biojutiklių platformose dėl gebėjimo kontroliuoti paviršiaus savybes, pvz., hidrofilinumą, laidumą ar molekulių prisijungimą [14]. Tipiniai SAM komponentai – alkanotioliai, kurie, prisitvirtina prie aukso paviršiaus per tiolio grupes [15,16]. SAM yra viena dažniausiai naudojamų metodikų biojutiklių kūrime, nes leidžia tiksliai valdyti paviršiaus savybes, sumažinti nespecifinią adsorbciją ir pagerinti biomolekulių sąveikos specifiką. Nors SAM sistemos yra labai plačiai naudojamos, jos turi tam tikrų apribojimų, susijusių su paviršiaus stabilumu, nespecifiniu adsorbcijos potencialu, bei jautrumu oksidacinei degradacijai [20]. Taip pat SAM formavimui reikia griežtai kontroliuojamų eksperimentinių sąlygų, o netolygus sluoksnio formavimasis gali paveikti jutiklio tikslumą. Tyrimuose buvo naudota aktyvios vietos maskavimo strategija, leidžianti tiksliai ir efektyviai įtvirtinti *T7* DNR polimerazę paviršiuje neprarandant jos aktyvumo.

SAM sluoksnių formavimas ant aukso paviršiaus, įskaitant ir ant aukso nanodalelių (AuNP), yra viena iš populiariausių savitvarkos technologijų. Tiolio grupes turinčios molekulės, tokios kaip 12-merkaptododekano rūgštis (12-MUA) ir 6-merkaptoheksanolis (6-MCH), stipriai jungiasi prie aukso paviršiaus per tiolio–aukso sąveikas [16,17]. Aukso nanodalelės turi šiuos privalumus:

- padidintą paviršiaus plotą biomolekulėms imobilizuoti;
- pagerintą signalų stiprumą (dėl paviršiaus plazmonų rezonanso efektų);
- geresnį imobilizuotų fermentų ar baltymų tankį ir funkcionalumą.

Šiame darbe pasirinktas plokščias aukso paviršius (QCM diskas) su savitvarkio sluoksniu, sudarytu iš 12-MUA ir 6-MCH mišinio, siekiant užtikrinti optimalų fermentų ir baltymų immobilizacijos valdymą.

SAM sluoksniai yra ypač tinkami DNR modifikuojančių fermentų imobilizacijai, nes jie:

- leidžia kontroliuoti fermento orientaciją paviršiuje;
- sumažina aktyvios vietos blokavimo riziką;

- išlaiko fermento funkcionalumą ilgalaikio stebėjimo metu [18].

Šiame tyrime, siekiant išvengti fermento aktyvios vietos užsiblokavimo, buvo taikomas aktyvios vietos maskavimo metodas, kai *T7* DNR polimerazė laikinai sujungiama su substratu prieš imobilizaciją, o po prisijungimo substratas pašalinamas. Tokiu būdu fermentas išlieka katalitiškai aktyvus po pritvirtinimo. Be to, naudojant EDC/NHS chemiją, buvo suaktyvintos karboksigrupės 12-MUA struktūroje, kurios leido kovalentiškai prisijungti aminogrupes turinčius baltymus.

Nepaisant didelio SAM technologijos potencialo, jų naudojimas turi tam tikrų apribojimų:

- Paviršiaus heterogeniškumas – netolygus molekulių pasiskirstymas gali sukelti skirtingus biomolekulių adsorbcijos lygius.
- Oksidacinis nestabilumas – SAM gali būti jautrūs oksidaciniam pažeidimui, ypač ilgalaikėse analizėse.
- Nespecifinė adsorbcija – jei nesubalansuota SAM sudėtis, gali didėti nespecifinių biomolekulių prisijungimas.

Per didelis sluoksnio tankumas – gali sukelti fermentų inaktyvaciją arba sumažinti prieinamumą substratams [19]. Todėl šio tyrimo metu buvo svarbu kruopščiai optimizuoti SAM formavimo sąlygas ir pasirinkti tinkamą tiolių santykį (pvz., 12-MUA:6-MCH), kad būtų užtikrintas geriausias biojutiklio veikimas.

Kvarcinės kristalo mikrobalansės (QCM) metodika

QCM yra itin jautri metodika, leidžianti stebėti masės pokyčius nanogramų lygiu realiuoju laiku. QCM veikia matuodama kvarcinio kristalo rezonansinio dažnio pokyčius, kurie tiesiogiai susiję su prisijungusių molekulių mase ant paviršiaus [20]. Šiame tyrime QCM buvo naudojama:

- stebėti *T7* DNR polimerazės ir BAFF baltymo imobilizaciją;
- vertinti DNR substratų sąveiką su imobilizuotais paviršiais;
- analizuoti fermento skilimą veikiant Proteinazei K;
- pritaikyti kinetinius modelius sąveikų dinamikos analizei.

QCM leidžia vertinti sąveikas be papildomų žymeklių (label-free), kas užtikrina natūralesnį biologinių procesų stebėjimą.

FTIR spektroskopija

FTIR (Fourier transformacijos infraraudonųjų spindulių spektroskopija) leidžia nustatyti funkcinę grupę ar baltymo antrinę struktūrą. Ji padeda įvertinti SAM formavimąsi ir imobilizuoto baltymo stabilumą bei struktūros pokyčius [24].

TYRIMO METODIKA

Šis skyrius pristato eksperimentinius darbus, skirtus įgyvendinti įvade iškeltus tyrimo tikslus. Dėmesys buvo skiriamas biojutiklių kūrimui, pagrįstam *T7* DNR polimerazės ir BAFF baltymo imobilizavimu ant auksu padengtų paviršių skirtingomis savitvarkių monosluoksnių (SAM) mišinių kompozicijomis. Eksperimentinis planas buvo parengtas remiantis išsamia literatūros apžvalga, ypatingą dėmesį skiriant fermentų orientacijai, paviršiaus chemijai ir molekulinių sąveikų dinamikai. Siekiant tiksliai įvertinti biomolekulių aktyvumą ir imobilizacijos efektyvumą, buvo taikytas paviršiui jautrių ir struktūrinių metodų derinys. QCM metodas buvo naudojamas paviršiaus sąveikoms stebėti realiu laiku, o Furjė transformacijos infraraudonųjų spindulių spektroskopija (FTIR) – cheminėms modifikacijoms ir baltymų struktūrinio vientisumo patvirtinimui. Kiekvienas biojutiklio kūrimo etapas – nuo paviršiaus funkcionalumo iki molekulinių sąveikų tyrimų – buvo sistemingai suplanuotas siekiant įvertinti imobilizuotų komponentų funkcionalumą ir stabilumą.

Neimobilizuotos T7 DNR polimerazės tyrimai

Neimobilizuotos *T7* DNR polimerazės elgsena buvo tiriama tirpale, siekiant nustatyti patikimą fermentinio aktyvumo atskaitos tašką. Šie preliminarūs tyrimai buvo skirti fermento natūraliai 3'→5' egzonukleazės veiklai charakterizuoti ir jo sąveikai su įvairiais DNR fragmentais įvertinti kontroliuojamomis sąlygomis. Suprasti fermento elgseną natūralioje būsenoje yra itin svarbu norint įvertinti vėlesnių imobilizacijos žingsnių poveikį ir užtikrinti, kad pastebėti veikimo pokyčiai atsirastų dėl sąveikos su paviršiumi, o ne dėl vidinio fermento kintamumo. Šio skyriaus rezultatai buvo naudojami kaip palyginimo pagrindas vėlesniuose imobilizuoto fermento sistemų etapuose.

DNR fragmentų išskyrimo iš agarozės gelio protokolas

Norint paruošti tam tikro ilgio DNR fragmentus egzonukleazės aktyvumui tirti, DNR buvo išskirta iš „Low DNA Mass Ladder“ naudojant agarozės gelio elektroforezę. Fragmentų separacija buvo atlikta 2 % TAE agarozės gelyje, o tikslinio ilgio juostos (100–2000 bp) buvo vizualizuojamos naudojant UV apšvietimą. Atrinktos DNR juostos buvo kruopščiai išpjautos ir išgrynintos naudojant GeneJET Gel Extraction Kit, vadovaujantis gamintojo protokolu. Kiekvieno fragmento (100 bp, 200 bp, 400 bp, 800 bp, 1200 bp ir 2000 bp) absorbancija buvo matuota „Nanodrop“ spektrofotometru ties 260 nm bangos ilgiu, leidžiant nustatyti jų koncentraciją ir apskaičiuoti A260/A280 santykį grynumui įvertinti. Fragmentai buvo paruošti galutine 0,25 mg/mL koncentracija kiekvienam 100 bp, 200 bp, 400 bp, 800 bp, 1200 bp ir 2000 bp ilgiui. Šis žingsnis buvo būtinas siekiant gauti švarius, aiškaus ilgio DNR substratus, užtikrinančius fermentinio skaidymo testų atkuriamumą.

Neimobilizuotos T7 DNR polimerazės 3′→5′ egzonukleazės aktyvumo tyrimai

Buvo tirtas neimobilizuotos *T7* DNR polimerazės egzonukleazės aktyvumas, siekiant nustatyti atskaitos tašką šio fermento veiklai tirpale. Šis etapas buvo itin svarbus siekiant atskirti paties fermento natūralų elgesį nuo bet kokių paviršiaus imobilizacijos poveikių, pasireiškiančių vėlesniuose eksperimentuose. Pagrindinis tikslas buvo įvertinti fermento natūralų 3′→5′ (žr. 4 pav.) egzonukleazės aktyvumą prieš dvigrandes DNR fragmentus, kurių ilgis, koncentracija ir reakcijos laikas skyrėsi. Išgryninus specifines juostas iš DNR žymeklio (ladder), buvo gauti dvigrandžiai DNR fragmentai, kurių ilgis siekė nuo 100 iki

2000 bazių porų. DNR koncentracijos buvo sureguliuotos iki 25 ng ir 12,5 ng vienai reakcijai. Tuo pačiu metu *T7* DNR polimerazė buvo naudojama 10 U galutinėje koncentracijoje kiekvienai reakcijai. Šios koncentracijos buvo pasirinktos siekiant atkartoti sąlygas, taikomas imobilizuoto fermento tyrimuose, ir užtikrinti formatų palyginamumą. Reakcijos buvo vykdomos 96-duobučių mikroplokštelėse, naudojant standartinį *T7* DNR polimerazei buferį (400 mM Tris-HCl (pH 7,5, 25 °C), 100 mM $MgCl_2$, 10 mM DTT), papildytą Mg^{2+} jonais, kurie būtini egzonukleazės aktyvumui. Fermentas ir DNR substratai buvo inkubuoti kambario temperatūroje (22–25 °C) tam tikrais laiko intervalais – nuo 1 valandos iki per naktį – siekiant atlikti laiko priklausomą DNR skaidymo kinetinę analizę.

DNR hidrolizė buvo stebima matuojant sugertį ties 260 nm bangos ilgiu, kuris atitinka nukleotidų aromatinių žiedų sugertį, naudojant mikrodėklo skaitytuvą. Likusi DNR koncentracija kiekvienu laiko momentu buvo apskaičiuojama, kad būtų įvertintas skaidymo greitis. Šie eksperimentai buvo vykdyti tokioje pačioje temperatūroje ir pagal tokius pačius laiko parametrus, kaip ir imobilizuoto fermento tyrimuose, siekiant užtikrinti, kad bet kokie būsimi palyginimai atspindėtų paviršiaus imobilizacijos įtaką, o ne skirtingas reakcijos sąlygas. Šis tyrimas suteikė esminių įžvalgų apie *T7* DNR polimerazės 3′→5′ egzonukleazės efektyvumą natūralioje būsenoje ir patvirtino jos tinkamumą biojutiklių sistemoms, kuriose fermento-substrato sąveikas gali paveikti paviršiaus apribojimai.

Imobilizuotos T7 DNR polimerazės tyrimai

Buvo atlikta eksperimentų serija su auksu padengtais QSense® jutikliais, siekiant ištirti T7 DNR polimerazės elgseną prisijungus prie paviršiaus. Šiame skyriuje pateikiami protokolai, skirti biojutiklio paviršiams paruošti, formuojant savitvarkius monosluoksnius (SAM) iš karboksilo ir hidroksilo grupėmis pasibaigiančių alkanotiolių mišinių, fermento aktyviojo centro apsaugai, fermento imobilizavimui bei jo egzonukleazės aktyvumo ir stabilumo įvertinimui po imobilizacijos. Apsaugotos (užmaskuotos) T7 DNR polimerazės imobilizavimas yra esminis žingsnis kuriant fermentais grįstus biojutiklius. Šie protokolai sukurti siekiant išlaikyti fermento funkcionalumą, kartu leidžiant fermentą patikimai prisitvirtinti prie paviršiaus, tinkamo pakartotiniam naudojimui ir kinetiniam stebėjimui.

Auksu padengtų QSense® diskų valymo protokolas

Prieš formuojant SAM sluoksnius, auksu padengti QSense® elektrodai buvo valomi standartizuotu elektrocheminiu metodu, siekiant užtikrinti eksperimentų atkuriamumą ir pašalinti paviršiaus teršalus. Elektrodų valymo procedūra apima ciklinės voltamperometrijos (CV) nuskaitymus 0.1 M H_2SO_4 tirpale, potencialų diapazone nuo -0.25 V iki 1.25 V (lyginant su Ag/AgCl nuorodiniu elektrodu). Ši procedūra leidžia oksiduoti ir redukuoti aukso paviršių: anodinės eigos metu vyksta aukso oksidacija, efektyviai pašalinanti organinius likučius, o katodinėje eigoje redukuojamas aukso oksidas, pašalinant neorganinius teršalus ir atkuriant švarų metalinį paviršių. Ši kontroliuojama elektrocheminė aktyvacija padidina paviršiaus glotnumą ir reaktyvumą, skatindama stabilių ir tvarkingų SAM struktūrų susidarymą per stiprias Au–S jungtis. Elektrocheminis valymas ir paviršiaus paruošimas buvo atliekamas naudojant Gamry Reference 600 potenciostatą/galvanostatą, užtikrinant tikslų potencialų ciklų valdymą ir eksperimentų atkuriamumą. Buvo atliekami trys nuoseklūs CV ciklai, o aiškūs oksidacijos ir redukcijos pikai patvirtina priemaišų pašalinimą ir sėkmingą paviršiaus regeneraciją. Šis standartizuotas elektrocheminio valymo protokolas yra labai svarbus siekiant užtikrinti pastovią paviršiaus chemiją, optimizuoti biomolekulių imobilizacijos efektyvumą ir pagerinti biojutiklių taikymų patikimumą.

SAM sluoksnio formavimo protokolas

Funkcionalizuoti paviršiai buvo sukurti formuojant mišrius savaime susitvarkančius monosluoksnius (SAM) naudojant tioliu modifikuotus alkano junginius: 12-merkaptododekano rūgštį (12-MUA, su -COOH grupėmis) ir 6-merkapto-1-heksanolį (6-MCH, su -OH grupėmis). SAM mišiniai su skirtingomis molinėmis proporcijomis (nuo 1:9 iki 9:1 MUA:MCH) buvo ruošiami etanolio tirpaluose (žr. 5 pav.). Auksu padengti QSense® jutikliai buvo panardinami į 1 mM tiolių mišinius (pvz., 0,1 mM 12-MUA ir 0,9 mM 6-MCH santykiu 1:9; 0,2 mM 12-MUA ir 0,8 mM 6-MCH santykiu 2:8 ir t. t.) ir inkubuojami per naktį kambario temperatūroje tamsoje, kad savaime susiformuotų SAM sluoksnis per stiprius aukso–tiolio ryšius (Au/12-MUA+6-MCH). Skirtingi molinių koncentracijų santykiai leido sistemingai tirti, kaip 12-MUA ir 6-MCH santykis veikia monosluoksnio struktūrą ir funkcionalumą. Po inkubacijos paviršiai buvo praplauti etanoliu, kad būtų pašalintos neprisijungusios molekulės, ir funkcionalizuoti auksu padengti elektrodai (Au/12-MUA+6-MCH) buvo perkelti į specialiai sukonstruotą elektrocheminę QCM mikrocelę, sujungtą su „Gamry Reference 600“ potenciosatu/galvanostatu. Ši sistema leido atlikti elektrocheminį valymą ir realiu laiku įvertinti elektrodo paviršiaus švarumą modifikacijos metu. Paruošti elektrodai buvo aktyvuoti naudojant EDC/NHS jungimo chemiją, leidžiančią kovalentiškai imobilizuoti *T7* DNR polimerazę ant funkcionalizuoto paviršiaus.

T7 DNR polimerazės aktyviojo centro maskavimo protokolas

Siekiant išsaugoti fermento T7 DNR polimerazės aktyvumą imobilizacijos metu, jo aktyvusis centras buvo laikinai maskuotas. Tam 0.69 µM koncentracijos fermentas buvo iš anksto inkubuojamas su dvigrandėmis DNR (dsDNR) molekulėmis 30 minučių kambario temperatūroje, švelniai maišant, kad užtikrintų gerą sąveiką ir prisijungimą prie fermento 3′→5′ egzonukleazės srities. Šis maskavimo žingsnis neleidžia aktyviajam centrui tiesiogiai kovalentiškai prisijungti SAM sluoksnio formavimo metu, taip užtikrinant teisingą fermento orientaciją ir išlaikytą aktyvumą po imobilizacijos.

SAM aktyvavimas ir T7 DNR polimerazės imobilizacijos strategija

SAM sluoksnio aktyvavimas yra būtinas fermento imobilizacijai – tai sustiprina paviršiaus reaktyvumą ir leidžia formuoti stiprius kovalentinius ryšius su karboksilo grupėmis. Tokia aktyvacija leidžia specifinę fermento imobilizaciją, kontroliuoja jo orientaciją paviršiuje ir išsaugo aktyvaus centro prieinamumą, o tai būtina efektyviam fermentiniam aktyvumui. Be to, SAM aktyvavimas sumažina nespecifinį adsorbciją, pagerina sistemos atkuriamumą ir padidina fermento stabilumą prieš pH, temperatūros ir buferio sudėties svyravimus, užtikrinant tolygų fermento pasiskirstymą biojutikliuose ir efektyvesnį signalų fiksavimą.

Eksperimentų serija buvo atlikta naudojant funkcionalizuotą auksu padengtą elektrodą (Au/12-MUA+6-MCH), kuris buvo montuojamas į specialiai sukonstruotą mažo tūrio (0.1 mL) pernašos QCM celę. QCM matavimai buvo atliekami naudojant Maxtek QCM-R sistemą (5 MHz). Naudojant realaus laiko srauto sąranką, buvo galima nuolat stebėti dažnio ir pasipriešinimo pokyčius, tiksliai įvertinant paviršiaus funkcionalizaciją ir vėlesnes biomolekulines sąveikas.Prieš aktyvuojant SAM sluoksnį ant auksu padengto elektrodo (Au/12-MUA+6-MCH), elektrodo plovimas buvo atliekamas naudojant nukleazių neturintį vandenį esant pastoviam 1 mL/min srauto greičiui 30 minučių kambario temperatūroje uždaroje QCM celėje. Karboksilo grupių aktyvavimui naudotas tirpalas, sudarytas iš 0.6 mg/mL NHS ir 0.4 mg/mL EDC 1× PBS buferyje, pH 7.4, esant 0.5 mL/min

srauto greičiui, 20 minučių kambario temperatūroje. Po aktyvavimo į sistemą buvo įvesta 0.69 μM maskuotos T7 DNR polimerazės tirpalo 1× PBS buferyje, esant 0.1 mL/min srautui 2 valandoms kambario temperatūroje. Fermento adsorbcija buvo stebima realiu laiku QCM būdu, o po imobilizacijos elektrodo plovimas buvo atliktas PBS buferiu, kad būtų pašalintos neprisijungusios molekulės.

Imobilizacijos eksperimentai buvo kartojami tris kartus siekiant užtikrinti rezultatų atkuriamumą, o duomenys buvo analizuojami remiantis Sauerbrey lygtimi ir kinetiniais modeliais (pirmos, antros ir n-osios eilės). Dažnio (Δf) ir pasipriešinimo (ΔR) pokyčiai suteikė kiekybinių įžvalgų apie jungimosi kinetiką ir bendrą biojutiklio veikimą. Apskaičiuoti vidutiniai dažnio pokyčiai patvirtino rezultatų patikimumą viso eksperimento metu. Bendras SAM mišinio struktūros ir aktyvavimo proceso, įskaitant T7 DNR polimerazės imobilizaciją ir QCM signalo pokyčius, schematinis vaizdas pateikiamas 6 paveiksle. Vėliau funkcionalizuotas jutiklis buvo veikiamas taikiniu – DNR substratu – esant Mg^{2+} jonams, kurie būtini T7 DNR polimerazės katalitinio centro aktyvavimui.

Imobilizuotos T7 DNR polimerazės 3′→5′ egzonukleazės aktyvumo tyrimai

Imobilizuotos T7 DNR polimerazės katalizinis aktyvumas buvo įvertintas siekiant nustatyti, ar po kovalentinio prijungimo prie aukso paviršiaus (Au/12-MUA+6-MCH) SAM modifikuoto elektrodo buvo išsaugota jos 3′→5′ egzonukleazės funkcija. Šis žingsnis buvo būtinas norint patvirtinti, kad fermentas išlaikė savo funkcionalumą po prijungimo prie paviršiaus, bei palyginti jo veikimą su laisvo fermento aktyvumu, esant identiškoms buferio ir substrato sąlygoms. Sėkmingai imobilizavus fermentą ant serijos SAM modifikuotų auksu dengtų elektrodų (Au/12-MUA+6-MCH), paviršius buvo paveiktas 15 ng dvigrandės DNR (dsDNR) fragmentų T7 DNR polimerazės buferio sąlygomis (400 mM Tris-HCl (pH 7.5, 25 °C), 100 mM $MgCl_2$, 10 mM DTT), kurių sudėtyje buvo Mg^{2+} kaip būtinas kofaktorius, ir inkubuotas 18 valandų kambario temperatūroje, kad prasidėtų egzonukleazės reakcija. Reakcijos produktai buvo vizualizuoti naudojant 2 % TAE agaro gelio elektroforezę, stebint substrato fragmentų skaidymo pokyčius. Eksperimentas buvo suplanuotas taip, kad kuo tiksliau atkartotų tirpalo fazės reakcijos sąlygas. Buvo naudojamas vienodo ilgio ir koncentracijos dsDNR substratas, kad būtų sumažinta variacija ir užtikrintas palyginamumas tarp paviršiuje prijungto ir laisvo fermento aktyvumo. Reakcijos trukmė buvo parinkta pagal optimalų aktyvumo laiką, nustatytą tirpalo pagrindu atliktuose tyrimuose.

Imobilizuotos T7 DNR polimerazės biojutiklio pakartotinio naudojimo protokolas

Siekiant įvertinti sukurto biojutiklio praktinį pritaikomumą ir stabilumą, buvo sukurtas pakartotinio naudojimo protokolas, skirtas tirti imobilizuotos T7 DNR polimerazės fermentinį aktyvumą per kelis egzonukleazės aktyvumo ciklus. Tyrimai siekė nustatyti, ar biojutiklis išlaiko 3′→5′ egzonukleazės aktyvumą per pakartotinius naudojimus, bei identifikuoti sąlygas, kurios optimizuoja fermento aktyvumo išlaikymą. Tyrimai buvo atlikti naudojant SAM modifikuotą aukso elektrodą (Au/12-MUA+6-MCH), kurio 12-MUA ir 6-MCH molinis santykis buvo 6:4. T7 DNR polimerazė buvo kovalentiškai imobilizuota naudojant anksčiau aprašytą 0.1 mL tūrio srautinę QCM celę. Fermento kiekis ant paviršiaus buvo nustatytas – maždaug 427.95 ± 0.60 ng. dsDNR fragmentai, kaip substratai, buvo įleidžiami į srautinę QCM sistemą T7 DNR polimerazės buferio sąlygomis (400 mM Tris-HCl (pH 7.5, 25 °C), 100 mM $MgCl_2$, 10 mM DTT) su Mg^{2+} kaip būtinų kofaktoriumi fermentinei veiklai. Kiekvienam ciklui buvo naudojama 1 ng dsDNR substrato, inkubuojant 45 ir 90 minučių kambario temperatūroje, taip simuliuojant greitoms

biojutiklio analizėms būdingas sąlygas. Po kiekvienos reakcijos paviršius buvo švelniai praplaunamas buferiu, pašalinant reakcijos produktus, o tas pats fermentinis paviršius buvo naudojamas kitam ciklui be regeneracijos. DNR substratų degradacijos efektyvumas kiekviename cikle buvo vertinamas naudojant 2 % TAE agaro gelio elektroforezę. Juostų intensyvumo pokyčiai buvo kiekybiškai analizuojami naudojant „TotalLab“ vaizdo analizės programinę įrangą, o optinių juostų tūriai buvo naudojami likutinės DNR koncentracijos po egzonukleazės reakcijos įvertinimui.

Imobilizuotos T7 DNR polimerazės hidrolizės tyrimo protokolas

Hidrolizės eksperimentai buvo atliekami naudojant Proteinazę K – plataus spektro serino proteazę – siekiant įvertinti imobilizuotos *T7* DNR polimerazės jautrumą proteolitiniam skaidymui. Šie tyrimai buvo skirti fermento stabilumo analizavimui bei QCM metodo tinkamumo realaus laiko paviršinių baltymų degradacijos stebėjimui įvertinimui. Sėkmingai imobilizavus fermentą ant SAM modifikuoto aukso elektrodo (Au/12-MUA+6-MCH), paviršius buvo veikiamas 1.4 µM Proteinazės K tirpalu 1× PBS buferyje (pH 7.4), kuris buvo tiekiamas pastoviu 0.1 mL/min srautu 2 valandas kambario temperatūroje. Hidrolizės procesas buvo stebimas realiu laiku naudojant QCM sistemą.

Pagrindinė baltymo hidrolinės reakcija apima T7 DNR polimerazės hidrolizę Proteinazės K pagalba:

T7 DNR polimerazė + Proteinazė K → Hidrolizuoti peptidai + Aminorūgštys

Šis tyrimas buvo skirtas įvertinti imobilizuotos T7 DNR polimerazės veikimą ir stabilumą skirtingų SAM mišinių sąlygose. Hidrolizės efektyvumo analizė buvo naudojama nustatyti optimalią SAM mišinio sudėtį, kuri užtikrina didžiausią fermento stabilumą. Be to, buvo atlikta kiekybinė kinetinių duomenų (pirmo, antro ir n-laipsnio) analizė, leidžianti suprasti, kaip imobilizacijos matrica veikia fermento hidrolizės jautrumą. Šie rezultatai suteikia įžvalgų į patikimesnių ir efektyvesnių fermentinių biojutiklių kūrimą įvairioms taikymo sritims.

BAFF biojutiklio kūrimas

SAM aktyvinimo ir BAFF imobilizavimo protokolas

Auksu dengto QSense® jutiklio valymo protokolas, taip pat SAM mišinio paruošimas, SAM aktyvinimas ir BAFF imobilizavimo procesas, naudojant specialiai sukonstruotą mažo tūrio (0,1 mL) srautinę QCM ląstelių sistemą, buvo atliktas tiksliai, kaip aprašyta ankstesniuose skyriuose, naudojant T7 DNR polimerazę. Visi parametrai ir proceso sąlygos buvo išlaikytos vienodos. 3:7 SAM mišinio sudėtis ant auksu padengtų elektrodų (Au/12-MUA+6-MCH) buvo specialiai parinkta siekiant užtikrinti sėkmingą BAFF baltymo imobilizavimo tyrimą.

SAM deaktyvinimas su BSA

Po sėkmingo BAFF imobilizavimo eksperimentų serijoje, naudojant auksu padengtą elektrodą (Au/12-MUA+6-MCH) su 3:7 SAM modifikuotu paviršiumi, nepasisavinusios paviršiaus vietos buvo deaktyvuotos taikant 1 mg/mL BSA tirpalą 1X PBS buferyje (pH 7,4). Šis žingsnis buvo atliktas siekiant užblokuoti nespecifinio prisijungimo vietas, naudojant specialiai sukonstruotą mažo tūrio (0.1 mL) srautinę QCM sistemą, esant

pastoviam srautui 0.1 mL/min 20 minučių kambario temperatūroje ir tamsoje, stebint dažnio pokytį (Δf) realiu laiku, kad būtų patvirtintas paviršiaus prisotinimas. Po deaktyvinimo elektrodo paviršius buvo plaunamas 1X PBS tirpalu (pH 7.4), taikant tas pačias srauto sąlygas, kad būtų pašalintas neprisijungęs BSA.

Galvijų serumo albuminas (BSA) dažnai naudojamas kaip blokavimo agentas biojutiklių taikymuose dėl palankių fizikocheminių savybių. BSA yra stabilus, vandenyje tirpus baltymas, gausus serume, turintis palyginti didelę molekulinę masę (~66,5 kDa), todėl yra veiksmingas paviršiaus prisotinimui. Dėl didelio krūvį turinčių aminorūgščių kiekio ir hidrofilinės prigimties, jis gali adsorbuotis ant paviršių elektrostatinių ir van der Waals sąveikų dėka, formuodamas stabilų, nespecifinį baltymų sluoksnį, kuris neleidžia prisijungti netikslingiems molekulių tipams. Svarbu tai, kad BSA neturi funkcinių grupių, kurios trukdytų specifinei tiriamosios analitės ir jutiklio sąveikai, todėl leidžia aptikti tik specifines sąveikas. Tai daro jį idealiu pasirinkimu nespecifinės baltymų adsorbcijos prevencijai, kuri kitaip galėtų sukelti triukšmą ir klaidingus rodmenis biojutiklių eksperimentuose. Be to, BSA žinomas dėl paviršiaus pasyvinimo išlaikymo ilgesnį laiką, kas užtikrina nuoseklų ir patikimą jutiklio veikimą. Taip pat BSA yra ekonomiškas, lengvai naudojamas ir suderinamas su daugeliu buferių sistemų, įskaitant 1X PBS (pH 7.4), todėl plačiai taikomas paviršiaus deaktyvinimo protokoluose.

Tikslinis DNR aptikimas su BAFF jutikliu

Po SAM deaktyvinimo ant auksu dengto elektrodo (Au/12-MUA+6-MCH/BAFF/BSA), BAFF biojutiklis buvo funkcionalizuotas įvedant specifinį viengubos grandinės DNR (ssDNR) fragmentą. Šis žingsnis buvo atliktas tikslingam aptikimui, naudojant specialiai sukonstruotą mažo tūrio (0.1 mL) srautinę QCM ląstelių sistemą, esant pastoviam srautui 0.1 mL/min 20 minučių kambario temperatūroje ir tamsoje, stebint dažnio pokytį (Δf) realiu laiku, kad būtų patvirtintas ssDNR prisijungimas. Po šio žingsnio biojutiklio paviršius buvo plaunamas 1X PBS buferiu (pH 7.4), taikant tokias pačias srauto sąlygas, kad būtų pašalintas neprisijungęs ssDNR. BAFF adsorbcija ir poimobilizacinis plovimas 1XPBS buferiniu tirpalu, paviršiaus deaktyvinimas BSA ir tikslinės DNR adsorbcija buvo atliekami realiu laiku, taikant QCM stebėjimą, siekiant sukurti veikiantį BAFF biojutiklių. Visas procesas buvo pakartotas tris kartus, siekiant užtikrinti pakartojamumą, o analizė atlikta remiantis Sauerbrey lygčių masei nustatyti ir kinetiniu modeliavimu. Buvo atlikta ir kiekybinė kinetinių modelių (pirmo, antro ir n-laipsnio) analizė, siekiant suprasti fermento ir imobilizavimo matricos sąveiką bei jos poveikį fermento hidrolizės jautrumui. Šie duomenys suteikia įžvalgų kuriant patvaresnius ir efektyvesnius fermentinius biojutiklis įvairioms taikymo sritims.

Šiame tyrime analizuojama neimobilizuotos ir imobilizuotos T7 DNR polimerazės sąveika ir jos 3'→5' egzonukleazės aktyvumas. Šiame skyriuje pateikiama detali analizė eksperimentų, atliktų su auksu padengtu elektrodu (Au/12-MUA+6-MCH), funkcionalizuotas skirtingais SAM paviršių moliniais santykiais. Eksperimentiniai tyrimai buvo atliekami naudojant auksu dengtus QCM jutiklius, daugiausia dėmesio skiriant T7 DNR polimerazei ir BAFF baltymui, siekiant pademonstruoti galimybę konstruoti bežymes DNR modifikuojančius fermentinius biojutiklius. Naudojant šiuos jutiklius, parodyta, kaip fermentų ir baltymų imobilizavimas ant auksinių paviršių gali būti veiksmingai atliktas ir stebimas realiu laiku. Sąveikos kinetika buvo vertinama atliekant išsamius skaičiavimus, siekiant įvertinti imobilizuotos T7 DNR polimerazės ir BAFF prisijungimo elgseną. Šie skaičiavimai buvo labai svarbūs siekiant suprasti, kaip fermentai sąveikauja su substratais būdami prisijungę prie kietojo paviršiaus ir kaip šis paviršius veikia fermento katalitinį aktyvumą. Rezultatai atskleidė svarbių įžvalgų apie biojutiklių funkcinį stabilumą ir veikimą bei jų pritaikymo potencialą realiose diagnostinėse situacijose.

Neimobilizuotos T7 DNR polimerazės tyrimai

Norint ištirti neimobilizuotos T7 DNR polimerazės elgseną, buvo atliekama DNR (Low DNA Mass Ladder) fragmentų hidrolizė, naudojant skirtingas DNR substratų koncentracijas. Low DNA Mass Ladder sudaro 100 bp–2000 bp ilgio DNR fragmentai. Šie fragmentai yra dvigrandžiai ir paprastai turi bukus galus. Abiejų DNR grandžių galai baigiasi tuo pačiu nukleotidu, todėl nėra laisvų galų [82,83]. Bukų galų DNR fragmentai paprastai yra stabilesni, tačiau gali būti mažiau efektyvūs specifinėms fermentinėms reakcijoms, tokioms kaip ligacija. T7 DNR polimerazė prisijungia prie bukų galų DNR fragmentų. Toks galas sudaro paprastą substratą fermento 3'→5' egzonukleazės aktyvumui. T7 DNR polimerazės 3'→5' egzonukleazės aktyvumas pašalina nukleotidus nuo DNR grandinės 3' galo [84]. Šis aktyvumas dažniausiai naudojamas koreguoti neteisingai įjungtus nukleotidus DNR sintezės metu, tačiau taip pat efektyviai hidrolizuoja DNR fragmentus, kai nevyksta polimerizacijos sintezė. Egzonukleazės aktyvumas progresyviai trumpina DNR fragmentą, tol, kol fermentas atsiskiria nuo DNR arba fragmentas visiškai suskaidomas. Fermentas skaido fosfodiesterinius ryšius tarp nukleotidų, atskirdamas nukleotidus po vieną nuo 3' galo [10,85].

Šio tyrimo dalyje buvo naudotas 1 µg Low DNA Mass Ladder kaip dvigrandės DNR (dsDNA) substratas, kuriam buvo taikoma 21 valandos reakcija T7 DNR polimerazės buferio sąlygomis (400 mM Tris-HCl (pH 7.5 prie 25 °C), 100 mM $MgCl_2$ ir 10 mM DTT). Rezultatai patvirtino, kad per 21 valandos in vitro reakciją, naudojant 12.5 U T7 DNR polimerazės, 1 µg Low DNA Mass Ladder buvo visiškai hidrolizuotas. Rezultatai pateikiami abiem reakcijoms – su fermentu ir be jo – 7 pav.

Norint ištirti neimobilizuotos T7 DNR polimerazės elgseną, buvo stebima skirtingo ilgio DNR fragmentų hidrolizė, naudojant skirtingas DNR substrato koncentracijas. Skirtingo ilgio DNR fragmentų degradacija fermentinės reakcijos metu buvo sekama matuojant sugertį ties 260 nm kas 30 sekundžių 1 valandos laikotarpiu. Šios sugerties vertės buvo konvertuotos į likusią DNR koncentraciją (8 pav.) kiekvienu laiko momentu. DNR hidrolizės reakcija iš pradžių buvo analizuojama pagal pirmos eilės kinetinį modelį, siekiant ištirti DNR skaidymo kinetiką. Norint nustatyti, ar reakcija vyksta pagal pirmos eilės kinetiką, buvo sudaryta laiko (t) ir likusios DNR koncentracijos natūrinio logaritmo, ln([S]), kreivė. Čia [S] reiškia likusią DNR koncentraciją kiekvienu laiko intervalu. Buvo atlikta linijinė regresijos analizė per pirmąsias 200 sekundžių, naudojant skirtingo ilgio

DNR fragmentus ir pradines substratų koncentracijas (25 ng ir 12.5 ng). Ši analizė leido apskaičiuoti nuolydį, laisvąjį narį ir R^2 reikšmę. Tiesinė priklausomybė šioje kreivėje patvirtina, kad reakcija vyksta pagal pirmos eilės kinetiką, kaip parodyta 9 ir 10 pav.

Norint toliau įvertinti pirmos eilės kinetinio modelio tinkamumą, eksperimentiniai duomenys buvo palyginti su teoriniu modeliu, gautu iš pirmos eilės kinetinės lygties, įvertinant pritaikymo tikslumą. Reakcijos pradinis greitis V_0 yra tiesiogiai proporcingas substrato koncentracijai [S], o tai išreiškiama lygtimis (3) ir (4). Naudojant iš eksperimentinių duomenų gautą nuolydį ir laisvąjį narį, buvo perskaičiuota likutinė DNR koncentracija įvairiems DNR ilgiams. Tiek eksperimentiniai, tiek modeliavimo duomenys pavaizduoti (11 ir 12 pav.), ir įvertintas pirmos eilės kinetinio modelio tinkamumas. Palyginimas parodė atitikimą viso reakcijos laikotarpio metu ($R^2 > 0.99$), nurodant, kad reakcija iš tikrųjų vyksta pagal pirmos eilės kinetiką – be reikšmingų difuzijos, fermento prisotinimo ar kitų trukdančių veiksnių poveikio.

Norint įvertinti T7 DNR polimerazės 3'→5' egzonukleazės aktyvumo Michaelis–Menten kinetiką, reakcijos pradinis greitis V_0 buvo perskaičiuotas pagal šias kinetines lygtis (5) ir (6). Sudarius reakcijos greičio V_0 ir substrato koncentracijos [S] grafiką (13 ir 14 pav.), duomenys buvo pritaikyti prie Michaelio–Menten lygties naudojant nelinijinę regresiją. Buvo įvertinti pagrindiniai kinetiniai parametrai – V_{max} ir K_m, o kreivės parodė fermento prisotinimą esant aukštoms substrato koncentracijoms. Buvo nustatyta, kad ilgesni DNR fragmentai turi didesnę K_m reikšmę (mažesnį fermento afinitetą), tačiau V_{max} išlieka panašus, o trumpesni fragmentai pasižymi mažesnėmis K_m reikšmėmis (didesniu afinitetu). Be to, 25 ng koncentracijoje V_{max} buvo šiek tiek didesnis nei 12.5 ng, o tai rodo fermento aktyvumą plačiame koncentracijų diapazone.

Michaelio–Menten duomenų hiperbolinė priklausomybė buvo tiesiškai transformuota naudojant Lineweaver-Burk metodą pagal (7) lygtų. Lineweaver-Burk kreivės (15 ir 16 pav.) patvirtino teorinį atitikimą, o apskaičiuoti K_m rodikliai (pvz., K_m = 1.38–6.57 s^{-1} prie 12.5 ng; K_m = 3.33–8.36 s^{-1} prie 25 ng) parodė, kad fermento aktyvumo metu substratas dažniausiai veikia prisotinto fermento sąlygomis.

Norint įvertinti kinetiką esant mažoms substrato koncentracijoms ([S] ≪ K_m), buvo naudota pirmos eilės kinetika, braižant ln(V_0) prieš ln([S]) grafiką (17 pav.). Gauta tiesinė priklausomybė su nuolydžiu ~0.4 rodo frakcinės eilės kinetiką – reakcijos greitis priklauso nuo substrato koncentracijos ne vientisa proporcija. Tokia kinetika gali būti susijusi su fermento-substrato sąveika, steriniu slopinimu ar difuzijos apribojimais. Nepaisant to, kad nuolydis rodo frakcinę eilę, bendras fermento aktyvumas vis tiek gerai atitiko klasikinę Michaelio–Menten kinetiką, todėl papildomos aukštesnės eilės analizės nebuvo atliktos.

Panašūs pseudo pirmos eilės greičio pastovūs dydžiai (k_{cat}) buvo nustatyti – 0.026 s^{-1} ir 0.023 s^{-1} prie 25 °C, pH 8.0 [86]. Literatūroje nurodyta, kad T7 DNR polimerazė naudojama 1 μM koncentracijoje, o šiame tyrime naudota ~1.6 μM (10 U fermento, jei 1 U = 1 nmol aktyvumo). Be to, literatūroje naudotas fluorescenciniu žymeniu (FAM) žymėtas substratas, kuris gali paveikti sąveikos dinamiką, taip pat į reakciją buvo įtraukti komponentai (pvz., tioredoksinas, BSA, Mg^{2+}), kurie stiprina fermento aktyvumą. Galiausiai, šie tyrimai su laisvu fermentu buvo naudojami kaip bazinis modelis, norint išanalizuoti, kaip skiriasi fermento kinetika, kai jis yra imobilizuotas. Imobilizacija gali turėti įtakos fermento prieinamumui, konformacijai bei vietinei substrato koncentracijai. Lyginant laisvo ir imobilizuoto fermento reakcijos greičius ir afinitetą substratui, buvo siekiama įvertinti imobilizacijos įtaką fermento veiksmingumui bei specifiškumui biojutiklių sistemose. Šie rezultatai buvo esminiai norint suprasti imobilizuoto fermento taikymo galimybes realiose aptikimo sistemose. Lentelėse 3 ir 4 pateikti T7 DNR polimerazės 3'→5' egzonukleazės aktyvumo su įvairaus ilgio DNR fragmentais kinetinių

duomenų rezultatai, naudojant atitinkamai 25 ng (lentelė 3) ir 12.5 ng (lentelė 4) pirminę substrato koncentraciją.

Imobilizuotos T7 DNR polimerazės tyrimai

QSense® jutiklio charakterizavimas po valymo

Ciklinės voltamperometrijos (CV) matavimai buvo atlikti esant potencialo intervalui nuo -0.25 V iki 1.25 V (lyginant su Ag/AgCl) 0.1 M H_2SO_4 tirpale, esant 100 mV/s skenavimo greičiui. CV matavimai buvo atlikti tris kartus siekiant užtikrinti rezultatų atkuriamumą. Tipiniai auksinio elektrodo voltamogramos parodytos 18 paveiksle. Vizualiai vertinant kreives, pastebimi aiškūs skirtumai, leidžiantys preliminariai įvertinti aukso paviršiaus kokybę. Ypač pastebima deguonies desorbcijos viršūnė ties maždaug 0.5 V, būdinga švariems aukso paviršiams. Ši viršūnė rodo tinkamą paviršiaus išvalymą ir aktyvavimą, patvirtinantį, kad paviršius paruoštas tolesnei biofunkcionalizacijai.

SAM paviršiaus charakterizavimas

FTIR spektroskopija buvo naudota tirti 12-MUA ir 6-MCH santykio poveikį SAM struktūrai ir fermento *T7* DNR polimerazės imobilizacijai. Spektrai atskleidė, kad karboksilo (COOH, ~1700 cm^{-1}) ir hidroksilo (OH, ~3300 cm^{-1}) grupių santykis turi reikšmingos įtakos fermento prisijungimui, stabilumui ir aktyvumui. Didelis COOH kiekis (9:1 santykis) pagerina fermento prisijungimą per elektrostatines ar kovalentines sąveikas, tačiau gali riboti fermento lankstumą. Tuo tarpu didelis OH kiekis (1:9 santykis) sukuria labiau hidrofilinį paviršių, skatinantį fermento aktyvumą, tačiau silpniau prisijungiantį fermentą. Subalansuotas 5:5 santykis užtikrina optimalią fermento imobilizaciją per COOH elektrostatines sąveikas ir OH vandenilinius ryšius. FTIR duomenys rodo, kad 5:5 SAM sudėtis užtikrina geriausią pusiausvyrą tarp fermento stabilumo ir veiksmingumo, nes sukuria tinkamą paviršiaus mikroaplinką, leidžiančią fermentui išlaikyti aktyvią konformaciją. Tolesni tyrimai nagrinėja T7 polimerazės imobilizaciją naudojant skirtingus SAM santykius.

T7 DNR polimerazės jutiklio rezultatų aptarimas

Fermento imobilizavimui taikomų SAM mišinių paviršių panaudojimas. QCM duomenų analizės charakterizavimas

QCM registruoja rezonansinio dažnio pokytį, proporcingą masei, nusėdusiai ant paviršiaus [90,91]. Eksperimentinė T7 DNR polimerazės imobilizavimo/adsorbcijos kinetikos ir sluoksnio storio tyrimo schema pateikta 20 paveiksle. Kiekvienas dažnio pokyčio taškas atspindi tris kartus pakartotų matavimų rezultatus, atliktus stabiliomis sąlygomis naudojant skirtingus SAM mišinių paviršius kambario temperatūroje. Esant fiziologinėms sąlygoms (pH 7.4), peptidinio ryšio susidarymas ir T7 DNR polimerazės adsorbcijos procesas ant auksu padengto elektrodo, prijungto prie QCM sistemos, lemia Δf pokyčius proceso metu. Tiesioginio stebėjimo QCM profilis atspindi T7 DNR polimerazės adsorbcijos procesą. Adsorbcijos metu buvo stebėtas staigus rezonansinio dažnio (Δf) kritimas po to, kai QCM jutikliai buvo inkubuojami su skirtingais SAM mišiniais padengtais auksuotais elektrodais. Rezonansinio dažnio pokyčių (Δf) vertės mažėjo proporcingai didėjant karboksilinių grupių kiekiui paviršiuje (žr. 20 pav.). Pirmasis staigus signalo pokytis siejamas su greitu

T7 DNR polimerazės adsorbcijos etapu ant SAM mišinio paviršiaus, kurį lemia: i) maksimalus masės pernašos greitis per ribinį sluoksnį virš savaime susiformavusio monosluoksnio (SAM), dėl kurio fermento koncentracija paviršiuje iš pradžių yra lygi nuliui; ii) visiškai prieinama sensoriaus paviršiaus adsorbcijai.

Po rezonansinio dažnio stabilizavimo 1X PBS buferiu (pH 7.4) kambario temperatūroje, pastovūs dažnio poslinkiai buvo pasiekti po 30–100 minučių (laikotarpis nuo 50 iki 80 min 1:9 SAM mišiniui ir nuo 50 iki 150 min 9:1 SAM mišiniui). Vėliau buvo atliktas skalavimo žingsnis su 1X PBS (pH 7,4) buferiu, siekiant pašalinti nesusijungusias T7 DNR polimerazės molekules nuo aukso paviršiaus ir/arba leisti fermentui persitvarkyti į mažesnės energijos konformacijas. Šie dinaminiai pokyčiai leido atsirasti papildomoms adsorbcijos vietoms paviršiuje, todėl stebėta lėta, bet pastovi adsorbcija iki visiško prisotinimo. Šiame etape pasiekiama dinaminė pusiausvyra tarp naujai adsorbuojamų T7 DNR polimerazės molekulių ir jų desorbcijos nuo SAM modifikuoto QCM jutiklio paviršiaus.

Nedideli rezonansinio dažnio pokyčiai T7 DNR polimerazei adsorbuojantis ant 7:3, 8:2 ir 9:1 SAM mišinių paviršių rodo, kad QCM jutiklio paviršius buvo visiškai padengtas fermento molekulėmis. Pažymėtina, kad apie 80 % visų molekulių buvo imobilizuota per pirmąsias 30 min kambario temperatūroje. Atsižvelgiant į QCM celės srauto konstrukciją ir pasirinktą srauto greitį (0.1 ml/min), toks pradinis kovalentinis prijungimas greičiausiai yra ribojamas fermento difuzijos per ribinį sluoksnį, o ne paviršiaus reakcijos. Duomenys rodo, kad didinant SAM mišinių koncentraciją, padidėja T7 DNR polimerazės kiekis, imobilizuotas ant paviršiaus. Darant prielaidą, kad imobilizacijos procesą riboja kinetika, adsorbuotas sluoksnis yra standžiai susijungęs su jutiklio paviršiumi, o viskoelastiniai efektai yra nereikšmingi (šiame tyrime <10), visi rezonansinio dažnio pokyčiai buvo pritaikyti Sauerbrey [92] lygties (13 lygtis) modeliui fermento masei apskaičiuoti. Šiame tyrime kovalentiškai pritvirtinta T7 DNR polimerazė elgiasi kaip standus sluoksnis (sklaidymo pokytis $\Delta D/(-\Delta f/n) < 4\times10^{-7}$ Hz^{-1}), todėl energijos sklaida nedaro įtakos rezonansinio dažnio matavimams. Sauerbrey modelis pakankamai tiksliai įvertina adsorbuoto sluoksnio masę. Naudojant Δfn reikšmes buvo apskaičiuota Au/12-MUA+6-MCH/T7 DNR polimerazės sluoksnio masė. Taip pat kiekviename žingsnyje buvo atlikta regresijos analizė, siekiant nustatyti susiformavusio monosluoksnio storį.

Kinetinių modelių charakterizavimas

Šiame tyrime naudojami pseudo-pirmos eilės (14 lygtis), pseudo-antros (15 lygtis) eilės ir savavališkos eilės (n) (16 lygtis) kinetiniai modeliai, siekiant išanalizuoti T7 DNR polimerazės kovalentinio prisijungimo kinetiką ant skirtingų SAM mišinių. Taikant 14-16 lygtis, darant prielaidą, kad matuotos koncentracijos atitinka fermento koncentraciją ant SAM paviršiaus. Atitikimo kreivės (21 pav.) parodytos kiekvienam modeliui, o parametrų reikšmės pateiktos kiekvienam SAM mišiniui. Koreliacijos koeficientai (R^2) visiems modeliams viršija 0.93 (išskyrus pseudo-antros eilės modelį 1:9 SAM mišiniui), o tai rodo gerą duomenų atitikimą. Pseudo-pirmos ir pseudo-antros eilės modeliai gerai atitiko eksperimentinius duomenis. Eksperimentinės adsorbcijos talpos ir teorinės reikšmės palyginimas pateiktas 21 pav. Nors n- eilės kinetinis modelis duoda kitokią m_{max} reikšmę, koreliacijos koeficientas išliko aukštas. Visgi pseudo-pirmos eilės modelis geriausiai atitiko tiek eksperimentinius duomenis, tiek jų teorinę analizę (m_{max} = 427.95 ng; R^2 = 0,992), artimai atitiko eksperimentinę reikšmę (436.34 ng).

Revellame ir kt. [94] išsamiai apžvelgė pseudo-pirmos ir pseudo-antros eilės kinetinius modelius fermentų imobilizacijai. Ezzati ir kt. [95] šiuos modelius išvedė remdamiesi Langmuir ir Freundlich izotermomis. Šiame tyrime pritaikyti tie patys modeliai

T7 DNR polimerazės kinetikos analizei, o jų rezultatai patvirtino pseudo-pirmos eilės modelio tinkamumą. Šiame skyriuje taip pat ištirta, ar imobilizuota T7 DNR polimerazė išlaiko savo funkcionalumą. Siekiant apsaugoti aktyvų fermento centrą, imobilizavimo metu fermentas buvo dalinai apsaugotas DNR molekulėmis, leidžiančiomis fermentui išlaikyti teisingą orientaciją. Pakako pridėti kofaktorių – magnį, kad fermentas atgautų aktyvumą. Specifiškumas buvo įvertintas, pasirinkus dvigrandinę DNR substratą, tinkamą 3'→5' egzonukleazės aktyvumui vertinti [96–98]. Po 18 valandų fermentinės reakcijos su buferiu, turinčiu magnio, ir 15 ng dvigrandinės DNR fragmento kambario temperatūroje, reakcijos produktai buvo išskirti agarozės geliu. Stebėti substrato fragmentų degradacijos pokyčiai (žr. 21 pav.). 5 lentelėje pateikti kinetinių skaičiavimų rezultatai. Rezultatai parodė, kad QCM sensorius su 427.95 ± 0.60 ng imobilizuotos T7 DNR polimerazės gali specifiškai skaidyti 15 ng DNR fragmentų per naktį kambario temperatūroje. Šie rezultatai rodo, kad 10 ng T7 DNR polimerazės imobilizavimas sukelia apie 1.20 Hz dažnio pokytį. Tai patvirtina, kad fermentas buvo pilnai funkcionalus visuose vertintuose SAM mišinių paviršiuose, o jo aktyvus centras liko apsaugotas nuo inaktyvacijos.

Naudojant struktūriškai pagrįstą, gerai suprojektuotą T7 DNR polimerazę, sistema leidžia analizuoti efektyvaus šio fermento imobilizavimo galimybes ir savybes ant QCM jutiklių paviršiaus. QCM metodas atspindi fundamentalią ir inovatyvią prieigą prie DNR modifikuojančiais fermentais pagrįstų biojutiklių tobulinimo. Rezultatai patvirtina, kad QCM pagrindu atliekamas DNR nustatymas yra itin jautrus [99–101], pasižymi greitu atsaku [102,103], tinka realaus laiko matavimams [104,105], yra nebrangus [106] ir gali būti naudojamas ne laboratorijos sąlygomis [107,108]. Naudojant QCM zondus, norint efektyviai nustatyti analitinį signalą, nereikia papildomų žymeklių, žymenų ar mediatorių. Kiekybiniai rezultatai rodo, kad aktyvųjį centrą turinti apsaugota T7 DNR polimerazė gali būti pilnai imobilizuota ant įvairios sudėties SAM mišinių paviršių neprarandant funkcionalumo. Patikimas QCM tyrimas patvirtino, kad T7 DNR polimerazė pasižymi specifiškumu, o paviršiaus prisotinimas pasiekiamas naudojant 6:4 santykio SAM mišinį, kai fermento kiekis paviršiuje pasiekia maksimalią imobilizacijos koncentraciją.

Kaip parodė tyrimai su neimobilizuota T7 DNR polimeraze, 1 μg (1000 ng) DNR buvo pilnai hidrolizuota per 21 valandą naudojant 12.5 U neimobilizuotos T7 DNR polimerazės, kas rodo šio fermento gebėjimą ilgalaikėje reakcijoje skaidyti didelį DNR kiekį. Imobilizuoto fermento tyrimuose 3 U (arba 427.95 ± 0.60 ng) T7 DNR polimerazės hidrolizavo tik 15 ng DNR, pabrėžiant katalizinio efektyvumo skirtumą tarp laisvos ir imobilizuotos fermento formos. Imobilizuotas fermentas pasižymi tik ~6.26 % efektyvumu (imobilizuotas fermentas skaido ~0.000066 ng DNR fragmento per 1 U T7 DNR polimerazės per sekundę; laisvas fermentas – ~1.06 ng DNR fragmento per 1 U per sekundę), lyginant rezultatus su neimobilizuotu fermentu per tą patį reakcijos laiką. Šis skirtumas greičiausiai susijęs su ribota difuzija, steriniais trukdžiais arba pakitusia fermento dinamika, kai jis yra imobilizuotas.

T7 DNR polimerazės biojutiklio pakartotinio panaudojimo charakterizavimas

Norint įvertinti imobilizuotos T7 DNR polimerazės pakartotinį panaudojamumą, fermentu funkcionizuoti QCM jutikliai, paruošti naudojant 6:4 santykio Au/12-MUA+6-MCH sluoksnį, buvo taikomi daugkartiniams DNR hidrolizės ciklams. Tyrimo tikslas buvo įvertinti, kiek fermentas išlaiko savo 3'→5' egzonukleazės aktyvumą po pakartotinio naudojimo, kas yra itin svarbu vertinant jo tinkamumą ilgalaikiuose biojutiklių taikymuose. Duomenys iš QCM analizės ir imobilizavimo efektyvumas naudojant užmaskuotą T7 DNR polimerazę 6:4 santykio SAM mišinyje pavaizduoti 22 pav. Staigus dažnio sumažėjimas po 40 minučių rodo greitą užmaskuotos T7 DNR polimerazės prisijungimą prie jutiklio

paviršiaus, kas atspindi efektyvų pradinį imobilizacijos etapą. Šis dažnio poslinkis (Δf) koreliuoja su ant paviršiaus imobilizuotos fermento masės kiekiu. Po pradinio prisijungimo dažnis stabilizuojasi, žymėdamas, kad sistema pasiekė pusiausvyrą, kai ant paviršiaus masės pokyčiai tampa minimalūs. Trijų eksperimentinių kartojimų metu gauti labai artimi Δf_{max} reikšmių rezultatai (–52.06 Hz, –52.37 Hz ir –52.59 Hz) rodo didelį pakartojamumą ir nuoseklų T7 DNR polimerazės imobilizacijos efektyvumą ant Au/12-MUA+6-MCH sluoksnio. Maža variacija tarp kartojimų leidžia manyti, kad imobilizacijos sąlygos buvo optimizuotos, užtikrinant stabilų fermento prisitvirtinimą ir sudarant patikimą platformą tolimesnei analizei ar pritaikymui.

Buvo taikytos dvi skirtingos inkubacijos trukmės – 45 ir 90 minučių – siekiant išnagrinėti, kaip reakcijos laikas veikia imobilizuoto fermento funkcinį stabilumą ir pakartotinį panaudojimą 6:4 santykio Au/12-MUA+6-MCH funkcionizuotuose elektroduose (23 pav.). Po kiekvieno reakcijos ciklo elektrodo paviršius buvo nuplaunamas ir pakartotinai naudojamas tomis pačiomis sąlygomis, imituojant praktinį jutiklio regeneravimą. Imobilizuotos užmaskuotos T7 DNR polimerazės pakartotinio panaudojimo stabilumas ir egzonukleazės aktyvumo efektyvumas buvo analizuojami taikant 2 % TAE agarozės gelio elektroforezę ir optinių juostų tūrio analizę. Eksperimentinėje schemoje buvo numatytos kontrolinės juostos („K“) – reakcija be fermento – ir nuoseklūs pakartotinio panaudojimo ciklai (1–5), kurie leido įvertinti egzonukleazės funkciją ir dvigrandės DNR fragmento skaidymo galimybes per kelis ciklus. 2 % TAE agarozės gelio elektroforezės vaizdas rodo DNR juostos intensyvumo pokyčius, nurodančius DNR substrato hidrolizės efektyvumo mažėjimą po kelių ciklų. Reakcijos trukmės – 45 minutės (a) ir 90 minučių (b) – buvo naudojamos skirtingoms substrato apdorojimo sąlygoms imituoti. Elektroforezės duomenys buvo konvertuoti į optinį juostos tūrį naudojant TotalLab sistemą, kad būtų galima kiekybiškai įvertinti juostų intensyvumo pokyčius, pateikiant objektyvią informaciją apie fermento pakartotinį panaudojimą ir santykinį aktyvumą. Tolimesnė analizė siekė koreliuoti optinį juostos tūrį su egzonukleazės aktyvumu kiekvieno pakartotinio ciklo metu, ypač jei stebimas aktyvumo mažėjimas.

Pakartotinio panaudojimo tyrimai, pagrįsti optinio juostos tūrio kiekybiniu įvertinimu, parodė (24 pav.), kad fermento aktyvumas reikšmingai sumažėja kiekvieno panaudojimo ciklo metu 45 minučių reakcijos sistemoje su 1 ng dvigrandės DNR fragmentu (Sistema A), nukrisdamas iki maždaug 25 % trečiame cikle ir beveik visiškai išnykdamas penktajame. Priešingai, fermento aktyvumas yra stabilesnis per kelis ciklus 90 minučių reakcijos sistemoje su tuo pačiu DNR kiekiu (Sistema B). Trečiajame panaudojimo cikle Sistema B išlaikė apie 50 % pradinio aktyvumo, o penktajame – apie 20 %, kas rodo geresnį stabilumą, palyginti su Sistema A.

Kumar ir kt. [96] nagrinėjo T7 DNR polimerazės struktūrinius ir funkcinius aspektus, pabrėždami jos didelį proceso efektyvumą [96–98]. Wuite ir kt. [97] tyrinėjo T7 DNR polimerazės mechanines savybes, išryškindami jos gebėjimą išvynioti DNR ir efektyviai atlikti egzonukleazės funkcijas. Šiame tyrime užmaskuota T7 DNR polimerazė buvo imobilizuota ant aukso paviršiaus ir pasiektas prisotinimas naudojant 6:4 santykio tiolintų jungiklių SAM mišinį. Šis metodas greičiausiai prisidėjo prie fermento stabilumo sukuriant palankią aplinką jo aktyvumui. Rezultatai rodo, kad imobilizacija reikšmingai veikia fermento pakartotinio naudojimo efektyvumą, priklausomai nuo reakcijos trukmės – 45 arba 90 minučių. Imobilizuoti fermentai gali būti apriboti, todėl jų sąveika su substratu yra ribota, o tai veikia jų aktyvumą ir bendrą efektyvumą, priklausomai nuo reakcijos trukmės [109]. Trumpesnės trukmės reakcijose, pavyzdžiui, 45 minučių, imobilizuotam fermentui gali nepakakti laiko pilnam substrato apdorojimui. Ribotas prieinamumas aktyviajam centrui gali lemti nevisišką substrato skaidymą ir greitesnį aktyvumo sumažėjimą pakartotinio naudojimo cikluose, galimai dėl dalinės denatūracijos ar aktyviojo centro

apribojimų. Tuo tarpu 90 minučių reakcijos trukmė suteikia daugiau laiko substrato apdorojimui, net jei fermento judėjimas ribotas. Ilgesnė trukmė gali užtikrinti tvirtesnę fermento ir substrato sąveiką, efektyvesnį reakcijos ciklą ir mažesnį imobilizacijos sukeliamą poveikį. Mūsų rezultatai rodo, kad 90 minučių trukmės reakcija leidžia fermentui geriau išlaikyti efektyvumą per kelis panaudojimo ciklus, taip pagerindama bendrą stabilumą.

Sėkminga užmaskuotos T7 DNR polimerazės imobilizacija ir stabilumas rodo, kad panašūs metodai gali būti taikomi ir kitiems fermentams, naudojamiems pramoninėje biokatalizėje. Imobilizuojant fermentus ant tinkamų paviršių galima pasiekti daugkartinio naudojimo ir stabilių katalizatorių, taip sumažinant kaštus ir pagerinant procesų efektyvumą. Tai itin aktualu didelio masto gamybos procesams, kur fermentų pakartotinis naudojimas yra itin svarbus. Farmacijos pramonėje imobilizuoti fermentai gali būti naudojami sudėtingų molekulių sintezei, vaistų kūrimui bei biotransformacijos procesuose [110]. Maisto pramonėje imobilizuoti fermentai gali būti naudingi siekiant pagerinti produktų galiojimo laiką, skonį ar sudedamųjų dalių apdorojimą [111]. Naudojant imobilizuotus fermentus biokuro gamyboje, galima padidinti biomasės konversijos į fermentuojamus cukrus efektyvumą [112]. Šiame tyrime parodytas T7 DNR polimerazės stabilumas ir pakartotinis naudojimas gali būti pritaikytas fermentams, dalyvaujantiems biomasės skaidyme, taip pagerinant bendrą biokuro gamybos efektyvumą ir tvarumą [113].

T7 DNR polimerazės biojutiklio hidrolizės charakterizavimas

Imobilizuotos T7 DNR polimerazės hidrolizė buvo įvertinta naudojant QCM metodą, stebint realaus laiko dažnio pokyčius po sąlyčio su Proteinaze K, siekiant charakterizuoti fermentinio jutiklio hidrolizę. Kaip parodyta 25 paveiksle, QCM duomenys rodo aiškius dažnio pokyčius, atitinkančius skirtingas SAM kompozicijas. Pradinis dažnio sumažėjimas patvirtina sėkmingą T7 DNR polimerazės imobilizaciją, kaip jau buvo aprašyta. Tuo tarpu vėlesnis dažnio padidėjimas po Proteinazės K poveikio rodo fermentinę hidrolizę ir masės sumažėjimą dėl baltymo hidrolizės. Hidrolizės efektyvumas skyrėsi priklausomai nuo SAM kompozicijos – tankiau supakuoti monosluoksniai pasižymėjo puikiu fermento stabilumu, o tai lėmė lėtesnį hidrolizės greitį. Dažnio pokyčiai (Δf) svyravo nuo –55 Hz iki –10 Hz priklausomai nuo SAM sudėties, o tai atitiko masės pokyčius nuo 10 iki 97.5 ng/mm². Duomenys rodo, kad specifinės SAM santykio variacijos daro įtaką fermento jautrumui hidrolizei, veikdamos jo stabilumą ir potencialą biojutiklių taikymuose. Šie rezultatai leidžia geriau optimizuoti paviršiaus chemiją siekiant pagerinti fermento imobilizaciją ir ilgaamžiškumą biojutiklių kūrime. Taikant klasikinę fermentinės katalizės teoriją, reakcija tarp substrato (S) ir fermento (E) vyksta per tarpinį aktyvų kompleksą (ES), kuris galiausiai suformuoja produktą (P). Šis procesas vyksta pagal dviejų pakopų mechanizmą (17 lygtis).

Šiame tyrime cheminė reakcija vyksta skystos-fazės/s kietosios fazės sąsajoje – tai reiškia, kad Proteinazė K (E) pirmiausia adsorbuojasi ant paviršiaus, o tuomet formuoja aktyvų kompleksą (ES) su imobilizuotu T7 DNR polimeraze (S). Todėl k_{ads} šiuo atveju tinkamiau vadinti adsorbcijos greičio konstanta, o k_{des} – fermento desorbcijos konstanta. Daroma prielaida, kad fermento adsorbcija ir desorbcija vyksta pagal paprastą Langmuir modelį. Tokiu atveju aktyvaus komplekso ES ir produkto P susidarymo greičiai gali būti aprašyti diferencialinėmis lygtimis 18 ir 19. Tačiau pastebėta, kad ši lygtis neatsižvelgia į fermento (šiuo atveju Proteinazės K) difuzijos apribojimus. Panašios problemos buvo pastebėtos ir analizuojant SPR duomenis [114]. Todėl buvo pritaikyta modifikuota reakcijos greičio lygtys (20 ir 21), įtraukianti fermento difuziją link elektrodo paviršiaus.

Skaičiavimams atlikti naudotas diferencialinių lygčių sprendimo metodas „Runge-Kutta“ [115], įgyvendintas per **odeint** funkciją „SciPy“ Python bibliotekoje. Optimizavimui naudotos šios pradinės reikšmės:

- $k_{ads} = 2.00\times10^{4}\ L\cdot mol^{-1}\cdot min^{-1}$
- $k_{des} = 2.00\times10^{-2}\ min^{-1}$
- $k_{cat} = 1.70\times10^{-3}\ min^{-1}$
- $\beta = 4.50\times10^{-3}$
- $\theta P = 2.00\times10^{-2}$

Kadangi QCM celėje fermento tirpalas tekėjo pastoviu greičiu, Proteinazės K koncentracija buvo laikoma pastovia: $[E] = 1.38\times10^{-6}\ mol\cdot L^{-1}$. 27 paveiksle pateikti T7 DNR polimerazės degradacijos rezultatai: mėlyni taškai žymi eksperimentinius duomenis, raudonos linijos – optimizuotus modelinius rezultatus. Matyti, kad duomenų optimizacija pasiekė didelį koreliacijos laipsnį (~0.9). Taip pat parodytos optimizuotų parametrų priklausomybės nuo fermento paviršiaus padengimo. T7 DNR polimerazės hidrolizė Proteinazės K pagalba, stebėta QCM sistema, suteikė vertingų įžvalgų apie fermentinės degradacijos kinetiką kietos–skystos fazės sąsajoje. Reakcija vyko pagal dviejų pakopų mechanizmą, būdingą fermentinei katalizei: pirmiausia Proteinazė K adsorbavosi ant paviršiaus, po to formavo aktyvų kompleksą su imobilizuotu fermentu. Klasikinės fermentinės kinetikos taikymas kartu su modifikuota lygtimi, apimančia fermento difuzijos poveikį, leido tiksliai aprašyti hidrolizės procesą.

Optimizavus kinetinius parametrus (k_{ads}, k_{des}, k_{cat}, β, θP), buvo pasiekta didelė modelio ir eksperimentinių duomenų koreliacija (~0.9). Tai patvirtina, kad modifikuotas fermentinis modelis, atsižvelgiantis į difuzijos ir adsorbcijos-desorbcijos dinamiką, yra patikimas QCM duomenų interpretavimui proteolizės metu. Tyrimas taip pat pabrėžė difuzijos apribojimų reikšmę paviršių fermentinėse reakcijose – kitaip nei tūrinėse reakcijose, šiuo atveju reakcijos greitis priklausė nuo Proteinazės K pernašos iki fermento sluoksnio. Šis metodinis požiūris, pagrįstas QCM matavimais ir pažangiu kinetiniu modeliavimu, gali būti pritaikytas tolesniems fermentų ir substratų sąveikos tyrimams biojutiklių paviršiuose, ypatingai tiriant baltymų stabilumą, fermentų specifiškumą ir paviršiaus funkcionalizavimo strategijas biojutiklių kūrime.

BAFF baltymo biojutiklio tyrimo rezultatai

SAM mišinių paviršių taikymas BAFF imobilizavimui. QCM duomenų analizės charakterizavimas

Eksperimentiniai BAFF baltymo imobilizavimo/adsorbcijos, SAM paviršiaus dezaktyvacijos ir taikinių ssDNR aptikimo kinetiniai sluoksnio storio tyrimo rezultatai pavaizduoti 28 paveiksle. Kiekvienas rezonanso dažnio pokytis atitinka tris kartus pakartotų matavimų rezultatus, atliktus pastoviomis sąlygomis naudojant 3:7 santykio SAM mišinio paviršius kambario temperatūroje. Fiziologinėmis sąlygomis (pH 7.4) peptidinės jungties susidarymas bei BAFF ir BSA adsorbcijos procesai ant auksu dengto QCM jutiklio paviršiaus lemia Δf pokyčius proceso metu. BAFF baltymo adsorbcijos metu (20–120 min intervale) buvo pastebėtas staigus rezonanso dažnio (Δf) kritimas po QCM rezonatoriaus ekspozicijos. Pirmasis staigus signalo pokytis susijęs su greita BAFF baltymo adsorbcija ant SAM mišinio paviršiaus, dėl: i) maksimalaus masės pernašos greičio per ribinį sluoksnį virš SAM paviršiaus, kai fermento koncentracija ties paviršiumi pradžioje yra lygi nuliui, ir ii) visiško jutiklio paviršiaus prieinamumo fermentų molekulėms prisijungti. Stabilizavus rezonanso dažnį su 1X PBS (pH 7.4) tirpalu kambario temperatūroje, pastovios būsenos dažnio pokytis buvo pasiektas po 110–120 min. Vėlesnis

plovimo etapas su 1X PBS (pH 7.4) tirpalu buvo atliktas siekiant pašalinti neprisijungusias BAFF baltymo molekules nuo aukso paviršiaus ir/arba leisti fermentui persitvarkyti į žemesnės energijos konformacijas. Šie dinaminiai pokyčiai paviršiuje sudarė papildomų adsorbcijos vietų, leidžiančių lėtai, bet stabiliai didėti adsorbuoto fermento koncentracijai ir pasiekti paviršiaus soties būseną. Šiame galutiniame etape pasiekiama dinaminė pusiausvyra tarp naujų BAFF baltymo molekulių, prisijungiančių prie paviršiaus, ir tų, kurios jį palieka. Nesant reikšmingų dažnio pokyčių BAFF adsorbcijos metu ant 3:7 SAM mišinio paviršių, galima daryti išvadą, kad visas QCM jutiklio elektrodas buvo padengtas ir prisotintas BAFF baltymo molekulėmis kambario temperatūroje.

SAM paviršiaus inaktyvacijos metu buvo atliktas BSA baltymo adsorbcijos procesas, kurio metu (120–150 min intervale) taip pat stebėtas staigus rezonanso dažnio (Δf) kritimas po QCM jutiklio veikimo. Pirmasis staigus signalo pokytis susijęs su greita BSA adsorbcija ant SAM mišinio paviršiaus. Stabilizavus rezonanso dažnį su 1X PBS (pH 7.4) tirpalu kambario temperatūroje, pastovios būsenos dažnio pokytis buvo pasiektas po 150–160 min. Vėlesnis plovimo etapas su 1X PBS (pH 7.4) tirpalu buvo atliktas siekiant pašalinti neprisijungusias BSA baltymo molekules nuo aukso paviršiaus arba leisti fermentui persitvarkyti į žemesnės energijos formas. Tokie dinaminiai pokyčiai sudarė papildomas adsorbcijos vietas, leidžiančias palaipsniui didinti adsorbuoto baltymo kiekį ir pasiekti soties būseną. Galutiniu etapu pasiekiama dinaminė pusiausvyra tarp naujų BSA/BAFF baltymų molekulių, prisijungiančių prie paviršiaus, ir tų, kurios jį palieka. Nesant reikšmingų dažnio pokyčių BSA adsorbcijos metu ant 3:7 SAM mišinio paviršių, galima teigti, kad visas QCM jutiklio elektrodas buvo padengtas ir prisotintas BSA baltymo molekulėmis kambario temperatūroje.

BAFF biojutikliui atliekant taikininės DNR detekciją, buvo vykdomas ssDNR aptamero adsorbcijos procesas, kurio metu (160–210 min intervale) stebėtas staigus rezonanso dažnio (Δf) kritimas po QCM jutiklio aktyvavimo. Pirmasis staigus signalo pokytis susijęs su greita ssDNR aptamero adsorbcija ant BAFF jutiklio paviršiaus. Stabilizavus rezonanso dažnį 1X PBS (pH 7.4) tirpalu kambario temperatūroje, pastovios būsenos dažnio pokytis buvo pasiektas po 210 min. Vėlesnis plovimas su 1X PBS (pH 7.4) tirpalu buvo atliktas siekiant pašalinti neprisijungusias ssDNR molekules arba/ir leisti baltymams persitvarkyti į žemesnės energijos konformacijas. Šie dinaminiai procesai sudarė papildomas adsorbcijos vietas, leidžiančias lėtai, bet nuosekliai didinti ssDNR kiekį paviršiuje ir galiausiai pasiekti soties lygį. Galutiniu etapu pasiekiama dinaminė pusiausvyra tarp naujų BAFF/BSA/DNR molekulių, prisijungiančių prie paviršiaus, ir tų, kurios jį palieka. Nesant reikšmingų dažnio pokyčių ssDNR adsorbcijos metu BAFF jutiklio paviršiuje, galima teigti, kad visas QCM jutiklio elektrodas buvo padengtas ir prisotintas ssDNR molekulėmis kambario temperatūroje.

Daroma prielaida, kad imobilizacijos procesas yra kinetiškai kontroliuojamas, adsorbuotas sluoksnis yra tvirtai susietas su jutikliu, o viskoelastiniai efektai yra nereikšmingi, todėl visų matavimų rezonanso dažnio pokyčiams įvertinti buvo taikyta Sauerbrey lygtis [92], leidžianti įvertinti sukauptą BAFF baltymo masę ant paviršiaus. Įstatant rezonanso dažnio pokytį Δfn, atitinkantį Au/12-MUA+6-MCH/BAFF/BSA/DNR sluoksnio Δm masės pokytį, buvo atlikta regresinė analizė kiekviename etape siekiant nustatyti susiformavusio modifikuoto monosluoksnio storį pagal išsamią procedūrą, aprašytą *T7* DNR polimerazės jutiklių skyriuje. 6 lentelėje pateikiama santraukos lentelė, kurioje detalizuojami BAFF ir BSA adsorbcijos bei DNR sąveikos kinetiniai parametria ir gauti rezultatai su auksiniu elektrodu.

IŠVADOS

1. T7 DNR polimerazės biojutiklių konstravimas ant auksu padengtų QCM elektrodų, funkcionalizuotų įvairiomis savaime susitvarkančių monosluoksnių (SAM) kompozicijomis, leido sukurti funkcionalius, stabilius ir efektyvius fermentinius paviršius. Tarp tirtų modelių, pseudo pirmos eilės kinetinis modelis geriausiai apibūdino imobilizacijos procesą, parodęs, kad imobilizuoti 10 ng T7 DNR polimerazės QCM sistemoje sukelia 1.20 Hz dažnio pokytį. Šis modelis apėmė spartų pradinį prisijungimą ir vėlesnę laipsnišką paviršiaus prisotinimo fazę, todėl jis pripažintas patikimu įrankiu fermento ir paviršiaus sąveikoms analizuoti bei jutiklio jautrumui optimizuoti.
2. Tyrimas patvirtino, kad T7 DNR polimerazės jutikliai išlaiko pakartotinio naudojimo galimybę keliuose reakcijos cikluose – po trijų ciklų buvo išlaikyta daugiau kaip 50 % egzonukleazės aktyvumo. Šis rezultatas pabrėžia ilgalaikį jutiklių stabilumą ir jų praktinį taikymą realiose diagnostinėse situacijose, kur būtinas daugkartinis naudojimas.
3. Imobilizuotos T7 DNR polimerazės fermentinis hidrolizės procesas, vykstantis veikiant Proteazei K, sėkmingai stebėtas realiu laiku naudojant QCM sistemą. Hidrolizė atitiko su paviršiumi susijusios proteolizės kinetinį modelį, kurio parametrai buvo optimizuoti pagal eksperimentinius duomenis: $k_{ads} = 2{,}00 \times 10^{4}\ L \cdot mol^{-1} \cdot min^{-1}$, $k_{des} = 2{,}00 \times 10^{-2}\ min^{-1}$, $k_{cat} = 1{,}70 \times 10^{-3}\ min^{-1}$, $\beta = 4{,}50 \times 10^{-3}$ ir $\theta P = 2{,}00 \times 10^{-2}$. Šios reikšmės rodo aiškiai apibrėžtą fermentinį skilimo procesą paviršiuje, patvirtindamos, kad su paviršiumi susijusi proteolizė gali būti tiksliai modeliuojama ir kiekybiškai vertinama naudojant iš QCM duomenų gautus kinetinius parametrus.
4. BAFF pagrindu sukurtas biojutiklis, suformuotas ant SAM modifikuoto auksu dengto paviršiaus, sėkmingai aptiko specifines DNR sekas – buvo išmatuota 27.9 ng DNR adsorbcija. Geriausiai BAFF–DNR sąveiką apibūdino n-os eilės kinetinis modelis, kuris tiksliai atspindėjo netiesinę adsorbcijos dinamiką, atsirandančią dėl sterinių trukdžių ir molekulinių persitvarkymų paviršiuje. Apskaičiuotas reakcijos greičio konstantos dydis – $0.227 \pm 0.020\ min^{-1}$ – patvirtino, kad BAFF sluoksnis išliko biologiškai aktyvus ir gebėjo realiuoju laiku atpažinti DNR.

REFERENCES

1. Dronina, J.; Bubniene, U.S.; Ramanavicius, A. The Application of DNA Polymerases and Cas9 as Representative of DNA-Modifying Enzymes Group in DNA Sensor Design (Review). *Biosens Bioelectron* **2020**, 112867, doi:10.1016/j.bios.2020.112867.

2. Clark, L.C.; Lyons, C. ELECTRODE SYSTEMS FOR CONTINUOUS MONITORING IN CARDIOVASCULAR SURGERY. *Ann N Y Acad Sci* **1962**, *102*, 29–45, doi:10.1111/j.1749-6632.1962.tb13623.x.

3. Newman, J.D.; Setford, S.J. Enzymatic Biosensors. *Mol Biotechnol* 2006, *32*, 249–268.

4. Sarvutiene, J.; Prentice, U.; Ramanavicius, S.; Ramanavicius, A. Molecular Imprinting Technology for Biomedical Applications. *Biotechnol Adv* **2024**, *71*, 108318, doi:10.1016/J.BIOTECHADV.2024.108318.

5. Dronina, J.; Samukaite-Bubniene, U.; Ramanavicius, A. Advances and Insights in the Diagnosis of Viral Infections. *Journal of Nanobiotechnology 2021 19:1* **2021**, *19*, 1–23, doi:10.1186/S12951-021-01081-2.

6. Dronina, J.; Samukaite-Bubniene, U.; Ramanavicius, A. Towards Application of CRISPR-Cas12a in the Design of Modern Viral DNA Detection Tools (Review). *Journal of Nanobiotechnology 2022 20:1* **2022**, *20*, 1–15, doi:10.1186/S12951-022-01246-7.

7. Namba, K.; Pattanayek, R.; Stubbs, G. Visualization of Protein-Nucleic Acid Interactions in a Virus. Refined Structure of Intact Tobacco Mosaic Virus at 2.9 Å Resolution by X-Ray Fiber Diffraction. *J Mol Biol* **1989**, *208*, 307–325, doi:10.1016/0022-2836(89)90391-4.

8. Filée, J.; Forterre, P.; Sen-Lin, T.; Laurent, J. Evolution of DNA Polymerase Families: Evidences for Multiple Gene Exchange Between Cellular and Viral Proteins. *J Mol Evol* **2002**, *54*, 763–773, doi:10.1007/s00239-001-0078-x.

9. Sengupta, S.; Spiering, M.M.; Dey, K.K.; Duan, W.; Patra, D.; Butler, P.J.; Astumian, R.D.; Benkovic, S.J.; Sen, A. DNA Polymerase as a Molecular Motor and Pump. *ACS Nano* **2014**, *8*, 2410–2418, doi:10.1021/nn405963x.

10. Hubscher, U.; Spadari, S.; Villani, G.; Maga, G. *DNA Polymerases: Discovery, Characterization and Functions in Cellular DNA Transactions*; World Scientific.; World Scientific: Singapore, 2009; ISBN 978-981-4299-16-9.

11. Hübscher, U.; Nasheuer, H.P.; Syväoja, J.E. Eukaryotic DNA Polymerases, a Growing Family. *Trends Biochem Sci* 2000.

12. Nyrén, P. Enzymatic Method for Continuous Monitoring of DNA Polymerase Activity. *Anal Biochem* **1987**, *167*, 235–238, doi:10.1016/0003-2697(87)90158-8.

13. Kellogg, D.E.; Rybalkin, I.; Chen, S.; Mukhamedova, N.; Vlasik, T.; Siebert, P.D.; Chenchik, A. TaqStart Antibody(TM): "Hot Start" PCR Facilitated by a Neutralizing Monoclonal Antibody Directed against Taq DNA Polymerase. *Biotechniques* **1994**, *16*, 1134–1137.

14. Merkens, L.S.; Bryan, S.K.; Moses, R.E. Inactivation of the 5′-3′ Exonuclease of Thermus Aquaticus DNA Polymerase. *BBA - Gene Structure and Expression* **1995**, *1264*, 243–248, doi:10.1016/0167-4781(95)00153-8.

15. Wang, Y.; Li, B.; Liu, J.; Zhou, H. T4 DNA Polymerase-Assisted Upgrade of a Nicking/Polymerization Amplification Strategy for Ultrasensitive Electrochemical Detection of Watermelon Mosaic Virus. *Anal Bioanal Chem* **2019**, *411*, 2915–2924, doi:10.1007/s00216-019-01737-x.

16. Blanco, L.; Salas, M. *Characterization and Purification of a Phage +29-Encoded DNA Polymerase Required for the Initiation of Replication (Phage 4.29 DNA Polymerase/Phage 429 Replication/Host Factor)*; 1984; Vol. 81;.

17. Summerer, D.; Marx, A. Dna Polymerase Selectivity: Sugar Interactions Monitored with High-Fidelity Nucleotides. *Angewandte Chemie - International Edition* **2001**, *40*, 3693–3695, doi:10.1002/1521-3773(20011001)40:19<3693::AID-ANIE3693>3.0.CO;2-O.

18. Tsai, Y.C.; Johnson, K.A. A New Paradigm for DNA Polymerase Specificity. *Biochemistry* **2006**, *45*, 9675–9687, doi:10.1021/bi060993z.

19. Ganai, R.A.; Johansson, E. DNA Replication-A Matter of Fidelity. *Mol Cell* 2016, *62*, 745–755.

20. Jain, R.; Aggarwal, A.K.; Rechkoblit, O. Eukaryotic DNA Polymerases. *Curr Opin Struct Biol* 2018, *53*, 77–87.

21. Béguin, P.; Chekli, Y.; Sezonov, G.; Forterre, P.; Krupovic, M. Sequence Motifs Recognized by the Casposon Integrase of Aciduliprofundum Boonei. *Nucleic Acids Res* **2019**, *47*, 6386–6395, doi:10.1093/nar/gkz447.

22. Johnson, K.A. Rapid Quench Kinetic Analysis of Polymerases, Adenosinetriphosphatases, and Enzyme Intermediates. *Methods Enzymol* **1995**, *249*, 38–61, doi:10.1016/0076-6879(95)49030-2.

23. Hirano, S.; Nishimasu, H.; Ishitani, R.; Nureki, O. Structural Basis for the Altered PAM Specificities of Engineered CRISPR-Cas9. *Mol Cell* **2016**, *61*, 886–894, doi:10.1016/j.molcel.2016.02.018.

24. Nishimasu, H.; Ran, F.A.; Hsu, P.D.; Konermann, S.; Shehata, S.I.; Dohmae, N.; Ishitani, R.; Zhang, F.; Nureki, O. Crystal Structure of Cas9 in Complex with Guide RNA and Target DNA. *Cell* **2014**, *156*, 935–949, doi:10.1016/j.cell.2014.02.001.

25. Gao, L.; T Cox, D.B.; Yan, W.X.; Manteiga, J.C.; Schneider, M.W.; Yamano, T.; Nishimasu, H.; Nureki, O.; Crosetto, N.; Zhang, F. Engineered Cpf1 Variants with Altered PAM Specificities. *Nature Publishing Group* **2017**, *35*, doi:10.1038/nbt.3900.

26. Tagami, N.; Yuda, J.; Goto, Y. Current Status of BAFF Targeting Immunotherapy in B-Cell Neoplasm. *Int J Clin Oncol* **2024**, *29*, 1676–1683, doi:10.1007/S10147-024-02611-2/FIGURES/1.

27. Smulski, C.R.; Eibel, H. BAFF and BAFF-Receptor in B Cell Selection and Survival. *Front Immunol* **2018**, *9*, doi:10.3389/FIMMU.2018.02285.

28. Rauch, M.; Tussiwand, R.; Bosco, N.; Rolink, A.G. Crucial Role for BAFF-BAFF-R Signaling in the Survival and Maintenance of Mature B Cells. *PLoS One* **2009**, *4*, doi:10.1371/JOURNAL.PONE.0005456.

29. Vigolo, M.; Chambers, M.G.; Willen, L.; Chevalley, D.; Maskos, K.; Lammens, A.; Tardivel, A.; Das, D.; Kowalczyk-Quintas, C.; Schuepbach-Mallepell, S.; et al. A Loop Region of BAFF Controls B Cell Survival and Regulates Recognition by Different Inhibitors. *Nat Commun* **2018**, *9*, 1–15, doi:10.1038/S41467-018-03323-8;TECHMETA.

30. Bossen, C.; Schneider, P. BAFF, APRIL and Their Receptors: Structure, Function and Signaling. *Semin Immunol* **2006**, *18*, 263–275, doi:10.1016/j.smim.2006.04.006.

31. Zhao, W.; Li, B.; Xu, S.; Huang, X.; Luo, J.; Zhu, Y.; Liu, X. Electrochemical Protein Recognition Based on Macromolecular Self-Assembly of Molecularly Imprinted Polymer: A New Strategy to Mimic Antibody for Label-Free Biosensing. *J Mater Chem B* **2019**, *7*, 2311–2319, doi:10.1039/C9TB00220K.

32. Ferrara, N. VEGF and Its Receptors. *Int Congr Ser* **2004**, *1262*, 283–286, doi:10.1016/J.ICS.2003.11.003.

33. Apte, R.S.; Chen, D.S.; Ferrara, N. VEGF in Signaling and Disease: Beyond Discovery and Development. *Cell* **2019**, *176*, 1248–1264, doi:10.1016/J.CELL.2019.01.021.

34. Li, Y.; Hye, J.L.; Corn, R.M. Detection of Protein Biomarkers Using RNA Aptamer Microarrays and Enzymatically Amplified SPR Imaging. *Anal Chem* **2007**, *79*, 1082, doi:10.1021/AC061849M.

35. Freeman, R.; Girsh, J.; Fang-Ju Jou, A.; Ho, J.A.A.; Hug, T.; Dernedde, J.; Willner, I. Optical Aptasensors for the Analysis of the Vascular Endothelial Growth Factor (VEGF). *Anal Chem* **2012**, *84*, 6192–6198, doi:10.1021/AC3011473.

36. Freeman, R.; Girsh, J.; Fang-Ju Jou, A.; Ho, J.A.A.; Hug, T.; Dernedde, J.; Willner, I. Optical Aptasensors for the Analysis of the Vascular Endothelial Growth Factor (VEGF). *Anal Chem* **2012**, *84*, 6192–6198, doi:10.1021/AC3011473.

37. Park, Y.; Hong, M.S.; Lee, W.H.; Kim, J.G.; Kim, K. Highly Sensitive Electrochemical Aptasensor for Detecting the Vegf165 Tumor Marker with Pani/Cnt Nanocomposites. *Biosensors (Basel)* **2021**, *11*, 114, doi:10.3390/BIOS11040114/S1.

38. Park, Y.; Hong, M.S.; Lee, W.H.; Kim, J.G.; Kim, K. Highly Sensitive Electrochemical Aptasensor for Detecting the VEGF165 Tumor Marker with PANI/CNT Nanocomposites. *Biosensors (Basel)* **2021**, *11*, doi:10.3390/BIOS11040114.

39. Velachi, V.; Bhandary, D.; Singh, J.K.; Cordeiro, M.N.D.S. Structure of Mixed Self-Assembled Monolayers on Gold Nanoparticles at Three Different Arrangements. *Journal of Physical Chemistry C* **2015**, *119*, 3199–3209, doi:10.1021/JP512144G.

40. Oberhaus, F. V.; Frense, D.; Beckmann, D. Immobilization Techniques for Aptamers on Gold Electrodes for the Electrochemical Detection of Proteins: A Review. *Biosensors (Basel)* 2020, *10*.

41. Luo, C.; Wei, N.; Sun, X.; Luo, F. Fabrication of Self-Healable, Conductive, and Ultra-Strong Hydrogel from Polyvinyl Alcohol and Grape Seed–Extracted Polymer. *J Appl Polym Sci* **2020**, *137*, 49118, doi:10.1002/APP.49118.

42. Yong, Y.; Bai, Y.; Li, Y.F.; Lin, L.; Cui, Y.; Xia, C. Preparation and Application of Polymer-Grafted Magnetic Nanoparticles for Lipase Immobilization. *J Magn Magn Mater* **2008**, *320*, 2350–2355, doi:10.1016/j.jmmm.2008.04.158.

43. Shen, D.; Huang, M.; Chow, L.M.; Yang, M. Kinetic Profile of the Adsorption and Conformational Change of Lysozyme on Self-Assembled Monolayers as Revealed by Quartz Crystal Resonator. *Sens Actuators B Chem* **2001**, *77*, 664–670, doi:10.1016/S0925-4005(01)00763-8.

44. Jing-jiang Yu, †; Yih Horng Tan, †; Xue Li, †; Pao-Kuang Kuo, ‡ and; Gang-yu Liu*, † A Nanoengineering Approach to Regulate the Lateral Heterogeneity of Self-Assembled Monolayers. *J Am Chem Soc* **2006**, *128*, 11574–11581, doi:10.1021/JA0631403.

45. Shams, S.; Bakhshi, B.; Tohidi Moghadam, T.; Behmanesh, M. A Sensitive Gold-Nanorods-Based Nanobiosensor for Specific Detection of Campylobacter Jejuni and Campylobacter Coli. *J Nanobiotechnology* **2019**, *17*, 43, doi:10.1186/s12951-019-0476-0.

46. Baruch-Shpigler, Y.; Avnir, D. Enzymes in a Golden Cage †. **2020**, doi:10.1039/c9sc05419g.

47. Pingarrón, J.M.; Yáñez-Sedeño, P.; González-Cortés, A. Gold Nanoparticle-Based Electrochemical Biosensors. *Electrochim Acta* **2008**, *53*, 5848–5866, doi:10.1016/j.electacta.2008.03.005.

48. Schneider, S.; Füser, M.; Bolte, M.; Terfort, A. Self-Assembled Monolayers of Aromatic Pyrrole Derivatives: Electropolymerization and Electrocopolymerization with Pyrrole. *Electrochim Acta* **2017**, *246*, 853–863, doi:10.1016/J.ELECTACTA.2017.06.046.

49. Dong, J.; Carpinone, P.L.; Pyrgiotakis, G.; Demokritou, P.; Moudgil, B.M. Synthesis of Precision Gold Nanoparticles Using Turkevich Method. *KONA Powder and Particle Journal* **2020**, *37*, 224–232, doi:10.14356/kona.2020011.

50. Petkova, G.A.; Záruba, K.; Žvátora, P.; Král, V. *Gold and Silver Nanoparticles for Biomolecule Immobilization and Enzymatic Catalysis*; 2012;

51. Masud, M.K.; Na, J.; Lin, T.-E.; Malgras, V.; Preet, A.; Ibn Sina, A.A.; Wood, K.; Billah, M.; Kim, J.; You, J.; et al. Nanostructured Mesoporous Gold Biosensor for

MicroRNA Detection at Attomolar Level. *Biosens Bioelectron* **2020**, 112429, doi:10.1016/j.bios.2020.112429.

52. Nelson, J.M.; Griffin, E.G. Adsorption of Invertase. *J Am Chem Soc* **1916**, *38*, 1109–1115, doi:10.1021/ja02262a018.

53. Nawawi, N.N.; Hashim, Z.; Rahman, R.A.; Murad, A.M.A.; Bakar, F.D.A.; Illias, R.M. Entrapment of Porous Cross-Linked Enzyme Aggregates of Maltogenic Amylase from Bacillus Lehensis G1 into Calcium Alginate for Maltooligosaccharides Synthesis. *Int J Biol Macromol* **2020**, *150*, 80–89, doi:10.1016/j.ijbiomac.2020.02.032.

54. Yang, Y.; Zhu, G.; Wang, G.; Li, Y.; Tang, R. Robust Glucose Oxidase with a Fe3O4@C-Silica Nanohybrid Structure. *J Mater Chem B* **2016**, *4*, 4726–4731, doi:10.1039/c6tb01355d.

55. Gomes, N.O.; Carrilho, E.; Machado, S.A.S.; Sgobbi, L.F. Bacterial Cellulose-Based Electrochemical Sensing Platform: A Smart Material for Miniaturized Biosensors. *Electrochim Acta* **2020**, *349*, doi:10.1016/j.electacta.2020.136341.

56. Xuan, F.; Luo, X.; Hsing, I.M. Sensitive Immobilization-Free Electrochemical DNA Sensor Based on Isothermal Circular Strand Displacement Polymerization Reaction. *Biosens Bioelectron* **2012**, *35*, 230–234, doi:10.1016/j.bios.2012.02.054.

57. Sheldon, R.A. Enzyme Immobilization: The Quest for Optimum Performance. *Adv Synth Catal* 2007, *349*, 1289–1307.

58. Jesionowski, T.; Zdarta, J.; Krajewska, B. Enzyme Immobilization by Adsorption: A Review. *Adsorption* 2014, *20*, 801–821.

59. Makaraviciute, A.; Ramanaviciene, A. Site-Directed Antibody Immobilization Techniques for Immunosensors. *Biosens Bioelectron* **2013**, *50*, 460–471, doi:10.1016/J.BIOS.2013.06.060.

60. Ahuja, T.; Mir, I.A.; Kumar, D.; Rajesh Biomolecular Immobilization on Conducting Polymers for Biosensing Applications. *Biomaterials* **2007**, *28*, 791–805, doi:10.1016/J.BIOMATERIALS.2006.09.046.

61. Eş, I.; Vieira, J.D.G.; Amaral, A.C. Principles, Techniques, and Applications of Biocatalyst Immobilization for Industrial Application. *Appl Microbiol Biotechnol* 2015, *99*, 2065–2082.

62. Nishida, H.; Kajisa, T.; Miyazawa, Y.; Tabuse, Y.; Yoda, T.; Takeyama, H.; Kambara, H.; Sakata, T. Self-Oriented Immobilization of DNA Polymerase Tagged by Titanium-Binding Peptide Motif. *Langmuir* **2015**, *31*, 732–740, doi:10.1021/la503094k.

63. Baniukevic, J.; Kirlyte, J.; Ramanavicius, A.; Ramanaviciene, A. Application of Oriented and Random Antibody Immobilization Methods in Immunosensor Design. *Sens Actuators B Chem* **2013**, *189*, 217–223, doi:10.1016/j.snb.2013.03.126.

64. Iwakura, M.; Rokubu, T. Immobilization of Dihydrofolate Reductase by Engineered Cysteine Residue Attached to Its C-Terminal End. *The Journal of Biochemistry* **1993**, *114*, 339–343, doi:10.1093/OXFORDJOURNALS.JBCHEM.A124178.

65. Kausaite-Minkstimiene, A.; Ramanaviciene, A.; Kirlyte, J.; Ramanavicius, A. Comparative Study of Random and Oriented Antibody Immobilization Techniques on the Binding Capacity of Immunosensor. In Proceedings of the Analytical Chemistry; American Chemical Society, August 1 2010; Vol. 82, pp. 6401–6408.

66. Lim, G.; Kim, J.; Kim, J.H. Optimization of the Masking Molecule for Active-Site-Protected Immobilization of Taq DNA Polymerase and Its Application. *Anal Biochem* **2013**, *432*, 139–141, doi:10.1016/j.ab.2012.09.033.

67. Lim, G.; Hwang, H.J.; Kim, J.H. Protected Immobilization of Taq DNA Polymerase by Active Site Masking on Self-Assembled Monolayers of ω-Functionalized Thiols. *Anal Biochem* **2011**, *419*, 205–210, doi:10.1016/j.ab.2011.08.022.

68. Zhang, H.; Hua, S.F.; Li, C. qiang; Zhang, L.; Fan, Y.C.; Duan, P. Effect of Graphene Oxide with Different Morphological Characteristics on Properties of Immobilized Enzyme in the Covalent Method. *Bioprocess Biosyst Eng* **2020**, doi:10.1007/s00449-020-02375-9.

69. Tarhan, T.; Ulu, A.; Sariçam, M.; Çulha, M.; Ates, B. Maltose Functionalized Magnetic Core/Shell Fe 3 O 4 @Au Nanoparticles for an Efficient L-Asparaginase Immobilization. **2019**, doi:10.1016/j.ijbiomac.2019.09.116.

70. Caruso, F.; Hyeon, T.; Rotello, V.; Dreaden, E.C.; Alkilany, A.M.; Huang, X.; Murphy, C.J.; El-Sayed, M.A. Nanomedicine Themed Issue The Golden Age: Gold Nanoparticles for Biomedicinew. *Chem. Soc. Rev* **2740**, *41*, 2740–2779, doi:10.1039/c1cs15237h.

71. German, N.; Ramanaviciene, A.; Ramanavicius, A. Dispersed Conducting Polymer Nanocomposites with Glucose Oxidase and Gold Nanoparticles for the Design of Enzymatic Glucose Biosensors. *Polymers (Basel)* **2021**, *13*, 2173, doi:10.3390/POLYM13132173/S1.

72. Ramanavicius, A.; German, N.; Ramanaviciene, A. Evaluation of Electron Transfer in Electrochemical System Based on Immobilized Gold Nanoparticles and Glucose Oxidase. *J Electrochem Soc* **2017**, *164*, G45–G49, doi:10.1149/2.0691704jes.

73. German, N.; Ramanavicius, A.; Ramanaviciene, A. Electrochemical Deposition of Gold Nanoparticles on Graphite Rod for Glucose Biosensing. *Sens Actuators B Chem* **2014**, *203*, 25–34, doi:10.1016/j.snb.2014.06.021.

74. German, N.; Popov, A.; Ramanaviciene, A.; Ramanavicius, A. Formation and Electrochemical Characterisation of Enzyme-Assisted Formation of Polypyrrole and Polyaniline Nanocomposites with Embedded Glucose Oxidase and Gold Nanoparticles. *J Electrochem Soc* **2020**, *167*, 165501, doi:10.1149/1945-7111/abc9dc.

75. German, N.; Ramanaviciene, A.; Voronovic, J.; Ramanavicius, A. Glucose Biosensor Based on Graphite Electrodes Modified with Glucose Oxidase and Colloidal Gold Nanoparticles. *Microchimica Acta* **2010**, *168*, 221–229, doi:10.1007/s00604-009-0270-z.

76. Li Ang, W.; Yun Seah, X.; Ching Koh, P.; Caroline, C.; Bonanni, A. Electrochemical Polymerase Chain Reaction Using Electroactive Graphene Oxide Nanoparticles as Detection Labels. *Cite This: ACS Appl. Nano Mater* **2020**, *2020*, 5489–5498, doi:10.1021/acsanm.0c00797.

77. Mazeiko, V.; Kausaite-Minkstimiene, A.; Ramanaviciene, A.; Balevicius, Z.; Ramanavicius, A. Gold Nanoparticle and Conducting Polymer-Polyaniline-Based Nanocomposites for Glucose Biosensor Design. *Sens Actuators B Chem* **2013**, *189*, 187–193, doi:10.1016/j.snb.2013.03.140.

78. Ramanaviciene, A.; Nastajute, G.; Snitka, V.; Kausaite, A.; German, N.; Barauskas-Memenas, D.; Ramanavicius, A. Spectrophotometric Evaluation of Gold Nanoparticles as Red-Ox Mediator for Glucose Oxidase. *Sens Actuators B Chem* **2009**, *137*, 483–489, doi:10.1016/j.snb.2009.01.021.

79. German, N.; Kausaite-Minkstimiene, A.; Ramanavicius, A.; Semashko, T.; Mikhailova, R.; Ramanaviciene, A. The Use of Different Glucose Oxidases for the Development of an Amperometric Reagentless Glucose Biosensor Based on Gold Nanoparticles Covered by Polypyrrole. *Electrochim Acta* **2015**, *169*, 326–333, doi:10.1016/j.electacta.2015.04.072.

80. Ramanaviciene, A.; German, N.; Kausaite-Minkstimiene, A.; Voronovic, J.; Kirlyte, J.; Ramanavicius, A. Comparative Study of Surface Plasmon Resonance, Electrochemical and Electroassisted Chemiluminescence Methods Based Immunosensor for the Determination of Antibodies against Human Growth Hormone. *Biosens Bioelectron* **2012**, *36*, 48–55, doi:10.1016/j.bios.2012.03.036.

81. Andreescu, S.; Luck, L.A. Studies of the Binding and Signaling of Surface-Immobilized Periplasmic Glucose Receptors on Gold Nanoparticles: A Glucose Biosensor Application. *Anal Biochem* **2008**, *375*, 282–290, doi:10.1016/j.ab.2007.12.035.

82. Watzke, A.; Gutierrez-Rodriguez, M.; Köhn, M.; Wacker, R.; Schroeder, H.; Breinbauer, R.; Kuhlmann, J.; Alexandrov, K.; Niemeyer, C.M.; Goody, R.S.; et al. A Generic Building Block for C- and N-Terminal Protein-Labeling and Protein Immobilization. *Bioorg Med Chem* **2006**, *14*, 6288–6306, doi:10.1016/J.BMC.2006.05.006.

83. Smulders, R.H.P.H.; Carver, J.A.; Lindner, R.A.; Van Boekel, M.A.M.; Bloemendal, H.; De Jong, W.W. Immobilization of the C-Terminal Extension of Bovine AA-Crystallin Reduces Chaperone-like Activity *. *Journal of Biological Chemistry* **1996**, *271*, 29060–29066, doi:10.1074/JBC.271.46.29060.

84. Makaraviciute, A.; Ruzgas, T.; Ramanavicius, A.; Ramanaviciene, A. Antibody Fragment Immobilization on Planar Gold and Gold Nanoparticle Modified Quartz Crystal Microbalance with Dissipation Sensor Surfaces for Immunosensor Applications. *Analytical Methods* **2014**, *6*, 2134–2140, doi:10.1039/c4ay00070f.

85. Sharifi, M.; Sohrabi, M.J.; Hosseinali, S.H.; Hasan, A.; Kani, P.H.; Talaei, A.J.; Karim, A.Y.; Nanakali, N.M.Q.; Salihi, A.; Aziz, F.M.; et al. Enzyme Immobilization onto the Nanomaterials: Application in Enzyme Stability and Prodrug-Activated Cancer Therapy. *Int J Biol Macromol* 2020, *143*, 665–676.

86. Viswanathan, M.; Golin, C.E.; Jones, C.D.; Ashok, M.; Blalock, S.J.; Wines, R.C.M.; Coker-Schwimmer, E.J.L.; Rosen, D.L.; Sista, P.; Lohr, K.N. Interventions to Improve Adherence to Self-Administered Medications for Chronic Diseases in the United States: A Systematic Review. *Ann Intern Med* **2012**, *157*, 785–795, doi:10.7326/0003-4819-157-11-201212040-00538.

87. Amiripour, F.; Ghasemi, S.; Naser Azizi, S. A Novel Non-Enzymatic Glucose Sensor Based on Gold-Nickel Bimetallic Nanoparticles Doped Aluminosilicate Framework Prepared from Agro-Waste Material. *Appl Surf Sci* **2020**, 147827, doi:10.1016/j.apsusc.2020.147827.

88. Jung F. Kang; Sheng Liao; Rainer Jordan, and; Ulman*, A. Mixed Self-Assembled Monolayers of Rigid Biphenyl Thiols: Impact of Solvent and Dipole Moment. *J Am Chem Soc* **1998**, *120*, 9662–9667, doi:10.1021/JA981187L.

89. Rivera-Gandía, J.; Cabrera, C.R. Self-Assembled Monolayers of 6-Mercapto-1-Hexanol and Mercapto-n-Hexyl-Poly(DT)18-Fluorescein on Polycrystalline Gold Surfaces: An Electrochemical Impedance Spectroscopy Study. *Journal of Electroanalytical Chemistry* **2007**, *605*, 145–150, doi:10.1016/j.jelechem.2007.03.021.

90. Cancino, J.; MacHado, S.A.S. Microelectrode Array in Mixed Alkanethiol Self-Assembled Monolayers: Electrochemical Studies. *Electrochim Acta* **2012**, *72*, 108–113, doi:10.1016/J.ELECTACTA.2012.04.009.

91. Bianco, M.; Aloisi, A.; Arima, V.; Capello, M.; Ferri-Borgogno, S.; Novelli, F.; Leporatti, S.; Rinaldi, R. Quartz Crystal Microbalance with Dissipation (QCM-D) as Tool to Exploit Antigen-Antibody Interactions in Pancreatic Ductal Adenocarcinoma Detection. *Biosens Bioelectron* **2013**, *42*, 646–652, doi:10.1016/j.bios.2012.10.012.

92. Migoń, D.; Wasilewski, T.; Suchy, D. Application of QCM in Peptide and Protein-Based Drug Product Development. *Molecules* **2020**, *25*, 3950, doi:10.3390/MOLECULES25173950.

93. Dixon, M.C. Quartz Crystal Microbalance with Dissipation Monitoring: Enabling Real-Time Characterization of Biological Materials and Their Interactions. *J Biomol Tech* **2008**, *19*, 151.

94. Cheng, C.; Shuman, S. DNA Strand Transfer Catalyzed by Vaccinia Topoisomerase: Ligation of DNAs Containing a 3' Mononucleotide Overhang. *Nucleic Acids Res* **2000**, *28*, 1893–1898, doi:10.1093/nar/28.9.1893.

95. Tabor, S.; Richardson, C.C. DNA Sequence Analysis with a Modified Bacteriophage T7 DNA Polymerase. *Proceedings of the National Academy of Sciences* **1987**, *84*, 4767–4771, doi:10.1073/PNAS.84.14.4767.

96. Joyce, C.M.; Steitz, T.A. Function and Structure Relationships in DNA Polymerases. *Annu Rev Biochem* **1994**, *63*, 777–822, doi:10.1146/ANNUREV.BI.63.070194.004021.

97. Bebenek, K.; Kunkel, T.A. Functions of DNA Polymerases. *Adv Protein Chem* **2004**, *69*, 137–165, doi:10.1016/S0065-3233(04)69005-X.

98. Dangerfield, T.L.; Kirmizialtin, S.; Johnson, K.A. Substrate Specificity and Proposed Structure of the Proofreading Complex of T7 DNA Polymerase. *Journal of Biological Chemistry* **2022**, *298*, 101627, doi:10.1016/j.jbc.2022.101627.

99. Dangerfield, T.L.; Johnson, K.A. Optimized Incorporation of an Unnatural Fluorescent Amino Acid Affords Measurement of Conformational Dynamics Governing High-Fidelity DNA Replication. *Journal of Biological Chemistry* **2020**, *295*, 17265–17280, doi:10.1074/JBC.RA120.015557.

100. Huang, T.; Nallathamby, P.D.; Gillet, D.; Xu, X.H.N. Design and Synthesis of Single Nanoparticle Optical Biosensors for Imaging and Characterization of Single Receptor Molecules on Single Living Cells. *Anal Chem* **2007**, *79*, 7708, doi:10.1021/AC0709706.

101. Huang, T.; Nallathamby, P.D.; Xu, X.H.N. Photostable Single-Molecule Nanoparticle Optical Biosensors for Real-Time Sensing of Single Cytokine Molecules and Their Binding Reactions. *J Am Chem Soc* **2008**, *130*, 17095, doi:10.1021/JA8068853.

102. Calvo, E.; Kanazawa, K.; Perrot, H.; Jimenez, Y. Combination of Quartz Crystal Microbalance with Other Techniques. *Piezoelectric Transducers and Applications* **2009**, 307–330, doi:10.1007/978-3-540-77508-9_13.

103. Norde, W. Adsorption of Proteins from Solution at the Solid-Liquid Interface. *Adv Colloid Interface Sci* **1986**, *25*, 267–340, doi:10.1016/0001-8686(86)80012-4.

104. Sauerbrey, G. Verwendung von Schwingquarzen Zur Wägung Dünner Schichten Und Zur Mikrowägung. *Zeitschrift für Physik 1959 155:2* **1959**, *155*, 206–222, doi:10.1007/BF01337937.

105. Jenny Malmström; Hossein Agheli; Peter Kingshott, and; Sutherland*, D.S. Viscoelastic Modeling of Highly Hydrated Laminin Layers at Homogeneous and Nanostructured Surfaces: Quantification of Protein Layer Properties Using QCM-D and SPR. *Langmuir* **2007**, *23*, 9760–9768, doi:10.1021/LA701233Y.

106. Revellame, E.D.; Fortela, D.L.; Sharp, W.; Hernandez, R.; Zappi, M.E. Adsorption Kinetic Modeling Using Pseudo-First Order and Pseudo-Second Order Rate Laws: A Review. *Clean Eng Technol* **2020**, *1*, 100032, doi:10.1016/J.CLET.2020.100032.

107. Ezzati, R. Derivation of Pseudo-First-Order, Pseudo-Second-Order and Modified Pseudo-First-Order Rate Equations from Langmuir and Freundlich Isotherms for Adsorption. *Chemical Engineering Journal* **2020**, *392*, 123705, doi:10.1016/J.CEJ.2019.123705.

108. Kumar, J.K.; Chiu, E.T.; Tabor, S.; Richardson, C.C. A Unique Region in Bacteriophage T7 DNA Polymerase Important for Exonucleolytic Hydrolysis of

DNA. *Journal of Biological Chemistry* **2004**, *279*, 42018–42025, doi:10.1074/JBC.M406103200.

109. Wuite, G.J.L.; Smith, S.B.; Young, M.; Keller, D.; Bustamante, C. Single-Molecule Studies of the Effect of Template Tension on T7 DNA Polymerase Activity. *Nature 2000 404:6773* **2000**, *404*, 103–106, doi:10.1038/35003614.

110. Bedford, E.; Tabor, S.; Richardson, C.C. The Thioredoxin Binding Domain of Bacteriophage T7 DNA Polymerase Confers Processivity on Escherichia Coli DNA Polymerase I. *Proceedings of the National Academy of Sciences* **1997**, *94*, 479–484, doi:10.1073/PNAS.94.2.479.

111. Triyana, K.; Rianjanu, A.; Nugroho, D.B.; As'ari, A.H.; Kusumaatmaja, A.; Roto, R.; Suryana, R.; Wasisto, H.S. A Highly Sensitive Safrole Sensor Based on Polyvinyl Acetate (PVAc) Nanofiber-Coated QCM. *Scientific Reports 2019 9:1* **2019**, *9*, 1–12, doi:10.1038/s41598-019-51851-0.

112. Matsumoto, K.; David, B.; Tiu, B.; Kawamura, A.; Advincula, R.C.; Miyata, T. QCM Sensing of Bisphenol A Using Molecularly Imprinted Hydrogel/Conducting Polymer Matrix. *Polym J* **2016**, *48*, 525–532, doi:10.1038/pj.2016.23.

113. Murray, B.; Narayanan, S. The Role of Wettability on the Response of a Quartz Crystal Microbalance Loaded with a Sessile Droplet. *Scientific Reports 2019 9:1* **2019**, *9*, 1–13, doi:10.1038/s41598-019-53233-y.

114. Fulgione, A.; Cimafonte, M.; Ventura, B. Della; Iannaccone, M.; Ambrosino, C.; Capuano, F.; Thérèse, Y.; Proroga, R.; Velotta, R.; Capparelli, R. QCM-Based Immunosensor for Rapid Detection of Salmonella Typhimurium in Food OPEN. *SciEntific RePoRTs* | **2018**, *8*, 16137, doi:10.1038/s41598-018-34285-y.

115. Galuska, L.A.; Muckley, E.S.; Cao, Z.; Ehlenberg, D.F.; Qian, Z.; Zhang, S.; Rondeau-Gagné, S.; Phan, M.D.; Ankner, J.F.; Ivanov, I.N.; et al. SMART Transfer Method to Directly Compare the Mechanical Response of Water-Supported and Free-Standing Ultrathin Polymeric Films. *Nature Communications 2021 12:1* **2021**, *12*, 1–11, doi:10.1038/s41467-021-22473-w.

116. Shpigel, N.; Sigalov, S.; Malchik, F.; Levi, M.D.; Girshevitz, O.; Khalfin, R.L.; Aurbach, D. Quantification of Porosity in Extensively Nanoporous Thin Films in Contact with Gases and Liquids. *Nature Communications 2019 10:1* **2019**, *10*, 1–9, doi:10.1038/s41467-019-12277-4.

117. Li, X.; Song, S.; Shuai, Q.; Pei, Y.; Aastrup, T.; Pei, Y.; Pei, Z. Real-Time and Label-Free Analysis of Binding Thermodynamics of Carbohydrate-Protein Interactions on Unfixed Cancer Cell Surfaces Using a QCM Biosensor OPEN. *Nature Publishing Group* **2015**, *5*, 14066, doi:10.1038/srep14066.

118. Guo, K.; Wustoni, S.; Koklu, A.; Díaz-Galicia, E.; Moser, M.; Hama, A.; Alqahtani, A.A.; Ahmad, A.N.; Alhamlan, F.S.; Shuaib, M.; et al. Rapid Single-Molecule Detection of COVID-19 and MERS Antigens via Nanobody-Functionalized Organic Electrochemical Transistors. *Nature Biomedical Engineering 2021* **2021**, 1–12, doi:10.1038/s41551-021-00734-9.

119. Plausinaitis, D.; Ratautaite, V.; Mikoliunaite, L.; Sinkevicius, L.; Ramanaviciene, A.; Ramanavicius, A. Quartz Crystal Microbalance-Based Evaluation of the Electrochemical Formation of an Aggregated Polypyrrole Particle-Based Layer. *Langmuir* **2015**, *31*, 3186–3193, doi:10.1021/LA504340U.

120. Ratautaite, V.; Plausinaitis, D.; Baleviciute, I.; Mikoliunaite, L.; Ramanaviciene, A.; Ramanavicius, A. Characterization of Caffeine-Imprinted Polypyrrole by a Quartz Crystal Microbalance and Electrochemical Impedance Spectroscopy. *Sens Actuators B Chem* **2015**, *212*, 63–71, doi:10.1016/J.SNB.2015.01.109.

121. Linqiu Cao *Carrier-Bound Immobilized Enzymes: Principles, Application and Design*; Wiley-VCH, 2005; ISBN 9783527312320.

122. Sassolas, A.; Blum, L.J.; Leca-Bouvier, B.D. Immobilization Strategies to Develop Enzymatic Biosensors. *Biotechnol Adv* **2012**, *30*, 489–511, doi:10.1016/J.BIOTECHADV.2011.09.003.

123. Adrio, J.L.; Demain, A.L. Microbial Enzymes: Tools for Biotechnological Processes. *Biomolecules 2014, Vol. 4, Pages 117-139* **2014**, *4*, 117–139, doi:10.3390/BIOM4010117.

124. Datta, S.; Christena, L.R.; Rajaram, Y.R.S. Enzyme Immobilization: An Overview on Techniques and Support Materials. *3 Biotech* **2013**, *3*, 1–9, doi:10.1007/S13205-012-0071-7/FIGURES/1.

125. Zdarta, J.; Meyer, A.S.; Jesionowski, T.; Pinelo, M. A General Overview of Support Materials for Enzyme Immobilization: Characteristics, Properties, Practical Utility. *Catalysts 2018, Vol. 8, Page 92* **2018**, *8*, 92, doi:10.3390/CATAL8020092.

126. Lee, H.J.; Wark, A.W.; Goodrich, T.T.; Fang, S.; Corn, R.M. Surface Enzyme Kinetics for Biopolymer Microarrays: A Combination of Langmuir and Michaelis-Men Ten Concepts. *Langmuir* **2005**, *21*, 4050–4057, doi:10.1021/LA046822H/ASSET/IMAGES/LARGE/LA046822HF00009.JPEG.

127. Runge, C. Ueber Die Numerische Auflösung von Differentialgleichungen. *Math Ann* **1895**, *46*, 167–178, doi:10.1007/BF01446807.

128. Hosseini-Koupaei, M.; Shareghi, B.; Saboury, A.A.; Davar, F.; Raisi, F. The Effect of Spermidine on the Structure, Kinetics and Stability of Proteinase K: Spectroscopic and Computational Approaches. *RSC Adv* **2016**, *6*, 105476–105486, doi:10.1039/C6RA20975K.

129. Teran, M.; Nugent, M.A. CHARACTERIZATION OF RECEPTOR BINDING KINETICS FOR VASCULAR ENDOTHELIAL GROWTH FACTOR-A USING SPR. *Anal Biochem* **2018**, *564–565*, 21, doi:10.1016/J.AB.2018.10.001.

130. Nonaka, Y.; Sode, K.; Ikebukuro, K. Screening and Improvement of an Anti-VEGF DNA Aptamer. *Molecules 2010, Vol. 15, Pages 215-225* **2010**, *15*, 215–225, doi:10.3390/MOLECULES15010215.

LIST OF PUBLICATIONS

Paper 1 **Dronina, J.**, Bubniene, U. S., Ramanavicius, A. The application of DNA polymerases and Cas9 as representative of DNA-modifying enzymes group in DNA sensor design (review). *Biosensors and Bioelectronics.* 112867 (2020) https://doi.org/10.1016/j.bios.2020.112867

Paper 2 **Dronina, J.**, Bubniene, U. S., Ramanavicius, A. Advances and Insights in the Diagnosis of Viral Infections. *Journal of Nanobiotechnology.* 348 (2021) https://doi.org/10.1186/s12951-021-01081-2

Paper 3 **Dronina, J.**, Bubniene, U. S., Ramanavicius, A. Towards application of CRISPR-Cpf1 in the design of modern viral DNA detection tools (Review). *Journal of Nanobiotechnology. 41* (2022). https://doi.org/10.1186/s12951-022-01246-7

Paper 4 **Dronina, J.**, Plausinaitis D., Bubniene, U. S., Ramanavicius, A. Real-time-flow and label-free assessment of *T7* DNA polymerase immobilization. *Materials Today Nano.* 100232 (2022). https://doi.org/10.1016/j.mtnano.2022.100232

Paper 5 **Sarvutiene, J.**, Prentice, U., Ramanavicius, S., Ramanavicius, A. Molecular imprinting technology for biomedical applications. *Biotechnology Advances.* 108318 (2024). https://doi.org/10.1016/j.biotechadv.2024.108318

Paper 6 V. Liustrovaite, V. Ratautaite, A. Ramanaviciene, I. Plikusiene, U. Malinovskis, D. Erts, **J. Sarvutiene**, A. Ramanavicius. Electrochemical sensor for vascular endothelial growth factor based on self-assembling DNA aptamer structure, *Science of the Total Environment*, 955, (2024), 177151. https://doi.org/10.1016/j.scitotenv.2024.177151

Paper 7 **Sarvutiene, J.**, Prentice, U., Ramanavicius, A. Advances in Duchenne Muscular Dystrophy: Diagnostic Techniques and Dystrophin Domain Insights. *International Journal of Molecular Sciences.* https://doi.org/10.3390/ijms26083579

Paper 8 Maciulis V., Stanciauskaite M., Balevicius S., Ramanaviciene A., Malinovskis U., Erts D., Ramanavicius A., **Sarvutienė J.**, Plikusiene I. Characterisation of binding kinetics for vascular endothelial growth factor with self-assembled DNA aptamer using total internal reflection ellipsometry. *Surfaces and Interfaces, 107453 (2025), ISSN 2468-0230.* https://doi.org/10.1016/j.surfin.2025.107453.

Paper 9 **Sarvutiene, J.**, Plausinaitis D., Prentice, U., Ramanavicius, A. Proteinase K-Assisted Proteolysis of Immobilized Enzymes and BAFF-Based DNA Biosensing: Comparative Insights from QCM Kinetic Modeling. *Talanta*. Submitted and accepted for publication

Paper 10 **Sarvutiene, J.**, Plausinaitis D., Prentice, U., Ramanavicius, A. Enhanced Reusability of Immobilized T7 DNA Polymerase in Multi-Cycle Exonuclease Reactions on Gold-Coated SAM Biosensor Platforms. *Materials Today Chemistry*. Submitted and accepted for publication

LIST OF CONFERENCE PRESENTATIONS

1. Chemija ir cheminė technologija 2024 “Enhancing Analytical Efficiency: Reusable DNA Enzymes in Biosensing Technology” 2024.05.17 Kaunas. Žodinis pranešimas. R. Alexander, J. Sarvutiene, U. Prentice https://cct-students.ktu.edu/wp-content/uploads/sites/367/2024/05/Chemija-ir-chemine-technologija_2024_Programa.pdf
2. OpenReadings 2025 Vilnius: ENHANCING *T7* DNA POLYMERASE IMMOBILIZATION FOR REUSABLE BIOSENSORS: Julija Sarvutiene, Deivis Plaušinaitis, Urte Prentice, Arunas Ramanavicius
3. PITTCON 2025 Bostonas: Affinity sensors for the determination of SARS-CoV-2 virus proteins: Arunas Ramanavicius, Viktorija Liustrovaite, Yana Karnitskaya, Maryia Drobysh, Ernestas Brazys, Alma Rucinskiene, Vilma Ratautaite, Ieva Plikusiene, Julija Sarvutiene, Urte Prentice, Sarunas Zukauskas, Almira Ramanaviciene
4. 8th World Chemistry Conference and Exhibition (WCCE-2025) June 23 - 24, 2025 at Prague, Czech Republic. Optimizing *T7* DNA Polymerase Immobilization for Reusable Biosensors: Real-Time QCM Monitoring for Sustainable DNA Analysis. U. Prentice, J. Sarvutiene

CURRICULUM VITAE

PERSONAL INFORMATION	
Name, Surname	Julija Sarvutienė
e-mail	julija.sarvutiene@ftmc.lt
EDUCATION	
2006 – 2011	Bachelor of Chemical Engineering, Kaunas University of Technology
2011 – 2013	Master of Chemistry, Vilnius University
2019 – 2024	PhD studies, Vilnius University, Center for Physical Sciences and Technology
PROFESSIONAL EXPERIENCE	
2006	Thermo Fisher Scientific (former UAB Fermentas), Junior specialist
2011 – 2013	Thermo Fisher Scientific, Quality Control Specialist
2013 – 2018	Thermo Fisher Scientific, Senior Quality Control Specialist
2018 – 2021	Thermo Fisher Scientific, Manager, Enzymes Quality Control Group
2021 – 2023	Thermo Fisher Scientific, Manager, Enzymes Manufacturing Group
2023 – Present	Thermo Fisher Scientific, Manager, Modification Enzymes value stream

Vilniaus universiteto leidykla
Saulėtekio al. 9, III rūmai, LT-10222 Vilnius
El. p. info@leidykla.vu.lt, www.leidykla.vu.lt
bookshop.vu.lt, journals.vu.lt
Tiražas 20 egz.